DYNAMICS ON NETWORKS

BY

LAN WANG

DISSERTATION

Submitted in partial fulfillment of the requirements
for the degree of Doctor of Philosophy in Mathematics
in the Graduate College of the
University of Illinois at Urbana-Champaign, 2020

Urbana, Illinois

Doctoral Committee:

Professor Lee Deville, Chair
Professor Jared Bronski
Associate Professor Zoi Rapti
Associate Professor Kay Kirkpatrick

ABSTRACT

The main focus of this thesis is to study the stability of fix points for a dynamical system. In the first part, we consider two dynamical models whose underlying graph can be represented by a single network. We first consider the Kuramoto model, a canonical model of coupled phase oscillators. We obtain two results on its partial phase-locked state, where a subset of oscillators remain close in phase while others drift away. Firstly, we derive an analytical criterion for the finite-N model to guarantee the existence of partial phase-locking for sufficiently strong coupling, by proving the existence of an attracting ball around a fixed point of a subset of the oscillators. Secondly, we deduce a deterministic condition for the model in the large N limit, giving almost sure existence of a partially entrained cluster of computable size. We then explore a social network model describing the formation of opinions. Two approaches, automorphism reduction method and "nearest-neighbor" mean-field analysis, are proposed to analyze its fix points and their stabilities. Both approaches aim to resolve the problem of the curse of dimensionality. For the first approach, we exploit the graph automorphism of the Petersen graph and find its three stable fix points, a consensus state, a balanced and an unbalanced state. For the second approach, we use the Erdös-Rényi graph to illustrate the idea of approximating a large system by an "averaged" smaller one by considering the distances of neighbors of a given vertex.

In the second part, we generalize the single-network case into complex networks to account for real-world problems. In particular, we study a node-aligned multilayer Kuramoto model that encapsulates multiple channels of connectivity among oscillators. Our primary goal is to understand how inter-layer connections affect system stability. We address this question from two aspects: the effect of inter-layer topologies and the effect of a weak inter-layer perturbation. For the first aspect, we discuss two specific topologies: a complete graph and a cycle-tree graph or one containing only no-edge-shared cycles, and explore their effects on the stability of a twisted fixed point of the Kuramoto model. For the second aspect, we focus on a duplex network and provide analytical treatment to measure the effect of an additional weak inter-layer coupling on the system stability using the standard perturbation theory. It is found that under specific conditions our system is always destabilized due to the line addition, conforming to the famously counter-intuitive Braess's Paradox.

To my family with endless love and respect

ACKNOWLEDGEMENTS

"A teacher affects eternity; he can never tell where his influence stops", this saying cannot be more accurate of my advisor, Jared Bronski. Without your patience and support, this work would be a stew of my overwhelming self-doubt and struggles. Words alone cannot express my gratitude to you, Prof. Bronski, for guiding my research career into fruition. I am also grateful to the committee members of my preliminary exam and thesis defense: Lee Deville, Zoi Rapti, and Kay Kirkpatrick, for listening to my research and providing useful insights on my work.

Besides doing research, teaching has also retained as a precious memory. "In learning you will teach, and in teaching you will learn." I have to say I have learned just as much from my students as I have taught them calculus. Thanks to my wonderful years with my Calculus I and II classes, I learned to listen more than talk, share more than acquire, and care more than inform. More importantly, they are a living reminder of how noble and charming education can be and they deserve great credit.

Looking back upon the past years, landing in a new country and adapting to a completely different culture was never easy - especially never so without my great friends. My gratitude goes to Stef and Tara for being exceptionally nice to me when my English was too poor to be understood. Also, thanks Shinhae for being my best study buddy and Haojian for being my best gossip buddy; Amir for growing a pleasant romantic memory in my mind; and Thilina for opening up the world of computer science that I found myself to enjoy. Finally, thanks to Donglei for being my driving instructor and one of closest friends throughout my Ph.D. years.

There is something special, I believe, that ties people together and makes them friends, but it is even more special to make them roommates. I cannot forget how Kaili Ma woke me up every morning at 7 a.m. with her signature fragrant and pungent breakfast cuisine. I cannot forget how Claire Wu cheered me up when she performed on a piano, the melodious sound soaring and the symphony flowing around stirred wonders in my soul. I cannot forget the countless days and nights Yuqi Kang companied with me in the Grainger library and how I became a more mature and open-minded person under her influence. My last roommate, Jimmy He, who has also become my boyfriend, my soulmate, my forever love, will never be thanked more. I was always wondering how lucky I am to meet someone such brilliant and thoughtful at the same time.

Finally, I cannot be more indebted to my amazing family. My dear mom, thank you for visiting the USA three times during my Ph.D. and provided me with completely unconditional love and support. Dad, thank you for being a great example and making me strong, hard-working and persistent. My twin sister, thank you for being so optimistic and funny that always make me smile through tears and forget all the troubles. And my very beloved grandmother, thank you for raising me once I was born and give me endless love all the time.

Especially, thank myself for trying to be a better me every day.

TABLE OF CONTENTS

Chapter 1

Introduction

Though it has been for nearly twenty years in the past, the severe wobble of the London Millennium Bridge on its opening day remains fresh in people's memory. In June 2000, when thousands of pedestrians walked across the bridge, significant shaking and swaying occurred out of nowhere, which made the government shut it down almost immediately. It took entirely two years for the engineers to fix this problem with appropriate modifications and make it reopen in 2002. Such wobbles in the first place seem to be utterly unexpected, though Cornell University mathematician Steven Strogatz and three others provided a reasonable explanation in their 2005 Nature paper [1]. According to Strogatz, this strange phenomenon arose from the resonance between the bridge and people's footsteps. As pedestrians crowded through the bridge, as he explained, their periodic footfalls energized the bridge, causing it to move sideways, and in turn, inducing people to adjust their gaits to conform to the movement of the bridge, and eventually fell in sync with each other. "Wobbling and synchrony are inseparable. They emerge together, as dual aspects of a single instability mechanism, once the crowd reaches a critical size," they stated in their paper [1]. Despite the studies on the vibration of the Millennium Bridge still yet to conclude, this incident vividly paints a picture and opens a door to a world of synchronization in real life.

In the natural world, synchronization phenomena are ubiquitous around us. As early as the 17th century, Dutch scientist Christiaan Huygens observed synchronization between pendulums. As the pendulums move back and forth, sound pulses travel through the wall the clocks hang on. These sound pulses create vibrations and interfere with the pendulum swing and eventually they synchronize. Oliveira and Melo developed a model explaining the phase-locking between pendulums and reported their results in a recent paper [2]. Other than this, synchronization is also widely observed in biological, chemical, physiological and social systems [3, 4]. For instance, fireflies flash concertedly during the night in forests [5]; fishes swim in schools deep in the ocean; birds flock in circles at sunset; human heart rhythms synchronize while co-sleeping [6]; the level of skin conductance tends to sync up as a couple sits face-to-face staring at each other [7]. More examples and references can be found in an excellent book by Strogatz [8].

Research on comprehending the essence of the synchronization phenomena has been ongoing for decades, with one primary focus on the mechanism within a population of oscillators that account for the synchronization. To understand the theoretical principles behind it, it is requisite to find a model with nonlinear interactions among oscillators that can be mathematically analyzed. However, finding such a model had been proved difficult especially for a large system. A pioneering breakthrough was firstly made by Winfree in his first paper [9]. He considered a phase model containing a huge population of interacting limit-cycle oscillators and realized that synchronization occurs when the oscillator coupling is strong enough. However, his model is still hard to solve

in its full generality. Followed his pace, Yoshiki Kuramoto, a Japanese physicist in the field of nonlinear dynamics, simplified the model even further. In 1975, he proposed a model of phase oscillators running at arbitrary intrinsic frequencies and coupled through the sine of their phase differences, which is known as the Kuramoto model nowadays. The beauty of this model lies in both its simplicity and complexity. On the one hand, the interaction among oscillators is simple enough to be mathematically tractable. On the other hand, it is rich enough to display a variety of different synchronization patterns and sufficiently flexible to be adapted to various contexts. Although nearly half a century has passed, research on the Kuramoto model never ceased. Many excellent reviews have been given on the Kuramoto model including Strogatz's work in 2000 [10] and Acebrón's survey in 2005 [11].

The simplest form of the Kuramoto model deals with equally-weighted, all-to-all, and purely sinusoidal couplings [12, 13]:

$$\dot{\theta}_i = \omega_i + \frac{\gamma}{N}\sum_{j=1}^{N}\sin(\theta_j - \theta_i) \qquad i = 1, 2, ..., N, \tag{1.1}$$

where N is the number of oscillators in the system, $\theta_i \in \mathbb{T}^1 = (-\pi, \pi]$ is a phase variable describing the state of the i^{th} oscillator, $\omega_i \in \mathbb{R}$ is the natural frequency of the i^{th} oscillator following a given distribution with a probability density $g(\omega)$, and $\gamma > 0$ is the coupling strength among the oscillators. Here, we scale γ by a factor of N, the cardinality of each oscillator's neighborhood, to ensure the model is well behaved as $N \to \infty$. Note that by choosing an appropriate rotation frame: $\theta = \theta - \Omega t$ where Ω is the first moment of $g(\omega)$, the equation (1.1) is equivalent to a system with the average natural frequency of oscillators being zero. Thus, without loss of generality, we can always assume $\sum_i \omega_i = 0$. Depending on various distributions of ω_i, different synchronization scenarios can occur in the parameter regions where incoherence is unstable. And for the Kuramoto model, its synchronization can be conveniently measured by a complex order parameter

$$re^{i\Psi} = \frac{1}{N}\sum_{j=1}^{N} e^{i\theta_j}, \tag{1.2}$$

where i is the imaginary unit, the radius $0 < r(t) < 1$ measures the phase coherence of the oscillator population and the angle $\Psi(t)$ represents the average phase. As $N \to \infty$, the radius vanishes when all the oscillators are out of synchrony and becomes positive in synchronized states. By a mean-field argument, Kuramoto suggested that the order parameter should undergo a phase transition at some critical coupling γ^*, with amplitude $\propto \sqrt{\gamma - \gamma^*}$: since the amplitude is small for $\gamma \gtrsim \gamma^*$ one expects only partial synchronization, meaning phase-locked and drifting oscillators co-exist in the system. Strogatz gives a nice survey in his paper from 2000 [10]. In particular, he mentions the Bowen lectures of Kopell in 1986, where she raises the possibility of doing a rigorous analysis for large but finite N and then trying to prove a convergence result as $N \to \infty$.

The general bifurcation picture described by Kuramoto has been established for the continuum model: Strogatz and Mirollo introduced the continuum model and showed that if the frequencies are distributed with density $g(\omega)$ then the incoherent state goes unstable exactly at the critical value $\gamma^* = \frac{2}{\pi g(0)}$ predicted by Kuramoto [14]. Strogatz, Mirollo and Matthews [15] showed that below the threshold γ^* the evolution decays to an incoherent state via Landau damping, and Mirollo and Strogatz computed the spectrum of the partially locked state in the continuum model [16]. This general picture has been expanded by a number of authors including Fernandez [17], Dietert [18] and Chiba [19]. See also the review paper of Acebrón, Bonilla, Pérez Vicente, Ritort and Spigler [11], particularly section II.

The partially phase-locked states in the finite-N Kuramoto model have received somewhat less attention in the literature than either fully phase-locked states of the finite-N model or partially phase-locked states in the continuum model. Back to 2004, Aeyels and Rogge [20] proved the existence of partial entrainment of a three-cell network and showed its local stability. They defined the partial entrainment as a subset of oscillators remaining close to one another, while not necessarily being close to any fixed configuration. Three years later, De Smet and Aeyels [16] derived an elegant result by quantifying the influence of the coupling strength γ on the size of the partial entrainment. A neat sufficient condition was formulated as an inequality for the natural frequency differences of oscillators bounded by a function of γ and N. In particular, a critical value of γ guaranteeing partial entrainment with respect to a given subset of oscillators was found with the use of trigonometric inequalities.

One of the goals of this thesis is to address the issue that relatively little work on partial synchronization for the Kuramoto model has been done. The two primary references we followed are Dorfler and Bullo's paper [21] on the full synchronization of the finite-N Kuramoto model and the above-mentioned work on the partial entrainment by De Smet and Aeyels [16]. We will present two independent but related results in Chapter 2. Firstly, we shall derive an analytical criterion that, for sufficiently strong coupling, guarantees the existence of a partially phase-locked state. We do this by defining a semi-norm and proving the existence of an attracting ball around a fixed point of a subset of the oscillators. We also prove the existence of a larger invariant ball such that any point in it asymptotically converges to the attracting ball. Secondly, we shall consider the large N (thermodynamic) limit for the Kuramoto system. We use a result of De Smet and Aeyels [16] on partial entrainment to show that when the natural frequencies of the oscillators are independent identically distributed with a unimodal distribution, their result reduces to a deterministic condition giving almost sure existence of a partially entrained state for sufficiently strong coupling.

The Kuramoto model formation considered in Chapter 2 is in its simplest version where the underlying topology is a complete graph. By dint of the simple structure of a complete graph, we are able to characterize its synchronization analytically in a fairly simple manner. Nevertheless, in many applications one would like to understand a more general topology. For a dynamical system with a more generalized underlying topology, the fixed points together with their respective stability

are not well understood. Throughout this thesis, we will always assume the underlying topology is an undirected graph. In Chapter 3, we will examine fixed points of a simple model for a social network in a more general setting. In particular, we discuss two types of underlying graphs of the system. First we consider the case in which the underlying graph has a great deal of symmetry. We shall use the Petersen graph as an example to illustrate our approach. The gist is to reduce the graph exploiting its automorphism group, so as to simplify the analysis process. The second approach applied to large random graphs with few symmetries. Specifically, we shall focus on the Erdös-Rényi random graph model with a large number of nodes and propose a novel mean-field technique to study the fixed points. We name this technique the "nearest-neighbor" mean-field analysis method. The meat is to measure the effect of interactions among nodes by the distance between them. Hence, instead of considering every individual communication, we can classify the nodes and evaluate the average interaction between groups, and therefore tackle the curse of the dimensionality problem caused by the large size of the graph. We find good qualitative agreement between the fixed points of the model on the Erdös-Rényi graph and the fixed points on the reduced "mean-field" graph.

Starting from Chapter 4, we turn our attention from the traditional single-layer network representation to the multilayer network representation. For dynamical systems in real-world problems that incorporate multiple channels of connectivity and various interactions among entities, the canonical single-layer network structure is too simple to model them correctly. This issue alone gives incentive to the complex network theory blooming in recent decades. In Chapter 4, we will study a node-aligned multilayer Kuramoto model and explore how the inter-layer connections affect the stability of the twisted phase-locking states of the model. In particular, we shall focus on two specific inter-layer topologies: a complete graph and a cycle-tree graph, which is a graph containing only no-edge-shared cycles. For the complete graph, we conclude that the inter-layer connections always impede the phase-locking by computing eigenvalues of the graph Laplacian directly. For the cycle-tree graph, we investigate by following a workflow from a single cycle to multiple cycles with a single hub, and finally to a tree of cycles. Along with the analysis, perturbation theory and algebraic graph theory are applied to find the change of the number of positive eigenvalues of the Jacobian resulting from the addition of inter-layer connections. We find that the effect of inter-layer connections depends on the number of layers in each cycle: it impedes the phase-locking only when there exist cycles containing too few layers.

In Chapter 4, we contrast two cases: one with full inter-layer connection and one without any such connections. However, considering the intermediate case of a partial inter-layer coupling, i.e., a subset of nodes on one layer is connected to another layer while others are not, what will happen if we add a weak inter-layer connection? How will this extra coupling effect the stability of the whole dynamic? We consider this question in Chapter 5. We put forward a two-layer Kuramoto oscillator system. This system is proposed as an analog to the famous Braess's Paradox that adding a road intended to help can adversely impact the traffic and increase the overall journey time. The

underlying graph is a node-aligned duplex network. For this system, our result enables analytical measurement of the effect of an extra coupling on the stability using the standard perturbation theory. It is found, counter-intuitively as the Braess's Paradox, that under specific conditions our system is always destabilized by the additional inter-layer coupling.

Chapter 2

Partial Synchronization of Kuramoto Model

2.1. Background

The literature on synchronization is large, and many different types of synchronization [22] have been studied including chaotic synchronization [23], phase synchronization [24], lag synchronization [25], generalized synchronization [26–28], etc. In this chapter, we will focus on a specific type, also a most heavily studied one, for a system of a large population of oscillators. We present the precise definition as follows:

Definition 2.1. *For a dynamical system:* $\frac{d\vec{\theta}}{dt} = f(\vec{\theta}, \vec{\lambda})$*, where* $\vec{\theta}$ *is a vector of the oscillators' phases and* $\vec{\lambda}$ *is a vector of parameters. For some* $i, j \in \{1, ..., N\}$*, we say the* i*th and* j*th oscillators are synchronized (or phase-locked or coherent) if*

$$\dot{\theta}_i(t) - \dot{\theta}_j(t) \to 0 \text{ as } t \to \infty, \tag{2.1}$$

and asynchronous (or drifting or incoherent) otherwise. Here, the overdot denotes the differentiation with respect to time t*. Moreover, if (2.1) is true for all pairs of oscillators, we say the system reaches full synchronization (or full phase-lock or coherence). If it is not true for any pair of oscillators, we say the system is asynchronous (or incoherent).*

The Kuramoto model:

$$\dot{\theta}_i = \omega_i + \frac{\gamma}{N} \sum_{j=1}^{N} \sin(\theta_j - \theta_i) \qquad i = 1, 2, ..., N, \tag{2.2}$$

is a canonical model for understanding the synchronization phenomenon. During the past decades, a great deal of work has been directed towards studying necessary and/or sufficient conditions on the critical coupling strength to make the Kuramoto system phase-lock [10, 11, 16, 20, 29–35]. One particularly useful result by Dorfler and Bullo [21] is an explicit sufficient condition on the frequency spread that guarantees phase-locking:

$$\gamma > \omega_{max} - \omega_{min}, \tag{2.3}$$

where $\omega_{max} := \max_i \omega_i$ and $\omega_{min} := \min_i \omega_i$. Under this condition, the Kuramoto model (2.2) supports full phase-locking for all possible distributions of the natural frequencies supported on $[\omega_{min}, \omega_{max}]$. On the other hand, the standard ℓ_1/ℓ_∞ estimate on the sum gives a necessary

condition on the coupling strength γ in order for the system to support a phase-locked state:

$$\gamma \geq \frac{N}{2(N-1)} \left(\omega_{max} - \omega_{min}\right) \approx \frac{1}{2} \left(\omega_{max} - \omega_{min}\right). \tag{2.4}$$

From Equation (2.4) it is easy to see that if ω_i are independent and identically distributed according to a distribution with unbounded support, then in the large N limit one can expect, at best, partial phase-locking, as the law of large numbers will guarantee that, with high probability, Equation (2.4) will be violated. To see this, note that

$$\mathbb{P}(\max_{i \in \{1 \ldots N\}} |\omega_i| < c) = (\mathbb{P}(|\omega_i| < c))^N.$$

If the support of the distribution is unbounded, then $(\mathbb{P}(|\omega_i| < c)) < 1$ for all c and thus $\lim_{N \to \infty} \mathbb{P}(\max_{i \in \{1 \ldots N\}} |\omega_i| < c) = 0$. So for fixed coupling strength γ, full-phase-locking occurs with vanishing probability in the large N limit. One can, of course, One can, of course, consider scaling γ with N — this involves extreme value statistics of the distribution [29] — but if one is taking γ to be fixed one must consider partial phase-locking or partial entrainment.

Partially locked states occur due to two factors. One is the inhomogeneity of the oscillators themselves. The difference in the natural frequencies of oscillators in the Kuramoto model is one example. Another factor had not been uncovered until eighteen years ago (2002) when Kuramoto and Battogtokh [36] found that, with certain initial conditions, oscillators with identical natural frequency can behave differently too. Since then, people started to realize that coupling inhomogeneity is also a factor of partial locking. This discovery was so fascinating that people gave it a sensational name, "the Chimera state", inspired by the mythological creature composed of a lions head, a goats body, and a serpents tail. Thenceforth a chimera state refers to a spatio-temporal pattern in which a population of identical oscillators is split into coexisting regions of phase-locked and drifting oscillations. This research field, though interesting and active, is out of the scope of this chapter. We will, instead, pay our attention to understanding the partially locked states for the classic Kuramoto model (2.2) that arose by the first factor.

The partially locked states in the finite N Kuramoto model have received less attention in the literature than either fully phase-locked states of the finite-N model or partial locked states in the continuum model. Among the finite-N results we do mention the work of Aeyels and Rogge [20] and particularly De Smet and Aeyels [16]. De Smet and Aeyels establish a partial entrainment result that will be important for the latter part of this chapter. To make the future argument clear, we shall first draw a distinction between partial phase-locking and partial entrainment (as used by De Smet and Aeyels): we will use partial phase-locking to refer to a subset of oscillators that approximately rotate rigidly. More precisely, a partially phase-locked subset S of oscillators is the one that satisfies: there exists a constant vector $\theta^* \in \mathbb{T}^N$ such that the translated phase vector

$\tilde{\theta} := \theta - \theta^*$ follows

$$\limsup_{t\to\infty} |\tilde{\theta}_i(t) - \tilde{\theta}_j(t)| \leq \delta(N) \qquad \forall\ i,j \in S, \tag{2.5}$$

where $\delta(N) \to 0$ as $N \to \infty$. Typically in this chapter $\delta \propto N^{-\frac{1}{2}}$, where N is the total number of oscillators. Following De Smet and Aeyels we use partial entrainment to mean that there exists a constant c small but independent of N such that

$$\limsup_{t\to\infty} |\theta_i(t) - \theta_j(t)| \leq c \qquad \forall\ \ i,j \in S. \tag{2.6}$$

Obviously this distinction is mainly important in the large N limit.

In this chapter, we present two independent but related results. Firstly, we consider partial phase-locking in the finite-N Kuromoto model. The essence is perturbing a phase-locked solution by adding in additional oscillators that are not phase-locked to the main group. We define a collection of semi-norms and associated cylindrical sets in the phase space. We show that under suitable conditions the semi-norms are decreasing in forward time, and thus the associated cylindrical sets are invariant in forward time. The invariance of the cylindrical sets in forward time implies the existence of a subset of oscillators that remain close in phase for all time, while the infinite directions of the cylinder correspond to the degrees of freedom of the remaining oscillators that are not phase-locked to the group. More precisely, we first consider a Kuramoto model with a small forcing term and prove a standard proposition showing that if the unperturbed Kuramoto problem admits a stable phase-locked solution then the perturbed problem admits a solution that stays near to this phase-locked solution. We then apply this proposition to the Kuramoto model itself by identifying a subset of oscillators with a small spread in natural frequency and treating the remaining oscillators as a perturbation. This will lead to a sufficient condition for the existence of a partially phase-locked solution in terms of the infimum over all subsets of oscillators of a certain function of the frequency spread in that subset. Under such condition, the number of unbounded oscillators is at most $N^{1/2}$. Finally, we present some supporting numerical experiments.

For the second result, we reconsider some earlier work of De Smet and Aeyels [16] in the case where the natural frequencies of the oscillators are independent and identically distributed random variables, in the large N limit. We analyze the condition derived in [16] for the existence of a positively invariant region and show that, in the large N limit, we can find a deterministic condition guaranteeing the existence of a positively invariant region for sufficiently large coupling constant γ. The theorem shows that, for the coupling strength γ sufficiently large and ω_i chosen independently and identically distributed from some reasonable distribution, then with probability approaching one as $N \to \infty$ there exists an entrained subset of oscillators of positive density. We also get (deterministic) bounds on the size of the partially entrained cluster.

2.2. Partial Phase-locking

2.2.1. *Main Result*

Our first result is to establish that, given a set of stable phase-locked oscillators, one can add to the system a second set of oscillators that do not phase-lock to the first without materially impeding the phase-locking. Before going into details, we first give some intuition why we expect this to be true. The following is reasonably well-known. Suppose that an autonomous ODE $\boldsymbol{x}_t = \boldsymbol{f}(\boldsymbol{x})$ has an asymptotically stable fixed point $\boldsymbol{x}_0$ where the linearization is coercive: $\boldsymbol{y}^T \nabla \boldsymbol{f}(\boldsymbol{x}_0)\boldsymbol{y} \leq -c\|\boldsymbol{y}\|^2$. If one makes a sufficiently small time-dependent perturbation to the ODE, $\boldsymbol{x}_t = \boldsymbol{f}(\boldsymbol{x}) + \epsilon g(\boldsymbol{x}, t)$ then there will be a small ball around the former fixed point that is invariant in forward time (trapping) – trajectories that begin in the region remain so for all time. To see this, let $\boldsymbol{x} = \boldsymbol{x}_0 + \boldsymbol{y}$ and note that

$$\boldsymbol{y}_t = \boldsymbol{f}(\boldsymbol{x}_0 + \boldsymbol{y}) + \epsilon \boldsymbol{g}(\boldsymbol{x}_0 + \boldsymbol{y}, t) \approx \nabla \boldsymbol{f}(\boldsymbol{x}_0)\boldsymbol{y} + \epsilon \boldsymbol{g}(\boldsymbol{x}_0 + \boldsymbol{y}, t), \tag{2.7}$$

$$\frac{1}{2}\frac{d}{dt}\|\boldsymbol{y}\|^2 \approx \boldsymbol{y}^T \nabla \boldsymbol{f}(\boldsymbol{x}_0)\boldsymbol{y} + \epsilon \boldsymbol{y}^T \boldsymbol{g} \lesssim -c\|\boldsymbol{y}\|^2 + \frac{\epsilon}{2}(\|\boldsymbol{y}\|^2 + \|\boldsymbol{g}\|^2). \tag{2.8}$$

Thus if $\|\boldsymbol{y}\|$ is of the right size: large enough that $-(c - \frac{\epsilon}{2})\|\boldsymbol{y}\|^2 + \frac{\epsilon}{2}\|\boldsymbol{g}\|^2 < 0$ but small enough to justify $\boldsymbol{f}(\boldsymbol{x}_0 + y) \approx \nabla \boldsymbol{f}(\mathbf{x}_0)\boldsymbol{y}$, then we find that $\frac{d}{dt}\|\boldsymbol{y}\|^2 \leq 0$ and orbits initially in the ball remain so for all time. The intuition, therefore, is that under perturbation the fixed point should smear out to an invariant ball of radius $\sqrt{\epsilon}$. Similar constructions are used in the PDE context to prove the existence of attractors [37–41]. In the proof of the actual theorem, of course, we will take a bit more care but this is the essential idea.

Our first goal is to define what we mean by a partially phase-locked solution. To this end, we shall define a family of semi-norms $\|\cdot\|_S$ indexed by a subset of oscillators $S \subseteq \{1, 2, 3, \ldots, N\}$ representing the collection of phase-locked oscillators.

Definition 2.2. *Given a non-empty index subset $S \subseteq \Omega = \{1, 2, 3, \ldots, N\}$, we define a semi-norm on a phase vector θ with respect to S as follows*

$$\|\theta\|_S^2 := \frac{1}{|S|} \sum_{i,j \in S, i \leq j} (\theta_i - \theta_j)^2, \tag{2.9}$$

where $|S|$ is the cardinality of the set S.

Remark 2.3. *The open semi-ball $\|\theta\|_S < R$ is a cylinder in $\mathbb{R}^N$ that is unbounded in $N - |S| + 1$ directions and is bounded in the remaining $|S| - 1$ directions. The unbounded directions correspond to the $N - |S|$ oscillators that are not phase-locked together with 1 direction corresponding to the common translation mode $\theta \mapsto \theta + \alpha \hat{\boldsymbol{1}}$ where α is a scalar and $\hat{\boldsymbol{1}}$ is an all-ones vector.*

Note that when taking the universal set, i.e., $S = \Omega$, we have

$$\|\theta\|_S^2 = \frac{1}{N} \sum_{1 \le i \le j \le N} (\theta_i - \theta_j)^2 = \|\theta - \langle\theta\rangle \hat{\mathbf{1}}\|^2, \tag{2.10}$$

where $\langle\theta\rangle$ refers to the mean of θ. In this case, the semi-norm reduces to the usual ℓ_2 norm modding out by the translation degree of freedom.

Of course these are only semi-norms, not norms, as there is always at least one null direction. However, we will slightly abuse notation by referring to sets $\|\theta\|_S < r$ as a ball of radius r since the whole idea is to mod out what is happening in the null directions. Having defined these seminorms we can use this to define partial phase-locking.

Definition 2.4. *Let $\mathbb{T}^1 = (-\pi, \pi]$ be a torus and $\mathbb{T}^N$ a N-dimensional torus. Denote*

- *$|\theta_1 - \theta_2|$: geodesic distance between $\theta_1 \in \mathbb{T}^1$ and $\theta_2 \in \mathbb{T}^1$.*
- *$\triangle(\alpha, N) := \{(\theta_1, \theta_2, ..., \theta_N) \in \mathbb{T}^N | \max_{i,j=1}^N |\theta_i - \theta_j| < \alpha\}$ for any $\alpha \in [0, \pi]$.*
- *$\bar{\triangle}(\alpha, N) := \{(\theta_1, \theta_2, ..., \theta_N) \in \mathbb{T}^N | \max_{i,j=1}^N |\theta_i - \theta_j| \le \alpha\}$ for any $\alpha \in [0, \pi]$.*

Definition 2.5. *We say the dynamical system (2.2) achieves partial phase-locking if there exists a subset of oscillators $S \subseteq \{1, 2, 3, \ldots, N\}$ such that the following is true: for some constant vector $\theta^* \in \mathbb{T}^N$, the translated phase vector $\tilde{\theta} := \theta - \theta^*$ satisfies*

$$\limsup_{t \to \infty} |\tilde{\theta}_i(t) - \tilde{\theta}_j(t)| \le \delta(N), \qquad \forall\ i, j \in S, \tag{2.11}$$

where $\delta(N) \to 0$ as $N \to \infty$.

Remark 2.6. *In two ways, partial phase-locking has a stronger requirement than partial entrainment (a constant invariant region), which we shall define later. For one, it requires a subset of oscillators remain close to a fixed configuration; for another, the phase distance between any pair of phase-locked oscillators (up to a fixed point) decreases to zero as $N \to \infty$.*

We need the following result from Dorfler and Bullo [21] to prove our main theorem.

Theorem 2.7 (Dörfler-Bullo)**.** *If $\gamma > \gamma_{critical} := \omega_{max} - \omega_{min}$, then the Kuramoto model (2.2) achieves full synchronization and all oscillators eventually have a common frequency $\omega_{avg} = \frac{1}{N} \sum_{j=1}^N \omega_j$. Also, the set $\bar{\triangle}(\alpha, N)$ is positively invariant for every $\alpha \in [\alpha_{min}, \alpha_{max}]$, and each trajectory starting in $\triangle(\alpha_{max}, N)$ approaches asymptotically $\bar{\triangle}(\alpha_{min}, N)$. Here, α_{min} and α_{max} are two angles that satisfy $\sin(\alpha_{min}) = \sin(\alpha_{max}) = \gamma_{critical}/\gamma$ and $\alpha_{min} \in [0, \pi/2), \alpha_{max} \in (\pi/2, \pi]$.*

In order to state our main theorem, we first need to define two functions $g(K, N)$ and $h(K, N)$ that will prove important to the subsequent analysis.

Definition 2.8. *For the Kuramoto model (2.2) with natural frequencies* $\{\omega_i\}_{i=1}^N$*, define two functions:*

$$g(K,N) = \min_{S\subset\Omega,|S|=N-K} \max_{i,j\in S} |\omega_i - \omega_j|, \tag{2.12}$$

$$h(K,N) = \frac{(N-K)}{N}\sqrt{1-\frac{2K}{(N-K)^{1/2}}}. \tag{2.13}$$

We note that $g(K,N)$ *depends implicitly on the set of natural frequencies* $\{\omega_i\}_{i=1}^N$*, and represents the minimum spread in frequencies over subsets of size* $N-K$*. The function* $h(K,N)$ *will arise in the subsequent analysis and* $\gamma h(K,N)$ *represents an estimate of the maximum spread in frequencies for* $N-K$ *oscillators to be phase-locked. Note that* $h(K,N)$ *is only defined for* $K \leq \frac{\sqrt{16N+1}-1}{8} \approx 0.5N^{\frac{1}{2}}$*.*

With Definition 2.8 we are ready to state our main theorem, which gives a sufficient condition on the existence of partially phase-locked states.

Theorem 2.9. *Suppose that there exists some integer* $K \leq \frac{\sqrt{16N+1}-1}{8}$ *such that* $g(K,N) < \gamma h(K,N)\}$*, then for some constant vector* $\theta^* \in \mathbb{T}^N$*, there exists a subset of oscillators* S *with* $|S| = N-K$ *such that*

1. **INVARIANCE** *There exists a constant* R *with* $R = O(1)$ *such that every oscillator with the initial phase condition* $\|\theta(0)-\theta^*\|_S < R$ *satisfies* $\|\theta(t)-\theta^*\|_S < R$ *for all* $t > 0$*. In other words, the ball* $\|\theta(t)-\theta^*\|_S < R$ *is invariant in forward time.*

2. **CONVERGENCE** *There exists a constant* $r = O(\frac{1}{\sqrt{N}}) \ll R$ *such that orbits that begin in the larger ball* $\|\theta(0)-\theta^*\|_S < R$ *converge to the smaller ball* $\|\theta(t)-\theta^*\|_S < r$ *asymptotically.*

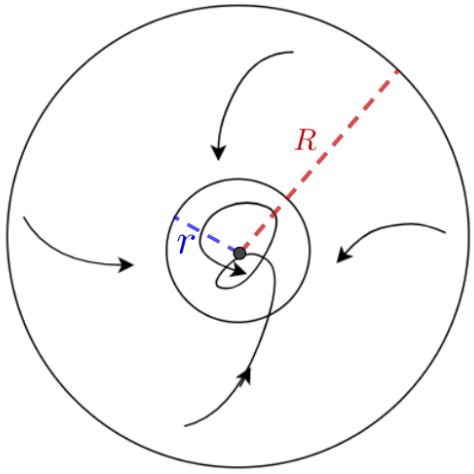

Figure 2.1: Attracting and invariant balls for a subset of $N-K$ oscillators

Remark 2.10. *We make a few remarks about this theorem. Firstly, we can actually derive analytical expressions for the sizes of the invariant and attracting balls, which are* $r = \frac{2K\gamma(N-K)^{1/2}}{N|\lambda_2|}$ *and* $R = \frac{N|\lambda_2|}{(N-K)\gamma}$*. Here,* λ_2 *is the second largest eigenvalue of the Jacobian matrix of Equation (2.2) at* θ^**. Note that* λ_2 *depends implicitly on* γ*, and as* γ *increases we expect* λ_2 *to become more negative.*

Secondly, The integer K *represents the number of free or non-phase-locked oscillators. The function* $h(K,N)$ *is only defined for* $K \leq \frac{\sqrt{16N+1}-1}{8} \approx 0.5N^{\frac{1}{2}}$ *for* N *large, so this theorem can only guarantee the existence a subset of mutually phase-locked oscillators with* $K \lesssim 0.5N^{\frac{1}{2}}$ *oscillators drifting away. This can probably be brought down with sharper estimates but we think it unlikely that the scaling could be improved without substantially changing the approach.*

Typically we will have $g(K,N) < \gamma h(K,N)$ *in an interval, so there will be a range of integers* K *for which the inequality is satisfied. In this situation, we would be primarily interested in the smallest such* K *that satisfies the inequality, as this would represent the largest partially phase-locked cluster. We denote such* K *as* K^**, i.e.,* $K^* = \underset{K}{\operatorname{argmin}}\{g(K,N) < \gamma h(K,N)\}$*.*

When $K = 0$*, corresponding to no free oscillators, the condition on* γ *in this theorem reduces to* $\gamma_{critical}(0) = \omega_{max} - \omega_{min}$*, which coincides with Theorem 2.7 of Dorfler and Bullo [21]. Thus this theorem can be viewed as a generalization of their result to the case of partial phase-locking.*

2.2.2. *Proof of Main Result*

In this section, we prove our first main result. A brief sketch of the main idea of the proof is as follows: we first prove a standard proposition: If we take the Kuramoto model in a parameter regime where there is a stable fixed point and we add a small perturbation, then there is an attracting ball of small radius around the former fixed point. In particular, any initial conditions that begin near the fixed point remain so for all time. We then use this result to study partial phase-locking by considering subsets of oscillators that could potentially phase-lock, and considering the remaining oscillators as a perturbation to these candidates for partial phase-locking.

Definition 2.11. *We say* θ^* *is a stable phase-locked solution of Equation (2.2) with frequencies* $\boldsymbol{\omega} = (\omega_1, \omega_2, ..., \omega_N)^T$ *if it satisfies (2.2)*

$$\omega_i = \frac{\gamma}{N} \sum_j \sin(\theta_i^* - \theta_j^*) \tag{2.14}$$

and J*, the Jacobian matrix at* θ^**, i.e,*

$$J_{ij}(\theta^*) = \begin{cases} \frac{\gamma}{N}\cos(\theta_i^* - \theta_j^*), & i \neq j, \\ -\frac{\gamma}{N}\sum_{k\neq i}\cos(\theta_i^* - \theta_k^*), & i = j \end{cases}$$

is negative semi-definite with a one dimensional kernel.

Proposition 2.12. *Suppose* θ^* *is a stable phase-locked solution. Consider the following perturbed*

Kuramoto model with perturbation ϵf_i:

$$\dot{\theta}_i = \omega_i - \frac{\gamma}{N}\sum_j \sin(\theta_i - \theta_j) + \epsilon f_i(\theta, t), \qquad i = 1, 2, ...N, \tag{2.15}$$

where ϵ is a small constant and $f_i's$ are functions bounded by a constant C, i.e., $\max_{\theta,t,i} |f_i(\theta, t)| \leq C$. Let

$$\begin{cases} r(\epsilon) = 2\epsilon C N^{1/2}/|\lambda_2|, \\ R = |\lambda_2|/\gamma, \end{cases} \tag{2.16}$$

where $\lambda_2 < 0$ is the second largest eigenvalue of the Jacobian matrix of (2.2) at θ^*. Then for $\epsilon < |\lambda_2|^2/(2CN^{1/2}\gamma)$, the following statements hold:
(1) The ball $\|\theta(t) - \theta^*\|_N < R$ is invariant in forward time.
(2) Every solution with $\|\theta(0) - \theta^*\|_N < R$ asymptotically converges to a smaller invariant ball with radius $r(\epsilon)$.

Proof. We will make a standard Lyapunov function calculation: the proof is sketched here, with details relegated to the Appendix. We will represent θ as $\theta = \theta^* + \tilde{\theta}$. Note that by rotational invariance we can assume $\tilde{\theta}$ is mean zero. Also note that the norm $\|\cdot\|_\Omega^2$ is equivalent to the standard Euclidean norm $\|\cdot\|^2$ on the subspace of mean zero functions: if $\tilde{\theta}$ has mean zero and $\hat{\mathbf{1}}$ is the vector of all ones then $\|\tilde{\theta} + \alpha\hat{\mathbf{1}}\|_\Omega^2 = \|\tilde{\theta}\|_\Omega^2 = \sum \tilde{\theta}_i^2$.

One can show an upper bound on $\frac{d}{dt}\|\tilde{\theta}\|^2$ is of the following form:

$$\frac{d}{dt}\|\tilde{\theta}\|^2 \leq 2\lambda_2\|\tilde{\theta}\|^2 + \gamma\|\tilde{\theta}\|^3 + 2\epsilon C N^{1/2}\|\tilde{\theta}\|.$$

To make $\frac{d}{dt}\|\tilde{\theta}\|^2$ negative, it suffices to require

$$\begin{cases} 2\epsilon C N^{1/2}\|\tilde{\theta}\| < |\lambda_2|\|\tilde{\theta}\|^2 \\ \gamma\|\tilde{\theta}\|^3 < |\lambda_2|\|\tilde{\theta}\|^2, \end{cases} \tag{2.17}$$

which is equivalent to

$$\frac{2\epsilon C N^{1/2}}{|\lambda_2|} < \|\tilde{\theta}\| < \frac{|\lambda_2|}{\gamma}. \tag{2.18}$$

Let $r(\epsilon) = 2\epsilon C N^{1/2}/|\lambda_2|$ and $R = |\lambda_2|/\gamma$, then by Gronwall's inequality [42], the semi-norm of $\tilde{\theta}$ is exponentially decreasing when $\tilde{\theta}$ is in the annulus of radii $r(\epsilon)$ and R, and then stays in the ball of radius $r(\epsilon)$ forever. So statements (1) and (2) are proved. ■

Now, we use Proposition 2.12 to prove Theorem 2.9.

Proof. For any integer K such that $0 \leq K < N$, consider $N - K$ oscillators in the Kuramoto model (2.2). By changing the order of labels, we can, w.l.o.g., focus on the first $N - K$ oscillators

and study the condition under which they will stably phase-lock. The evolution can be written as follows

$$\dot{\theta}_i = \omega_i - \frac{\gamma}{N}\sum_{j=1}^{N}\sin(\theta_i - \theta_j) \tag{2.19}$$

$$= \omega_i - \frac{\gamma}{N}\sum_{j=1}^{N-K}\sin(\theta_i - \theta_j) - \frac{\gamma}{N}\sum_{j=N-K+1}^{N}\sin(\theta_i - \theta_j) \tag{2.20}$$

$$= \omega_i - \frac{\tilde{\gamma}}{N-K}\sum_{j=1}^{N-K}\sin(\theta_i - \theta_j) + \epsilon f_i, \tag{2.21}$$

where $\tilde{\gamma} = \gamma\frac{N-K}{N}$ is a modified coupling strength on the first $N-K$ oscillators and ϵf_i represents the effect of the remaining K oscillators. Then we have $\epsilon = \frac{\gamma}{N}$, $f_i = \sum_{j=N-K+1}^{N}\sin(\theta_j - \theta_i) \leq K$. The strategy is to treat the effect of the remaining K oscillators as a perturbation and then apply Proposition 2.12.

We first consider the unperturbed problem

$$\dot{\theta}_i = \omega_i - \frac{\tilde{\gamma}}{N-K}\sum_{j=1}^{N-K}\sin(\theta_i - \theta_j), \qquad i = 1, 2, ..., N-K. \tag{2.22}$$

Define

$$\gamma_0 = \max_{i,j=1}^{N-K}|\omega_i - \omega_j|.$$

By Theorem 2.7 if the spread in frequencies satisfies

$$\gamma_0 < \tilde{\gamma} = \frac{\gamma(N-K)}{N}, \tag{2.23}$$

then the system (2.22) phase-locks. Plus, the set $\bar{\triangle}(\alpha, N-K)$ is positively invariant for every $\alpha \in [\alpha_{min}, \alpha_{max}]$, and each trajectory starting in $\triangle(\alpha_{max}, N-K)$ approaches asymptotically $\bar{\triangle}(\alpha_{min}, N-K)$, where $\alpha_{min} \in [0, \pi/2)$, $\alpha_{max} \in (\pi/2, \pi]$ and $\sin(\alpha_{min}) = \sin(\alpha_{max}) = \frac{\gamma_0}{\tilde{\gamma}}$. From these, it is clear to see that under a rotating frame with frequency ω_{avg}, Equation (2.22) has a fixed point θ^* such that $\theta^* \in \bar{\triangle}(\alpha_{min}, N-K)$.

Suppose L is the Jacobian matrix of (2.22) at the fixed point θ^*, i.e,

$$L_{ij} = \begin{cases} \frac{\tilde{\gamma}}{N-K}\cos(\theta_i^* - \theta_j^*) & i \neq j \\ -\frac{\tilde{\gamma}}{N-K}\sum_k \cos(\theta_i^* - \theta_k^*) & i = j. \end{cases}$$

Since $\theta^* \in \bar{\triangle}(\alpha_{min}, N-K)$ and $\alpha_{min} \in [0, \frac{\pi}{2})$, we have $\cos(\theta_i^* - \theta_j^*) > 0$ and L is a negative semidefinite Laplacian matrix with eigenvalues $\lambda_1 = 0 > \lambda_2 \geq \lambda_3 \geq ... \geq \lambda_{N-K}$, so the solution is stably phase-locked.

We next consider the effect of the perturbation term ϵf_i where $\epsilon = \frac{\gamma}{N}$ and $f_i = \sum_{j=N-K+1}^{N} \sin(\theta_j - \theta_i) \leq K$. Proposition 2.12 guarantees the existence of an invariant ball for the first $N-K$ oscillators when

$$\epsilon = \frac{\gamma}{N} < \frac{|\lambda_2|^2}{2K(N-K)^{1/2}\tilde{\gamma}}, \tag{2.24}$$

or equivalently, when

$$\gamma < \sqrt{\frac{1}{2K(N-K)^{3/2}}} \cdot N|\lambda_2|. \tag{2.25}$$

The eigenvalue λ_2 depends implicitly on γ so we need a lower bound on the magnitude of λ_2 to close the argument and guarantee that (2.25) can be satisfied. Since the kernel of L is spanned by $(1, 1, 1, \ldots, 1)$, we can consider the operator $-L$ acting on the space of mean-zero vectors. For any column vector $\boldsymbol{x}$ with length of $N-K$ and $\sum_i x_i = 0$, we have, on the one hand,

$$\begin{aligned}
\boldsymbol{x}^T(-L)\boldsymbol{x} &= \frac{\gamma}{N}\sum_{i,j}\cos(\theta_i^* - \theta_j^*)x_i^2 - \frac{\gamma}{N}\sum_{i,j}\cos(\theta_i^* - \theta_j^*)x_i x_j \\
&= \frac{\gamma}{2N}\sum_{i,j}\cos(\theta_i^* - \theta_j^*)(x_i - x_j)^2 \\
&\geq \frac{\gamma}{2N}\min_{i,j}\cos(\theta_i^* - \theta_j^*)\sum_{i,j}(x_i - x_j)^2 \\
&= \frac{\gamma}{N}\min_{i,j}\cos(\theta_i^* - \theta_j^*)\left((N-K)\sum_i x_i^2 - \sum_{i,j} x_i x_j\right) \\
&= \frac{\gamma(N-K)}{N}\min_{i,j}\cos(\theta_i^* - \theta_j^*)\|\boldsymbol{x}\|^2 \\
&\geq \frac{\gamma(N-K)}{N}\sqrt{1 - \frac{\gamma_0^2}{\tilde{\gamma}^2}}\|\boldsymbol{x}\|^2,
\end{aligned}$$

where the last inequality comes from $\sin(\alpha_{min}) = \sin(\alpha_{max}) = \frac{\gamma_0^2}{\tilde{\gamma}^2}$. On the other hand,

$$\boldsymbol{x}^T(-L)\boldsymbol{x} \leq \frac{\gamma}{2N}\sum_{i,j}(x_i - x_j)^2 = \frac{\gamma(N-K)}{N}\|\boldsymbol{x}\|^2.$$

Therefore we have the inequality

$$\frac{\gamma(N-K)}{N}\sqrt{1 - \frac{\gamma_0^2}{\tilde{\gamma}^2}} \leq |\lambda_2| \leq \frac{\gamma(N-K)}{N}. \tag{2.26}$$

Combining Equations (2.25) and (2.26), we can conclude that an invariant ball for the first

$N-K$ oscillators with radius $R = \frac{|\lambda_2|N}{\gamma(N-K)}$ exists when

$$\gamma_0 = \max_{i,j=1}^{N-K} |\omega_i - \omega_j| < \tilde{\gamma}\sqrt{1 - \frac{2K}{(N-K)^{1/2}}}. \tag{2.27}$$

Therefore, we have proven the first part of Theorem 2.9. In fact, since the above argument holds regardless of the subset of oscillators we choose, we can go through every subset holding $N-K$ elements and target the one with the smallest K such that (2.27) holds. So we derive a sufficient condition: $g(K,N) \leq \gamma h(K,N)$, where functions g and h are respectively defined in (2.12) and (2.13). The existence of an invariant ball of $N-K^*$ oscillators where

$$K^* := \min_K \{K \in \mathbb{N} : g(K,N) \leq \gamma h(K,N)\} \tag{2.28}$$

is guaranteed.

Similarly as Proposition 2.12, it can be concluded that if $\|\theta(0) - \theta^*\|_S < R$, then all the oscillators in S asymptotically converges to the invariant ball $\|\theta(t) - \theta^*\|_S < r$, where $r = \frac{2\gamma K(N-K)^{1/2}}{N|\lambda_2|}$. Therefore, we have a proof for the second part of Theorem 2.9. ■

2.2.3. *Experiments*

We have performed numerical experiments using Matlab on the Kuramoto model (2.2) to illustrate our first theorem. In the first three experiments, all of the oscillator frequencies are chosen to be i.i.d. Gaussian random variables with small variance except for one, two or three whose natural frequency is chosen to be large compared with others (the free oscillators). In the last experiment, we consider a case where all oscillators have independent Cauchy distributed natural frequencies.

Example 2.13 (One free oscillator)**.** The first experiment depicts a case with $N = 20$ oscillators with coupling strength $\gamma = 1$. The frequencies $\omega_1, \omega_2, ..., \omega_{19}$ are chosen to be Gaussian random variables with mean 0 and variance $\frac{\gamma}{N}$, and the frequency ω_{20} is chosen to be $\gamma + 0.1$. One can easily check $K^* = 1$ by its definition, meaning there exists at most one free oscillator. The cluster of the phase-locked oscillators eventually moves at a common angular frequency $\bar{\omega}$. We use the change of variables $\tilde{\theta}_i(t) = \theta_i(t) - \bar{\omega}t$ for $i = 1, 2, ..., N$ to work in the frame of reference which the phase-locked cluster is expected to be stationary. With a slight abuse of notation, we rewrite $\tilde{\theta}$ as θ. The left graph in Figure 2.2 exhibits the evolvement of the phases θ_i on the real line with respect to time t under the rotation frame; the right graph represents the phase trajectories on a torus. It can be seen that there exists a large phase-locked cluster of 19 oscillators depicted by the blue curves, and a free oscillator whose phase trajectory is associated with the red curve rotating fast around the torus.

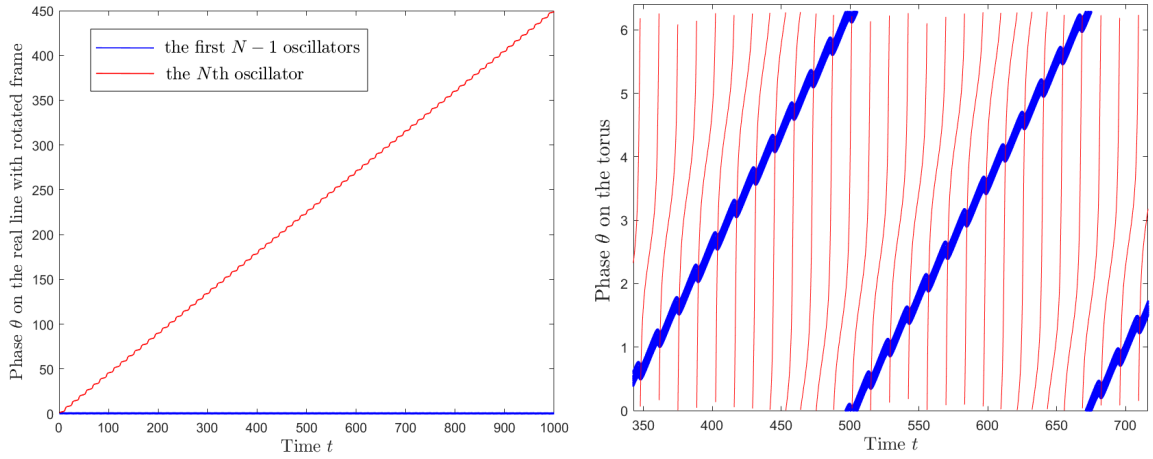

Figure 2.2: A cluster of 19 phase-locked oscillators and 1 free oscillator.

For a more clear inspection, we zoom in a small portion of the right graph of Figure 2.2 and redraw the trajectories under the rotation frame. This gives us Figure 2.3. It shows the trajectories of the phase-locked oscillators and illustrates the effect of the free oscillator on the phase-locked cluster. One can see a periodic disturbance when the free oscillator passes through the cluster, though this is not sufficient to break up the cluster.

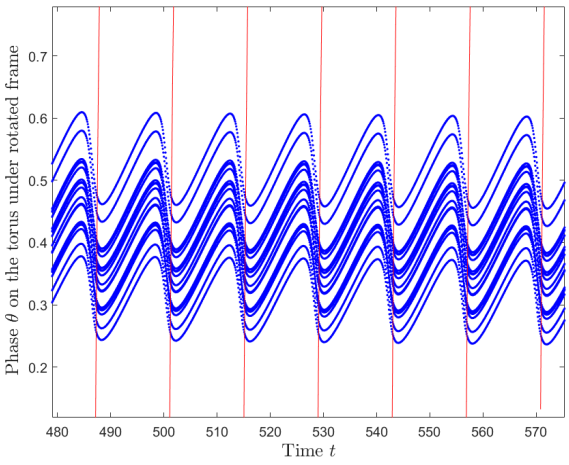

Figure 2.3: Phase trajectories on the torus under a rotated frame

The fundamental frequencies of the phase trajectory of a phase-locked oscillator ξ are expected to be related to the angular frequencies of the free oscillator $\tilde{\omega}$. In fact, we have $\tilde{\omega} = 2\pi\xi$, which can be observed from Figure 2.3. Every time a free oscillator completes a full-circle rotation, it creates a periodic disturbance when passing through the phase-locked cluster and the cluster moves forward a period. To make it more precise, we apply discrete Fourier transform on one of the blue curves and obtain Figure 2.4.

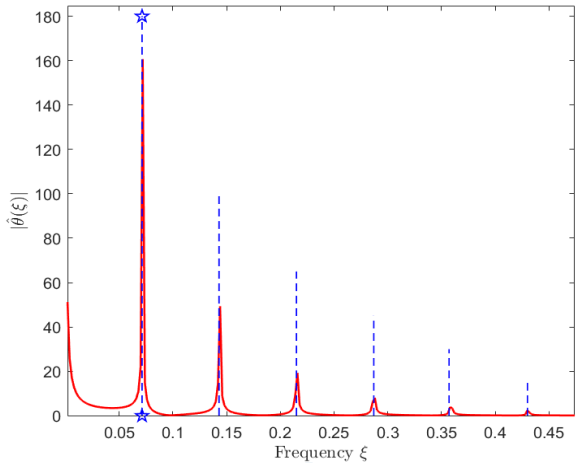

Figure 2.4: Single-sided amplitude spectrum of a locked phase trajectory

The fundamental frequency, as seen in Figure 2.4, is $\xi = 0.0714$, associated with the highest peak denoted by the blue dashed line with the star marker. Other peaks correspond to all but the first harmonic. On the other hand, the angular frequencies of the free oscillator can be computed by $\frac{\theta(T)-\theta(T/2)}{T/2}$ where $T = 1000s$ is the total running time. And the calculation gives us $\tilde{\omega}_{20} = 0.4483$. One can easily check $\tilde{\omega} = 2\pi\xi$.

Example 2.14 (Two free oscillators)**.** In this example, we still consider a system of $N = 20$ oscillators with coupling strength $\gamma = 1$. The difference is that we require two instead of one oscillator to have significantly large natural frequencies. More precisely, The frequencies $\omega_1, \omega_2, ..., \omega_{18}$ are chosen to be Gaussian random variables with mean 0 and variance $\frac{\gamma}{N}$, and the two free oscillators are chosen to have frequencies $\omega_{19} = \gamma + 0.1$ and $\omega_{20} = 1.5\gamma + 0.01$. As expected, $K^* = 2$, and as before we work in the coordinate system that rotates with the mean frequency of the cluster of 18 oscillators. The numerical results are depicted in Figure 2.5: a set of eighteen phase-locked oscillators with quasi-periodic disturbances as the two free oscillators pass through the cluster.

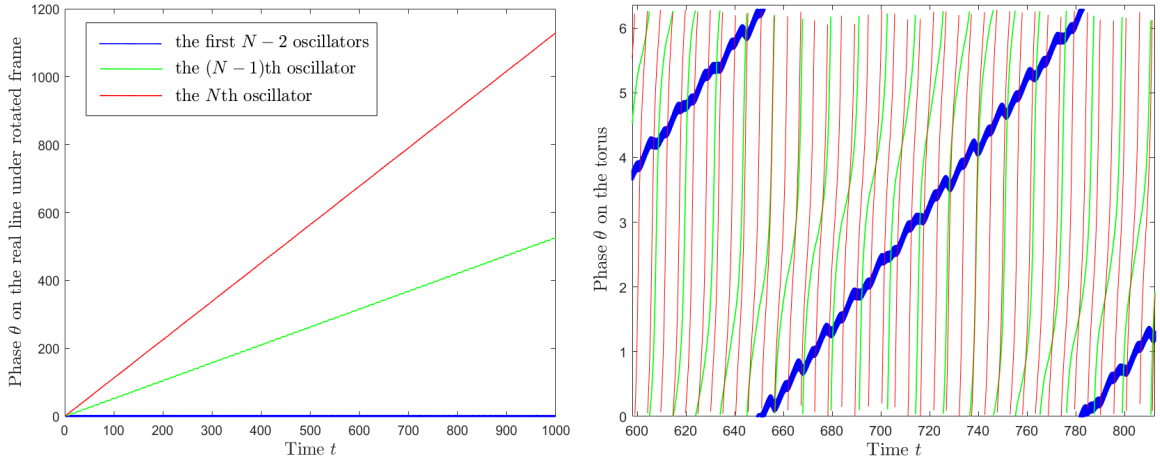

Figure 2.5: A cluster of 18 phase-locked oscillators and 2 free oscillators.

The left graph in Figure 2.5 shows the phases of the oscillators in the cluster, which appear to be quasi-periodic. The effect of the two free oscillators on the phase-locked ones can be seen from the right graph in Figure 2.5. Enlarging a portion of this graph and redrawing the trajectories under the rotation frame give Figure 2.6.

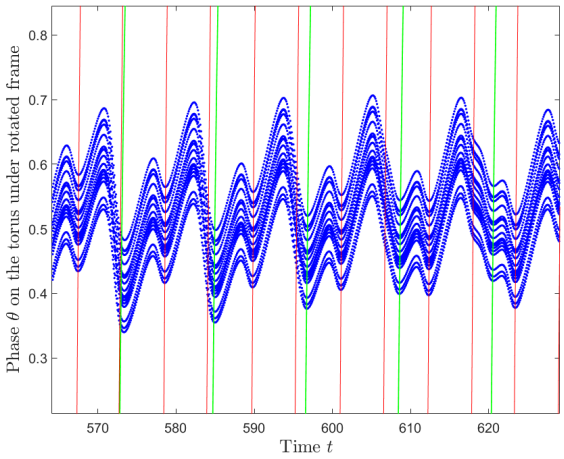

Figure 2.6: Phase trajectories on the torus under a rotated frame

Same as above, we expect a relationship between the fundamental frequencies of the phase trajectory of a phase-locked oscillator ξ and the angular frequencies of the free oscillator $\tilde{\omega}$: $\tilde{\omega} = 2\pi\xi$, Again, we apply discrete Fourier transform on one of the blue curves and obtain Figure *2.7*.

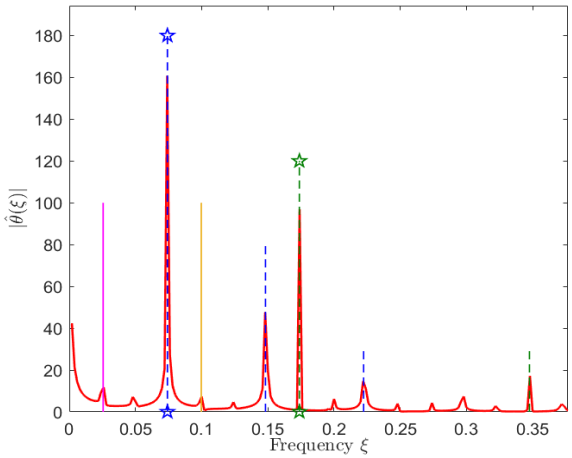

Figure 2.7: Single-sided amplitude spectrum of a locked phase trajectory

The fundamental frequencies, as seen in Figure 2.7, are $\xi_1 = 0.0741$ and $\xi_2 = 0.1738$, associated with the two highest peaks denoted by the dashed lines with the star markers. Other peaks denoted by the blue dashed lines are associated with the higher-order harmonics of the wave with the fundamental ξ_1, i.e. multiples of ξ_1; and those denoted by the green ones are the higher-order harmonics of the wave with the fundamental ξ_2, i.e. multiples of ξ_2. The remaining small peaks

are combinations of harmonics of the two waves. For instance, the pink line locates a frequency $\xi = \xi_2 - 2\xi_1$ and the yellow one a frequency $\xi = \xi_2 - \xi_1$. Moreover, the angular frequencies of the two free oscillators can be computed by $\frac{\theta(T)-\theta(T/2)}{T/2}$ where $T = 1000s$ is the total running time. And the calculation gives us $\tilde{\omega}_{19} = 0.4656$ and $\tilde{\omega}_{20} = 1.0920$. It can be easily seen that $\tilde{\omega} = 2\pi\xi$ holds.

Example 2.15 (Three free oscillators)**.** By increasing the natural frequency of one more oscillator, the system of $N = 20$ oscillators with coupling strength $\gamma = 1$ evolves into a partial phase-locked state with 3 free oscillators. The natural frequencies of such three oscillators are set to be $\omega_{18} = \gamma + 0.1$, $\omega_{19} = 1.5\gamma + 0.01$ and $\omega_{20} = 2\gamma + 0.2$. The other 17 oscillators' natural frequencies follow Gaussian distribution: $\omega_i \sim N(0, \gamma/N)$ for $i = 1, 2, ..., 17$. These 17 oscillators eventually phase lock and move at a common frequency $\bar{\omega}$. Considering phase trajectories on the real line with a rotation frame by applying a translation on the frequency: $\omega - \bar{\omega}$ gives the left graph of Figure 2.8. The phase trajectories on the torus is depicted in the right graph.

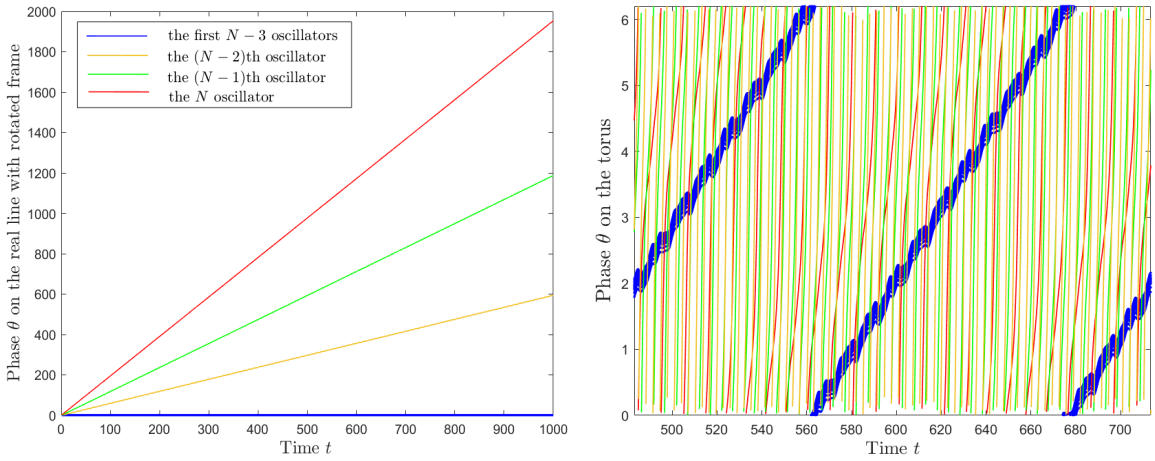

Figure 2.8: A cluster of 17 phase-locked oscillators and 3 free oscillators.

Same as the first two examples, we zoom in a small portion of the right graph of Figure 2.8 and redraw the trajectories under the rotation frame, which yields Figure 2.9.

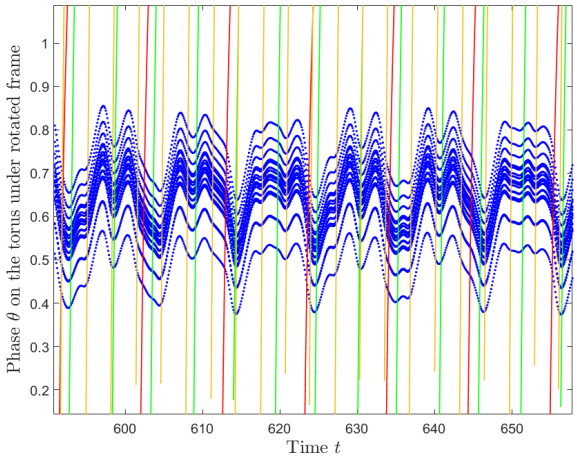

Figure 2.9: Phase trajectories on the torus under a rotated frame

The phase trajectories of the phase-locked oscillators in the cluster, depicted as blue curves in Figure 2.9, appear to be quasi-periodic. Following the same methodology, we apply discrete Fourier transform on one of the blue curves and obtain Figure 2.10.

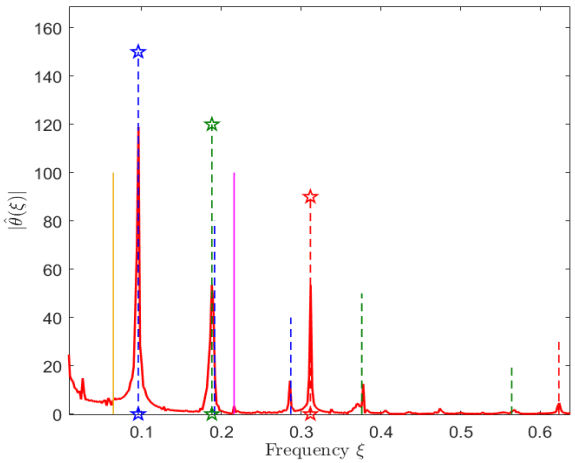

Figure 2.10: Single-sided amplitude spectrum of a locked phase trajectory

We again examine the relation between the fundamental frequencies of the phase-locked waves ξ and the angular frequencies of the three free oscillators $\tilde{\omega}$: $\tilde{\omega} = 2\pi\xi$. In fact, one can see from Figure 2.10 that $\xi_1 = 0.0957$, $\xi_2 = 0.1880$ and $\xi_3 = 0.3116$, associated with the three highest peaks denoted by the dashed lines with the star markers. And also, direct calculation gives $\tilde{\omega}_{18} = 0.6013$, $\tilde{\omega}_{19} = 1.1815$ and $\tilde{\omega}_{19} = 1.9581$. Clearly $\tilde{\omega} = 2\pi\xi$ holds in this case too. Furthermore, the blue dashed lines in the graph represent harmonics of the wave with the fundamental ξ_1; the yellow ones with the fundamental ξ_2; and the red ones with the fundamental ξ_3. The remaining small peaks are combinations of harmonics of the three waves. For instance, the peak denoted by the yellow line represents a frequency of $2\xi_2 - \xi_3$ and the one denoted by the pink line represents a frequency

of $\xi_3 - \xi_1$.

Remark 2.16. *In the previous three experiments, with one, and more than one free oscillators, the solutions appeared to be periodic and quasi-periodic respectively. It is worth noting that it would probably be quite difficult to prove the existence of a periodic or quasi-periodic solution. Even if one were able to do so, a linear stability analysis of the solution would likely be highly non-trivial. In the case of a periodic solution, the stability analysis would involve a Floquet problem; these types of problems are difficult to solve in any but the simplest of cases. The spectrum of quasi-periodic operators is even more difficult to understand: in the case of a quasi-periodic Schrödinger operator the spectrum typically lies on a Cantor set [43], rather than simple bands and gaps as in the periodic case. However, by showing the existence of a small exponentially attracting ball we can answer the same physical question in a much easier way.*

Example 2.17 (Cauchy distributed oscillators)**.** The first three numerical experiments were instructive but obviously somewhat contrived in that we picked one, two or three of the oscillators frequencies by hand to ensure that we had some free oscillators.

In this experiment, we take $N = 500$ oscillators with coupling strength $\gamma = 5$. The frequencies $\omega_1, \omega_2, ..., \omega_{500}$ were chosen to be standard Cauchy random variables with constant scale 0.01, i.e., $\omega_i \sim 0.01 \cdot Cauchy(0, 1)$. Since Cauchy random variables have broad tails, we expect large outliers to be relatively common (as compared with, for instance, a Gaussian distribution). In the experiment depicted here, $\omega_{\max} - \omega_{\min} = 7.2161 > \gamma = 5$, so the condition for full phase-locking is not satisfied. However, partial phase-locking is guaranteed if there exists some integer K such that $g(K) < \gamma h(K)$.

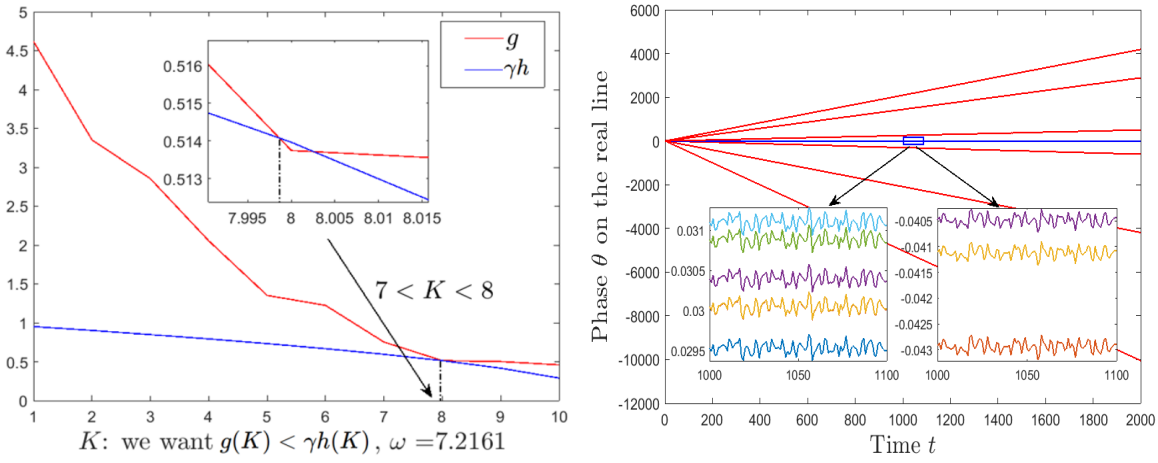

Figure 2.11: Partially phase-locked oscillators with Cauchy distributed frequencies.

The graphs of functions $g(K, N)$ and $\gamma h(K, N)$ with respect to K are drawn in the left graph of Figure 2.11. From it, it is clear to see $K^* = 7$, and thus, we are guaranteed the existence of a phase-locked cluster of at least $N - 7 = 493$ oscillators. The theorem does not say much about the basin of attraction, except to guarantee that it has a radius of at least $O(1)$. The right graph

in Figure 2.11 displays the evolution of the oscillator phases θ_i with respect to time t. The red curves represent the trajectories of 494 phase-locked oscillators while the blue curves represent 6 free oscillators. This example shows that $N - K^*$ is a strict lower bound of the size of the phase-locked cluster.

2.3. Almost sure Entrainment

2.3.1. *Main Result*

Our goal in this section is to understand the probability of partial entrainment in the Kuramoto model with randomly distributed frequencies, particularly in the large N limit. The results in the previous section used a relatively strong definition of partial phase-locking, in that we required a subset of oscillators to remain close to an equilibrium configuration. This resulted in fairly strong control on $\|\theta - \theta^*\|_S$; however, while it allowed a large number of non-phase-locked oscillators, the percentage as a fraction of the total number had to remain small. In considering the limit $N \to \infty$, one would really like to allow the possibility that a fixed percentage of the oscillators, possibly small but independent of N, would fail to phase lock. To this end, we utilize a pretty result of De Smet and Aeyels [16] that guarantees that a subset of oscillators remains close to one another, while not necessarily being close to any fixed configuration: partial entrainment.

Theorem 2.18 (Aeyels-DeSmet)**.** *For the finite-N Kuramoto model (2.2), if*

$$\min_{S\subset\Omega,|S|=N-K} \max_{i,j\in S} |\omega_i - \omega_j| < \gamma\sqrt{\frac{N}{N-K}}\left(\frac{2N-4K}{3N}\right)^{\frac{3}{2}}, \tag{2.29}$$

then there exists a subset $S \subset \{1, ..., N\}$ with $|S| = N - K$ such that there is an invariant region:

$$\exists c > 0 \ s.t. \ |\theta_i(t) - \theta_j(t)| < c, \ \forall t \geq 0, \ \forall i, j \in S,$$

i.e., the Equation (2.2) achieves partial entrainment for at least $N - K$ oscillators.

Remark 2.19. *The above result is very strong, in the sense that it establishes entrainment when a positive fraction of the oscillators is free. This is what one would expect from experiments, applications, and the original physical arguments of Kuramoto. On the other hand, it does not give very much information about the dynamics. While the angles of the entrained subset of oscillators are guaranteed to remain close to one another, there can in principle be $O(1)$ changes in the relative positions of the oscillators, and thus, the order parameter is not guaranteed to be constant. One expects that, on average, the free oscillators will not contribute to the order parameter (though there is no proof of that) but even defining a "reduced" order parameter based only on the entrained oscillators. The most that one can say is that the order parameter is bounded from above and below.*

If we denote the right-hand side of Inequality (2.29) as $\tilde{h}(K, N)$ and let $\rho = \frac{K}{N}$ represent the

density of unlocked oscillators, then it is clear that in this new variable ρ that

$$g(\rho) = \min_{S\subset\Omega, \frac{|S|}{N}=1-\rho} \max_{i,j\in S} |\omega_i - \omega_j|, \tag{2.30}$$

$$\tilde{h}(\rho) = \sqrt{\frac{1}{1-\rho}} \left(\frac{2-4\rho}{3}\right)^{\frac{3}{2}}. \tag{2.31}$$

In terms of ρ, the inequality (2.29) becomes $g(\rho) < \gamma\tilde{h}(\rho)$. Note the function $\tilde{h}(\rho)$ is only well-defined when $\rho \leq \rho_{max} = \frac{1}{2}$, which suggests that at most half of the oscillators can be phase-locked. By considering the large N limit of the Kuramoto model, we obtain our second main result as follows.

Theorem 2.20. *Consider the Kuramoto model (2.2) where the natural frequencies $\{\omega_i\}_{i=1}^N$ are chosen independently and identically distributed from a distribution with the following properties:*

- *The distribution has a density $f(x)$ that is symmetric and unimodal with support on the whole line – the density is increasing on $\mathbb{R}^-$ and decreasing on $\mathbb{R}^+$.*
- *The maximum of the density occurs at $\omega = 0$.*

Define the function $g_\infty(\rho)$ implicitly by

$$\int_{-\frac{g_\infty}{2}}^{\frac{g_\infty}{2}} f(x)dx = 1-\rho, \tag{2.32}$$

and the function $\tilde{h}(\rho)$ by

$$\tilde{h}(\rho) = \sqrt{\frac{1}{1-\rho}} \left(\frac{2-4\rho}{3}\right)^{\frac{3}{2}}.$$

Let γ^* be the smallest value of γ such that there exists a solution to

$$g_\infty(\rho) = \gamma\tilde{h}(\rho), \qquad \rho \in (0, \frac{1}{2}]. \tag{2.33}$$

Then γ^* is a threshold coupling strength for partial entrainment in the following sense: let $\mathbb{P}_{N,\gamma}$ denote the probability that the Kuramoto model admits a partially entrained state with $O(N)$ oscillators. Then

$$\lim_{N\to\infty} \mathbb{P}_{N,\gamma} = 1, \qquad \forall\gamma > \gamma^*.$$

Moreover we have bounds on the size of the largest partially entrained cluster: if $N_{cluster}$ denotes the number of the oscillators belonging to the largest partially entrained cluster then

$$1 - \rho_{min} \leq \frac{N_{cluster}}{N} \leq \int_{-\gamma}^{\gamma} f(\omega)d\omega.$$

Here, ρ_{min} is defined as the smallest ρ-coordinate of the intersection points of $g_\infty(\rho)$ and $\gamma\tilde{h}(\rho)$. The inequality holds in the sense that

$$\lim_{N\to\infty} \mathbb{P}(N_{cluster} \geq (1-\rho_{min})N - O(N^{\frac{1}{2}+\epsilon})) = 1, \tag{2.34}$$

$$\lim_{N\to\infty} \mathbb{P}(N_{cluster} \leq N\int_{-\gamma}^{\gamma} f(\omega)d\omega + O(N^{\frac{1}{2}+\epsilon})) = 1. \tag{2.35}$$

Remark 2.21. *This is, of course, a sufficient condition for partial phase-locking and not a necessary one. Based on what is known about the continuous Kuramoto model and the physical arguments on the finite-N Kuramoto model, one expects (and the numerics to be presented later to support this) that partial entrainment occurs for much smaller values of γ than are required by the theorem.*

As far as the hypotheses go, the second condition – that the maximum of the density of the distribution occurs at $\omega = 0$ – can be assumed w.l.o.g. by working in a co-rotating frame. In the first condition, the assumption of symmetry is not really required and was adopted mostly for ease of exposition, but the assumption that the density is unimodal enters into the proof in a more substantial way. The difference between unimodality and multimodality is essential, for instance, they have distinct supercritical bifurcation behaviours [44].

By the definition of g_∞, it is clear that $g_\infty = 2F^{-1}(1-\frac{\rho}{2})$. Under the assumptions of symmetry and unimodality, it is easy to verify that both $g_\infty(\rho)$ and $\tilde{h}(\rho)$ are decreasing functions with positive second derivatives. In fact, if one can show $(g_\infty - \tilde{h})(\rho)$ is a convex function when $\rho \leq \frac{1}{2}$, then it follows that these functions can be equal, i.e., $g_\infty(\rho) = \tilde{h}(\rho)$, at no more than two distinct values of ρ, which implies in the continuum limit the range of possible entrained cluster sizes is an interval. Plus, as the coupling strength γ increases, ρ_{min} decreases until the first intersection point vanishes, which implies that partial synchronization becomes full synchronization. For instance, when the natural frequencies ω_i follow a standard Gaussian distribution, the graph of the functions g_∞ and $\gamma\tilde{h}$ is shown as below.

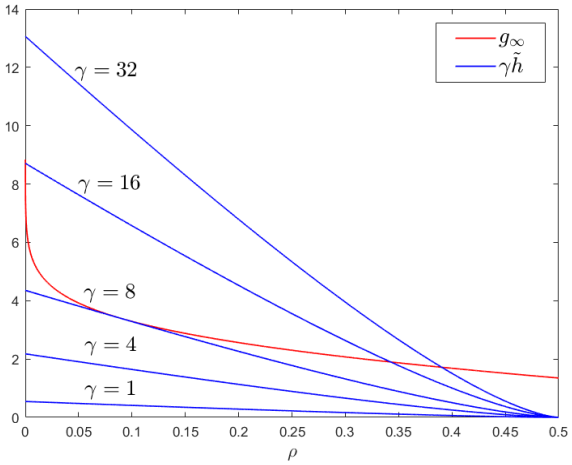

Figure 2.12: Intersections of g_∞ and $\gamma\tilde{h}$ for Gaussian distribution.

2.3.2. *Proof of Main Result*

To prove Theorem 2.20, one should first prove that under the assumptions of the distribution of ω_i, in the limit $N \to \infty$ the function $g(\rho)$ tends to a deterministic function $g_\infty(\rho)$, which is Proposition 2.22 stated below. The equation (2.34) in Theorem 2.20 then follows directly.

Proposition 2.22. *Suppose that the natural frequencies $\{\omega_i\}_{i=1}^N$ satisfy the assumptions in Theorem 2.20, $f(x)$ is its probability density function and $F(x)$ is its cumulative distribution function. Then, with high probability, $g(K,N)$ converges to a deterministic function $g_\infty(\rho)$ defined by the Equation (2.32). More precisely, we have the estimate*

$$\lim_{N\to\infty} \mathbb{P}(|g(K,N) - g_\infty(\frac{K}{N})| \leq N^{-\frac{1}{2}+\epsilon}) = 1. \tag{2.36}$$

Proof (Sketch of proof). Define $a = F^{-1}(1-\frac{\rho}{2})$ so that we have $g_\infty = 2a$. First, using the law of large number theorem, one can easily show $g(\rho) \leq 2a$ with probability one. What is less obvious to show is that $g(\rho) \geq 2(a-\delta)$ with probability one where $\delta = \frac{1}{2}N^{-\frac{1}{2}+\epsilon}$ and $\epsilon > 0$. In other words, we need to prove

$$\mathbb{P}(A) \to 0 \text{ as } N \to \infty, \tag{2.37}$$

where A is the event that "there exists an interval with length $L = 2(a-\delta)$ containing more than $(1-\rho)N$ points". Notice that if no intervals of Length L with ω_k at an endpoint contain more than m points then no any other interval does. So it is only necessary to focus on N intervals $\{[\omega_i, \omega_i + L] : i = 1, 2, ..., N\}$. Moreover, the interval centered at zero maximizes the probability that a point lies in the interval, i.e., $I = [-L/2, L/2]$ gives the largest $\mathbb{P}(x \in I)$ among all intervals of length L. Based on these observations, it is not hard to see

$$\mathbb{P}(A) \leq N \sum_{M=(1-\rho)N}^{N} \binom{N}{M} p^M (1-p)^{N-M}, \tag{2.38}$$

where $1-\rho = \int_{-a}^{a} f(x)dx$ and $p = \int_{-L/2}^{L/2} f(x)dx = \int_{-a+\delta}^{a-\delta} f(x)dx$. Using the Stirling approximation, one can prove that the right-hand side of the inequality (2.38) approaches zero as N approaches infinity. So we are done. This is the main idea of our proof. The full proof can be found in Appendix A.2. ■

Proposition 2.22 suggests Equation (2.34), a probabilistic lower bound on the number of oscillators in a partially entrained cluster. On the other hand, the probabilistic upper bound, given by Equation (2.35) in Theorem 2.20, is implied by the central limit theorem. We formalize it in the following proposition.

Proposition 2.23. *Consider the finite N Kuramoto model (2.2) where the frequencies ω_i are independent and identically distributed according to a distribution with a density $f(\omega)$ that is symmetric*

and monomodal, with the unique maximum of f occuring at $\omega = 0$. Then the probability that there is any partially entrained cluster containing more than

$$N \int_{-\gamma}^{\gamma} f(\omega) d\omega + O(N^{\frac{1}{2}+\epsilon})$$

tends to zero as $N \to \infty$.

Proof (Sketch of proof). The proof of this is straightforward and similar to previous arguments, so we just give the broad strokes. The basic observation is that from the usual ℓ_1/ℓ_∞ estimate we have that a subset of oscillators cannot be partially entrained if

$$\omega_{max} - \omega_{min} \geq 2\gamma.$$

By the usual central limit theorem arguments, the number of ω_i lying in an interval I is, for N large, approximately $\int_I f(\omega)$. Since f is symmetric and monomodal the interval of length $|I| = 2\gamma$ which maximizes $\int_I f(\omega)$ is the symmetric one, so the largest cluster will, with high probability, have no more than $\int_{-\gamma}^{\gamma} f(\omega) d\omega$. ■

Remark 2.24. *It is worth comparing this with the minimum cluster size guaranteed by Theorem 2.20. The condition $g_\infty(\rho) \leq \gamma \tilde{h}(\rho)$ defines the largest guaranteed cluster size $1 - \rho^*$ as a somewhat complicated implicit function of the coupling strength γ, but this simplifies greatly in the limit of large coupling strength γ. In the limit $\gamma \gg 1$ we have that $\rho \ll 1$ and the partial synchronization condition becomes $g_\infty(\rho) \leq \gamma \tilde{h}(0) = \gamma (2/3)^{\frac{3}{2}}$. Thus the theorem guarantees a partially locked cluster of size at least*

$$\approx \int_{-(\frac{2}{3})^{\frac{3}{2}}\frac{\gamma}{2}}^{(\frac{2}{3})^{\frac{3}{2}}\frac{\gamma}{2}} f(\omega) d\omega$$

for large γ.

2.3.3. *Experiments*

In this section, we provide two numerical experiments to support Theorem 2.20. In the first example, we consider oscillators with Gaussian distributed natural frequencies. In the second example, we consider oscillators whose natural frequencies follow a Cauchy distribution.

Example 2.25. For the case of Gaussian distributed natural frequencies ω_i, the function $g_\infty(\rho)$ is the inverse function of the error function:

$$g_\infty(\rho) = 2\sqrt{2}\,\mathrm{erf}^{-1}(1 - \rho).$$

Numerical calculations show that, in the thermodynamic limit, the minimum coupling strength to guarantee the existence of partially entrained states is $\gamma^* \approx 8.0027\sigma$, where σ is the variance

of the Gaussian distribution (it is clear from scaling that the critical coupling strength should be proportional to the variance). For this critical value of γ, we have $g_\infty(\rho) = \gamma^* \tilde{h}(\rho)$ at $\rho \approx .0901$. Thus, for Gaussian distributed frequencies, Theorem 2.20 guarantees the birth of a partially entrained cluster containing all but about 9.01% of the oscillators.

Plus, to verify Proposition 2.22, we consider $N = 10000$ oscillators with coupling strength $\gamma = 10$ and suppose the natural frequencies follow a standard Gaussian distribution $\mathcal{N}(0, 1)$. Then we should have $g \approx g_\infty \pm 0.01$. The graphs of g and g_∞ shown in Figure 2.13 have verified this.

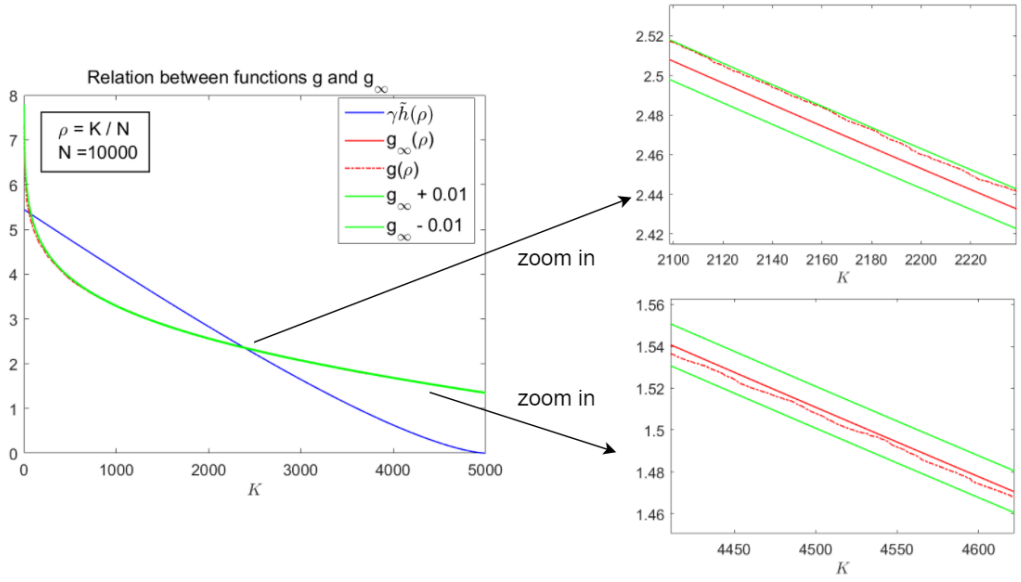

Figure 2.13: A comparison between functions g and g_∞ for Gaussian distribution

Example 2.26. For the case of Cauchy distributed natural frequencies ω_i, their CDF and PDF are as follows:

$$f(x; k, \lambda) = \frac{1}{k\pi(1 + (\frac{x-\lambda}{k})^2)}, \tag{2.39}$$

$$F(x; k, \lambda) = \frac{1}{\pi} \arctan(\frac{x - \lambda}{k}) + \frac{1}{2}, \tag{2.40}$$

where k is the scale parameter and λ is the location parameter specifying the location of the peak of the distribution. We consider the case where $\lambda = 0$. the function $g_\infty(\rho)$ is the inverse function of the error function:

$$g_\infty(\rho) = 2 \tan(\frac{\pi}{2}(1 - \rho)).$$

Numerical calculations show that, in the thermodynamic limit, the minimum coupling to guarantee the existence of partially entrained states is $\gamma^* \approx 21.4950k$ (it is clear from scaling that the critical coupling strength should be proportional to the scale parameter). For this critical value of γ we have $g_\infty(\rho) = \gamma^* \tilde{h}(\rho)$ at $\rho \approx .2258$. Thus, for Cauchy distributed frequencies, Theorem 2.20 guarantees the birth of a partially entrained cluster containing all but about 22.58% of the oscillators.

Similarly as before, to verify Proposition 2.22, we consider $N = 10000$ oscillators with coupling strength $\gamma = 50$ and suppose the natural frequencies follow a Cauchy distribution with $k = 1$ and $\lambda = 0$. Then we should have $g \approx g_\infty \pm 0.01$. The graphs of g and g_∞ are shown below:

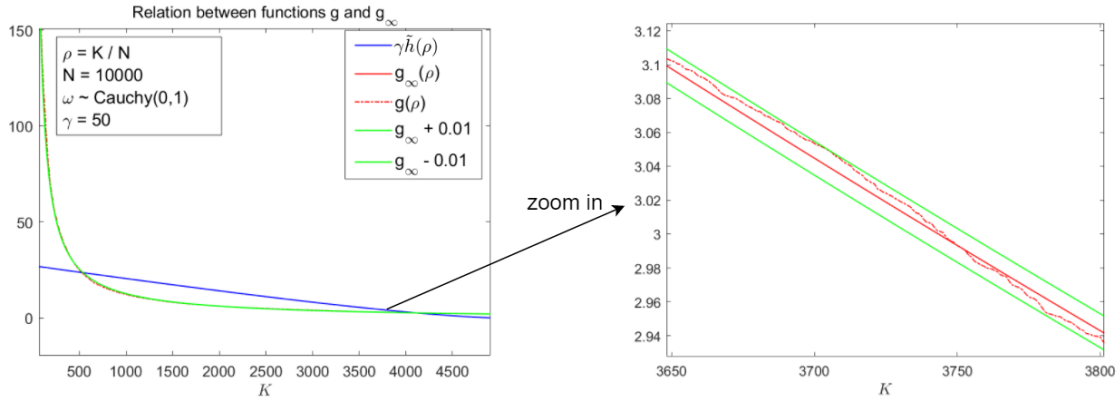

Figure 2.14: A comparison between functions g and g_∞ for Cauchy distribution

Now, we do a simulation to verify Theorem 2.20, our second main result about partial synchronization for the oscillators with Cauchy distributed natural frequencies.

Fix $k = 1$, $N = 500$, $\omega_1 = 0$ and $\omega_i \sim f(x; 1, 0)$ for $i = 2, ..., N$, then direct calculation gives $\gamma^* = 21.4950$. Define $\Phi_{1i} = \theta_i(\frac{T}{2}) - \theta_1(\frac{T}{2})$, $\Phi_{2i} = \theta_i(T) - \theta_1(T)$ and $\Psi_i = (\Phi_{2i} - \Phi_{1i}) \times \frac{2}{T}$. Then we have

$$\Psi_i \to \omega_{i\infty} - \omega_{1\infty} \text{ as } T \to \infty, \tag{2.41}$$

and thus, Ψ_i approaches zero if θ_i is locked with θ_1. Now, define a relative frequency difference: $d = 10^{-5} \times (\max_i(\Psi_i) - \min_i(\Psi_i))$, where 10^{-5} is a custom scale we choose to classify phase-locked oscillators. If $\Psi_i \leq d$, we regard θ_i as the oscillator that locks with θ_1. To see the effect of γ on the partial entrainment, we vary γ from 1 to 25, and for each γ, use 5 samples of ω_i to solve Equation (2.2) numerically up to time $T = 500$ with a time step $dt = 0.1$. Then we compute the average number of oscillators in the largest cluster with frequency difference less than d, i.e, $\Psi_i \leq d$, over the 5 simulations. The histogram graphs of the amount of oscillators corresponding to $\gamma = 5$ and $\gamma = 25$ are drawn separately in Figure 2.15, where the x-axis is the frequency difference Ψ_i and the y-axis is the average number of oscillators satisfying $\Psi_i \in (x - \frac{d}{2}, x + \frac{d}{2})$. The graphs show, as we expected, the size of the largest cluster of phase-entrained oscillators is larger for $\gamma = 25$ than which of $\gamma = 5$.

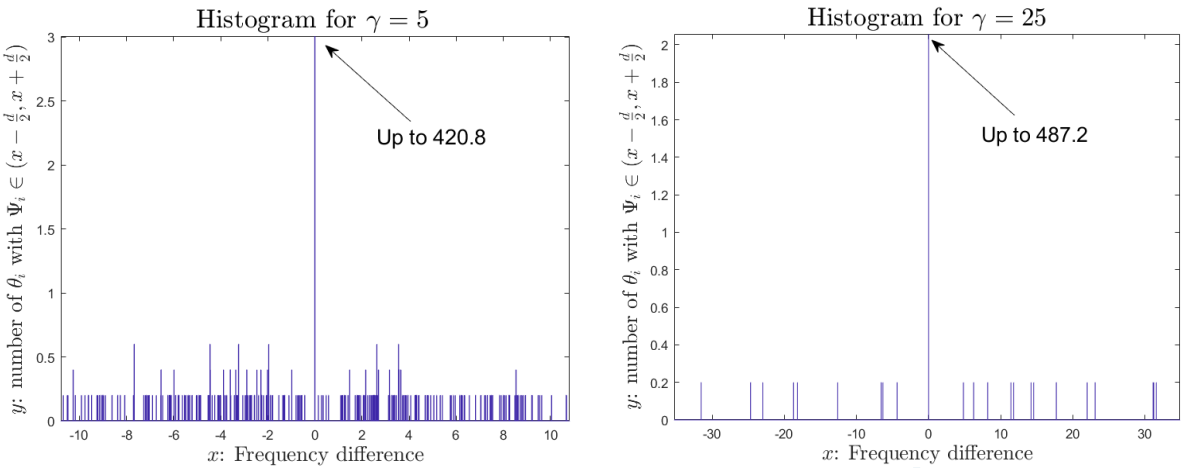

(a): $\gamma = 5$ (b): $\gamma = 25$

Figure 2.15: Histogram graphs of average number of phase-entrained oscillators

To make our argument more clear, we will define three parameters P_{numeric}, P_{lower} and P_{upper} and make a careful comparison among them.

First, let P_{numeric} denote the average percentage of oscillators in the largest phase-entrained cluster over the 5 simulations. For instance, the right graph in Figure 2.15 shows that $P_{\text{numeric}} = \frac{487.2}{500} \approx 97\%$ when $\gamma = 25$.

Second, notice that if we have

$$|\omega_i - \omega_j| > 2\gamma \geq \frac{2\gamma}{N} |\sum_{j=1}^{N} \sin(\theta_j - \theta_i)|, \tag{2.42}$$

then the ith oscillator and jth oscillator will never synchronize. Thus, by the law of large number, the percentage of oscillators that lock together must be less than $\int_{-\gamma}^{\gamma} f(x;1,0)dx$. Let P_{upper} denote this percentage, i.e., $P_{\text{upper}} = \int_{-\gamma}^{\gamma} f(x;1,0)dx$.

Finally, according to Theorem 2.20, we know that as $\gamma > \gamma^* = 21.4950$, there are at least $n = (1 - \rho_{\min}) \times N$ oscillators locking together, where $\rho_{\min}$ is defined as the ρ-coordinate of the first intersection point of g_∞ and $\gamma\tilde{h}$. Let P_{lower} denote the percentage of oscillators in the largest phase-entrained cluster derived from this theorem, i.e., $P_{\text{lower}} = 1 - \rho_{\min}$.

Obviously, we have the following inequality

$$P_{\text{lower}} \leq P_{\text{numeric}} \leq P_{\text{upper}}. \tag{2.43}$$

To check Inequality (2.43), we consider $\gamma = 16, 17, ..., 30$ and draw the graphs of $P_{\text{numeric}}, P_{\text{upper}}$ and P_{lower} corresponding to each γ as below. Note that when $\gamma < \gamma^* = 21.4950$, functions g_∞ and $\gamma\tilde{h}$ have no intersections, so our theorem cannot guarantee any cluster of phase-entrained oscillators.

Therefore, $P_{\text{lower}} = 0$ when $\gamma < \gamma^* = 21.4950$, as seen in Figure 2.16.

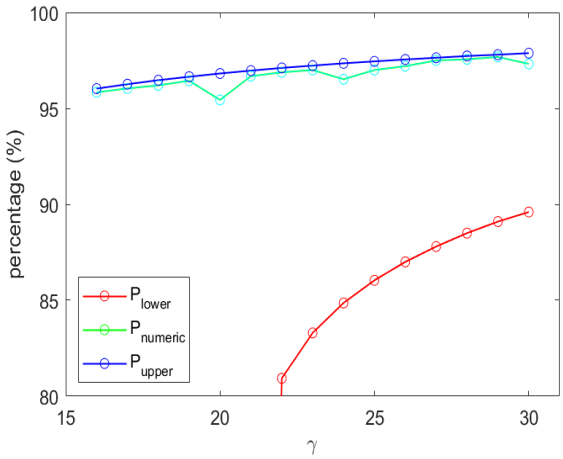

Figure 2.16: A comparison among P_{numeric}, P_{lower} and P_{upper} for Cauchy distribution

Moreover, we consider the asymptotic value of the percentage of locked oscillators for large coupling strength γ. Note that as γ grows large, $\rho_{\min}$ tends to approach zero, and thus, $\tilde{h}(\rho)$ approaches $(\frac{2}{3})^{\frac{3}{2}}$. From Equation (2.33), we have

$$g_\infty(\rho) \to (\frac{2}{3})^{\frac{3}{2}}\gamma \approx 0.544\gamma \text{ as } \rho \to 0.$$

Using the definition of g_∞ as given by (2.32), it is easy to compute that $\rho_{\min} = 2\int_{(\frac{2}{3})^{\frac{3}{2}}\frac{\gamma}{2}}^{\infty} f(x)dx \approx 2\int_{0.272\gamma}^{\infty} f(x)dx$. Thus, when γ is large,

$$P_{\text{lower}} \sim 1 - 2\int_{0.272\gamma}^{\infty} f(x)dx. \tag{2.44}$$

Denote the right-hand side as $P_{\text{lower asym}}$, i.e., $P_{\text{lower asym}} = 1 - 2\int_{0.272\gamma}^{\infty} f(x)dx$. Then for Cauchy distribution, $(1 - P_{\text{lower asym}}) \sim \frac{1}{\gamma}$, i.e., the percentage of unlocked oscillators is inversely proportional to the coupling strength when the strength is large. On the other hand, for P_{upper}, by its definition, we have for any $\gamma > 0$,

$$P_{\text{upper}} = 1 - 2\int_{\gamma}^{\infty} f(x)dx. \tag{2.45}$$

From (2.44) and (2.45), it is easy to see that as γ grows large, P_{lower} tends to approach P_{upper}. We make the comparison by considering γ=1000, 2000, 3000, ..., 10000 in the following graph:

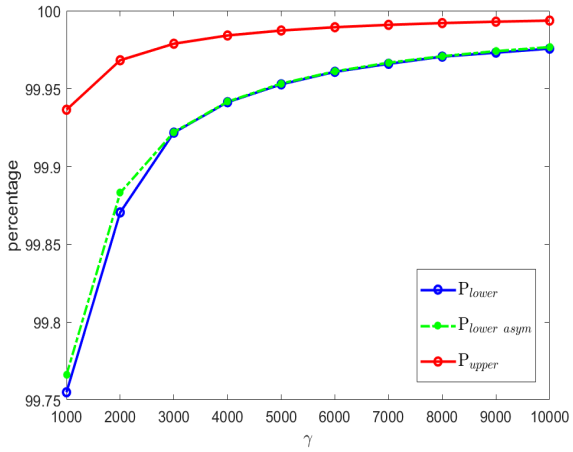

Figure 2.17: A comparison between P_{lower} and P_{upper} for Cauchy distribution

Eventually, we quantify a useful measure of coherence, the order parameter r, defined as

$$r(t) = \left| \frac{1}{N} \sum_{j=1}^{N} e^{i\theta_j(t)} \right|, \tag{2.46}$$

with respect to $\gamma = \gamma^*/2, \gamma^*, 2\gamma^*$ separately. Not surprisingly, $r(t)$ gets closer to 1 with faster convergence rate for larger coupling strength γ. See Figure 2.18 below.

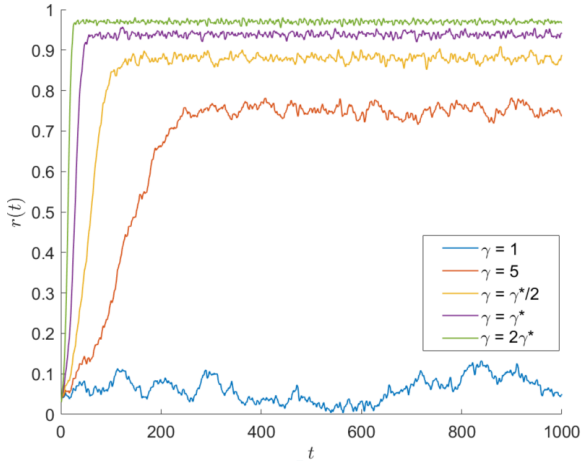

Figure 2.18: Order parameter $r(t)$ for different coupling strengths

2.4. Conclusion

In this chapter, we derive an explicit expression of a sufficient condition on the coupling strength γ to achieve partial phase-locking in the classical finite-N Kuramoto model (2.2) with an arbitrary distribution on the oscillators' natural frequencies. Compared with a recent report on the full

phase-locking given by F.Dörfler and F.Bullo [21], this is a more generalized result encompassing a wide range of patterns from zero to $O(N^{\frac{1}{2}})$ free oscillators. Interestingly, we realize that oscillators with singular natural frequencies, regardless of how large, present little effect on the behavior of the cluster of phase-locked oscillators, and if such cluster exists, there is only one big group with all but at most K oscillators. Mean-field calculations suggest that phase-locking should occur when $K \propto \tau N$ for τ small enough. The present approach, in the setting of a strong definition of partial phase-locking where we require a subset of oscillators to remain close to an equilibrium configuration, is sufficient to prove phase-locking when $K = O(N^{\frac{1}{2}})$. If weakening the requirement to only partial entrainment, where a subset of oscillators remains close to one another while not necessarily being close to any fixed configuration, then we will have more free oscillators. De Smet and Aeyels [16] actually considered the scenario where $O(N)$ free oscillators exist. In the large N limit, using their sufficient condition on the partial synchronization for a finite-N system, we show that this condition can be reduced to a deterministic one giving almost sure existence of a partially entrained state.

The underlying graph of the Kuramoto model we consider in this chapter is a complete graph. An all-to-all topology like so is simple and elegant, thus enabling abundant past research. As the exploration has matured, the fixed points (also known as steady states), as well as their stability in the dynamical system with a complete underlying structure, are well-understood. However in practice, the real systems could be sparse or asymmetric or both. With a lack of desirable properties on the graph topology itself, it is not only analytically but also numerically harder to investigate the fixed points in these systems, especially when the system grows in size. In the next chapter, we will discuss two types of more generalized graphs: one with symmetry but not fully connected and one with few symmetry but involves a large population of objects. A separate method will be proposed per graph to examine the fixed points in the context of a specific social network in its respective graph configuration. We hope these methods shed some light on the study of dynamical systems with general underlying topologies.

Chapter 3

Analysis on Social Dynamics

3.1. Background

Studies on the social network defined as a system consisting of a finite set or sets of actors and the relation or relations among them [45] can be dated back to mid-twentieth. Here, actors refer to social entities such as discrete individuals, corporations, or collective social units. Opinion dynamics, as one of the processes studied, play a crucial role to understand human interactions in our society. For instance, Parsegov *et al.* [46] proposed a novel multidimensional model describing the evolution of agents' opinions on several interdependent topics. They provided rigorous examination on the stability properties of their model including the convergence of the agents' opinions. Das *et al.* [47] considered a problem of modeling how people update opinions based on their neighbors' opinions. They established an analytical model for opinion formation and informational influence based on carefully designed online experiments, and explored the effect of the size of the neighborhood as well as stubborn nodes on the convergence of opinions. Quattrociocchi *et al.* [48] focused on how different sizes and interaction patterns of the information system may affect the opinions' distribution. In particular, they investigated the effect of media communication patterns and showed that plurality and competition within information sources lead to stable configurations where multiple distant cultures coexist. For more references see [49–53].

Among all concepts of social network analysis, one of the most important branches is the balance theory. The idea of it was first brought up by Heider [54] in his study on attitudes and cognitive organizations, where he stated that a stable social network requires every triad (a subset of three actors) has even number of negative relation affects. In essence, these networks are ones that satisfy the aphorism "enemy of my enemy is my friend". People call such a structure a balanced state. More precisely, a network is balanced, if, when two people like each other (a positive relation in the network), then they are consistent in their evaluation of all other people, and when they dislike each other (a negative relation in the network), then they disagree in the evaluation of all other people. Recently, Agbanusi and Bronski [55] proposed a model for the co-evolution of opinions and positions in a social network in order to understand the dynamics and emergence of balance. In their paper, the underlying topology considered is a complete graph. This chapter aims to extend their result to other interesting graphs such as the Petersen graph and the Erdös-Rényi graph.

First, we define their model explicitly. Consider a simple undirected graph Γ with N vertices

and $|E|$ edges, where E is the edge set, i.e.,

$$E = \{(v_i, v_j) : i < j \text{ and } v_i, v_j \text{ are two vertices in the graph}\}. \tag{3.1}$$

Each node represents an actor and each edge represents the relation between a pair of actors. There are two types of variables in the model:

- Position $x_i(t)$ is associated with vertex v_i in the graph and represents the position actor i on some issue. The larger the size of a vertex, the stronger position where an actor stands, i.e., the larger x_i is. Besides, a solid vertex represents a positive position while a hollow one negative position.
- Opinion $\gamma_{ij}(t)$ is associated with an edge in the graph and represents the degree of friendliness between actor i and actor j, with $\gamma_{ij}(t) > 0$, associated with a solid edge, representing friendliness; and $\gamma_{ij}(t) < 0$, associated with a dashed edge, antagonism.

Let $\boldsymbol{x}$ denote the vector of the actors' positions and $\boldsymbol{\gamma}$ the (lexicographically ordered) inter-actor opinions. Define a Dirichlet energy as

$$D(\boldsymbol{x}, \boldsymbol{\gamma}) = \sum_{(i,j)\in E} \gamma_{ij}(x_i - x_j)^2, \tag{3.2}$$

which represents the total amount of disharmony in the system. The goal is to target the state with the minimum energy under some constraints and analyze its stability. So examining the gradient flow in the configuration space is a necessity. This problem is equivalent to understanding the dynamics of constricted and interacted oscillators. Compared with the Kuramoto model studied in Chapter 2, we use the position x to represent oscillators in our current model instead of the phase configuration represented by angle θ. Additionally, each pair of nodes' positions interact via a linear function while the coupling strength γ is a variable dependent on the positions themselves. In consideration of reality, it is natural to assume the following constraints on this dynamic:

$$g_1 := \frac{1}{|E|} \sum_{(i,j)\in E} \gamma_{ij} = Q > 0, \tag{3.3}$$

$$g_2 := \frac{1}{|E|} \sum_{(i,j)\in E} \gamma_{ij}^2 = P > 0, \tag{3.4}$$

$$g_3 := \sum_{i=1}^{N} x_i^2 = R > 0, \tag{3.5}$$

where P, Q and R are positive constants.

- The first constraint (3.3) requires the mean of the opinions to be positive. This can be interpreted as a societal pressure toward civil discourse: while some people may hold negative opinions of others, the average opinion must be positive.

- The second constraint (3.4) excludes extreme personal opinion. The Cauchy-Schwarz inequality implies that $P - Q^2 \geq 0$. The quantity $\nu^2 := P - Q^2$ defines the opinion variance and represents some socially acceptable range of opinions.
- The third constraint (3.5) excludes extreme personal position. We will assume, w.l.o.g., $R = 1$ throughout this chapter. Otherwise, just rescale x_i for all i.

Following the method of Lagrange multipliers, the constrained free energy is given by

$$\mathscr{D} := \sum_{(i,j)\in E} \gamma_{ij}(x_i - x_j)^2 - \frac{\mu}{|E|} \sum_{(i,j)\in E} \gamma_{ij} - \frac{\tau}{|E|} \sum_{(i,j)\in E} \gamma_{ij}^2 - \lambda \sum_{i=1}^{N} x_i^2 \tag{3.6}$$

$$= D - \mu g_1 - \tau g_2 - \lambda g_3, \tag{3.7}$$

where μ, τ and λ are the three Lagrange multipliers enforcing the constraints (3.3)-(3.5). W.l.o.g., assume that $\gamma_{ji} = \gamma_{ij}$ for all $(i,j) \in E$ (see paper [55] for more details). Let L be the Laplacian matrix corresponding to (3.2), i.e. a $|V| \times |V|$ matrix whose entry at the ith row and jth column is

$$L_{ij} = \begin{cases} \sum\limits_{i\neq k} \gamma_{ik}, & i = j, \\ -\gamma_{ij}, & i \neq j, (i,j) \in E \text{ or } (j,i) \in E, \\ 0, & \text{otherwise.} \end{cases} \tag{3.8}$$

Notice that the positions $x_i(t)$ and the opinions $\gamma_{ij}(t)$ evolve according to a constrained gradient flow generated by the negative gradient vector field: $\dot{x}_i = -\frac{\partial \mathscr{D}}{\partial x_i}$ and $\dot{\gamma}_{ij} = -\frac{\partial \mathscr{D}}{\partial \gamma_{ij}}$, or more explicitly,

$$\dot{x}_i = -2 \sum_{j:(i,j)\in E \text{ or } (j,i)\in E} \gamma_{ij}(x_i - x_j) + 2\lambda x_i = -2(L\boldsymbol{x})_i + 2\lambda x_i, \tag{3.9}$$

$$\dot{\gamma}_{ij} = -(x_i - x_j)^2 + \frac{\mu}{15} + \frac{2\tau}{15}\gamma_{ij}, \tag{3.10}$$

with over-dots denoting differentiation with respect to time t.

By understanding the stability of the above gradient flow, the authors [55] made a few conclusions on the complete graph:

- For a small spread of opinions, the whole system on a complete graph converges to a consensus state where everyone stands at the same position on some issue.
- For a larger spread of opinions, a stable balanced state occurs where all people divide into two groups with opposing views.
- Except for consensus and balanced states, all other steady solutions are completely unbalanced and unstable based on the numerical results.

In the following part of this chapter, we will first extend their results from the complete graph to an interesting cubic symmetric graph, the Petersen graph, following a method of

reduction where the theory of graph automorphism serves as the key. This method only applies to graphs with symmetric structure. For large random graphs, however, such nice architecture vanishes, and thus, a different approach is required. We will, as a result, propose a "nearest-neighbor" mean-field analysis technique on graphs with few symmetry and particularly carry out our treatment on the Erdös-Rényi graph for scrutinization.

3.2. Social Dynamics on Petersen Graph

3.2.1. *Notation and Preliminaries*

The Petersen graph is one of the favorite graphs among graph theorists. It is a cubic symmetric graph with 10 vertices and 15 edges, i.e., $|V| = 10$ and $|E| = 15$. The 10 vertices are indexed by $C(5,2) = 10$ two-element subsets of a five-object set. Two vertices are joined by an edge if the corresponding subsets are disjoint. This gives us a regular graph of degree three, with automorphism group S_5 (up to isomorphism) corresponding to all permutations of the underlying five-element set, as shown below.

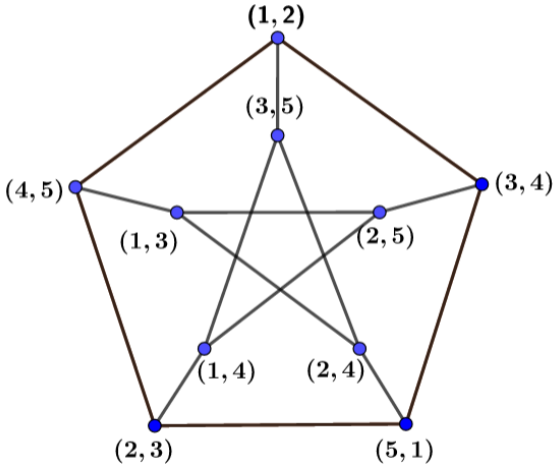

Figure 3.1: The Petersen graph

Though the symmetric group S_5 has a large number of subgroups (156), the total number of different automorphism classes of its subgroups (up to isomorphism) is much smaller (16). We display a complete list of the automorphism classes as below:

$$\{Z_1(\text{trivial group}), Z_2, Z_3, Z_4, D_4, Z_5, Z_6, S_3, D_8, D_{10}, A_4, S_2 \times S_3, GA(1,5), S_4, A_5, S_5\}. \qquad (*)$$

Definition 3.1. *An **automorphism of a graph** is a permutation of the vertices that preserve adjacency. More precisely, if σ is an automorphism of a graph G, then (v_1, v_2) is an edge in G if and only if $(\sigma(v_1), \sigma(v_2))$ is an edge in G. The equivalence classes of the vertices of G under*

the action of the automorphism are called ***vertex orbits****. The equivalence classes of the edges are called* ***edge orbits****.*

Clearly, each automorphism group in (∗) is an automorphism of the Petersen graph. Applying these automorphism groups on the Petersen graph and regarding each group orbit as a single element will give us associated reduced graphs. By virtue of the structure of the reduced graphs, we aim to find all states on the Petersen graph that minimizes the Dirichlet energy (3.2) and then study the stability of these states.

The consensus state, where everyone stands at the same position, i.e., $x_i(t) \equiv x_j(t)$ for any pair (i, j), is the simplest state among all. We will show, probably not surprisingly, that this state is a stable fixed point and almost every initial condition converges exponentially to consensus, i.e, it is a global minimizer, when the variance $\nu^2 = P - Q^2$ is sufficiently small. To start with, directly applying Agbanusi and Bronski's result [55] gives the following lemma:

Lemma 3.2. *Suppose $L(\gamma(t))$ is the graph Laplacian on the Petersen graph, then $\boldsymbol{x} = \frac{1}{\sqrt{10}}\mathbf{1}_{10}$ is a global minimizer, i.e., $\boldsymbol{x}(t) \to \frac{1}{\sqrt{10}}\mathbf{1}_{10}$ as $t \to \infty$, if L is positive semi-definite with a one-dimensional kernel.*

Using Lemma 3.2 it is not hard the derive our first theorem in this chapter:

Theorem 3.3. *If $P < \frac{31}{30}Q^2$, or in other word, the variance $\nu^2 = P - Q^2 < \frac{1}{30}Q^2$, then L is positive semi-definite with a one-dimensional kernel and thus the consensus state is a global minimizer.*

Proof. Recall our assumption $\gamma_{ij} = \gamma_{ji}$ and the graph Laplacian

$$L_{ij} = L_{ij}(\gamma) := \begin{cases} \sum\limits_{i \neq k} \gamma_{ik}, & i = j, \\ -\gamma_{ij}, & i \neq j, (i,j) \in E \text{ or } (j,i) \in E, \\ 0, & \text{otherwise.} \end{cases} \tag{3.11}$$

We write each opinion as a mean plus a mean-zero part, i.e., $\gamma_{ij} = Q + \tilde{\gamma}_{ij}$ for each $(i, j) \in E$, where the mean-zero part $\tilde{\gamma}_{ij}$ satisfies

$$\frac{1}{|E|}\sum_{(i,j)\in E} \tilde{\gamma}_{ij} = 0, \qquad \frac{1}{|E|}\sum_{(i,j)\in E} \tilde{\gamma}_{ij}^2 = P - Q^2. \tag{3.12}$$

Notice that each vertex in the Petersen graph has degree 3. The corresponding graph Laplacian takes the form $L = QL_0 + \tilde{L}$, where $L_0 = 3I - A$ with A as the adjacency matrix of the Petersen graph, and $\tilde{L}$ is a matrix with $L_{ij}(\tilde{\gamma})$ as an entry at the ith row and jth column. First, we take a look at the eigenvalues of L_0. ng the fact that the trace of a matrix is the sum of all its eigenvalues, it is easy to obtaiNotice that the adjacency matrix A satisfies $A^2 + A = 2I + J$ where I is the identity matrix and J denote the 10×10 matrix of all 1's. Suppose λ is an eigenvalue of A,

then since $(2I + J)$ has eigenvalue 12 with multiplicity 1 and eigenvalue 2 with multiplicity 9, we have that one eigenvalue of A satisfies $\lambda^2 + \lambda = 2$ and nine others satisfy $\lambda^2 + \lambda = 12$. Usin $\det(A - \lambda I) = (\lambda - 3)(\lambda + 2)^4(\lambda - 1)^5$. Thus, the minimum non-zero eigenvalue of L_0 is 2. Let $\sigma_{min}(\cdot)$ denote the minimum non-zero eigenvalue, then we have

$$\sigma_{min}(L_0) = 2. \tag{3.13}$$

Next, we make an important observation: the matrix L_0 commutes with every graph Laplacian, and thus, can be simultaneously diagonalized. Hence it suffices to estimate the most negative eigenvalue of $\tilde{L}$. The latter can be estimated by the Hilbert-Schmidt inequality. More explicitly, we have

$$\sigma_{min}(\tilde{L}) \geq -\|\tilde{L}\|_{HS}, \tag{3.14}$$

where $\|\cdot\|_{HS}$ denotes the Hilbert-Schmidt norm. According to its definition,

$$\|\tilde{L}\|_{HS}^2 = \sum_{i,j}(\tilde{L}_{ij})^2 = 2\sum_{(i,j)\in E}\tilde{\gamma}_{ij}^2 + \sum_i(\sum_{j\in S_i}\tilde{\gamma}_{ij})^2 \leq 2\sum_{(i,j)\in E}\tilde{\gamma}_{ij}^2 + 3\sum_i(\sum_{j\in S_i}\tilde{\gamma}_{ij}^2) = 8|E|(P - Q^2). \tag{3.15}$$

where $S_i = \{j : (i,j) \in E \text{ or } (j,i) \in E\}$. We used Cauchy-Schwarz inequality in a middle step when deriving (3.15). Combining the spectrum estimations of L_0 and $\tilde{L}$, (3.13) and (3.15), we eventually obtain the following inequality:

$$\sigma_{\min}(L) \geq 2(Q - \sqrt{2|E|(P - Q^2)}), \tag{3.16}$$

where $|E| = 15$. By requiring the right-hand side to be positive, we derive a sufficient condition to guarantee that the consensus state is a global minimizer as follows:

$$P < \frac{31}{30}Q^2, \text{ or equivalently, } \nu^2 = P - Q^2 \ < \frac{1}{30}Q^2. \tag{3.17}$$

■

Except for the consensus state, plenty of other steady states exist on the Petersen graph due to its highly symmetric structure. To study these states, we propose a method of reduction by applying graph automorphisms. We will try to shed light on the power of this reduction method and show how it simplifies the process of analysis in the next part.

3.2.2. *Method of Reduction*

We shall discuss the main idea of our method of reduction in this section. Consider a state that is invariant under a non-trivial automorphism group of the Petersen group (see the list (∗) above). Regarding the vertices on the same orbit under the automorphism group as one vertex gives us a reduced graph. Figure 3.2 is an example by taking the automorphism group as $S_2 \times S_3$

generated by permutations (123) and (12)(45).

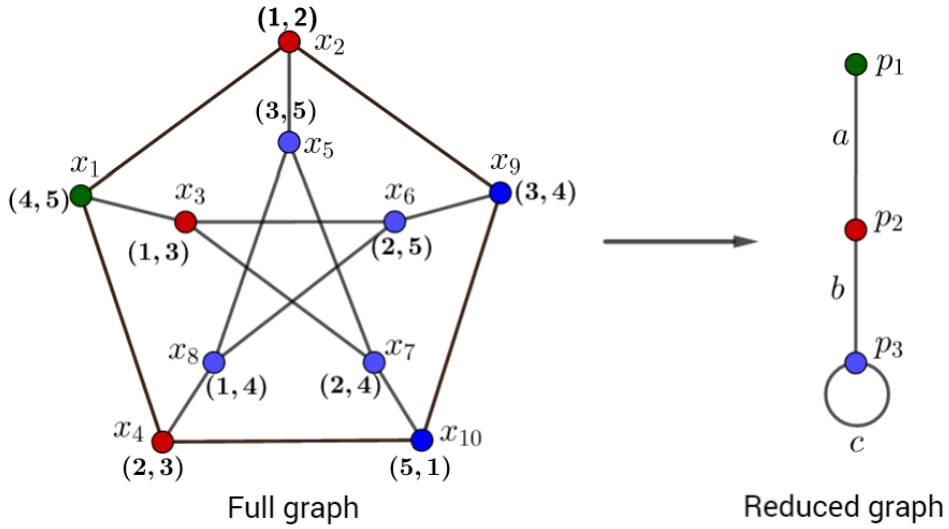

Figure 3.2: A reduction on the Petersen graph

The left image of Figure 3.2 is the original Petersen graph with 10 vertices and 15 edges, while the right one is the reduced graph with 3 vertices and 3 edges under $S_2 \times S_3$. To make it more clear, notice that the vertex orbits of this automorphism are

$$\begin{aligned} O_1 &= \{(4,5)\} = \{x_1\}, \\ O_2 &= \{(1,2),(1,3),(2,3)\} = \{x_2, x_3, x_4\}, \\ O_3 &= \{(3,5),(2,5),(2,4),(1,4),(3,4),(1,5)\} = \{x_5, x_6, x_7, x_8, x_9, x_{10}\}. \end{aligned}$$

Each orbit is represented by a vertex in the reduced graph. Suppose p_1, p_2, p_3 represent the three new vertices and a, b, c the three new edges, then minimizing the Dirichlet energy (3.2) with the third constraint (3.5) leads to a reduced optimization problem:

$$\min_{p_1,p_2,p_3} \quad 3a(p_1 - p_2)^2 + 6b(p_2 - p_3)^2, \tag{3.18}$$

$$\text{subject to:} \quad p_1^2 + 3p_2^2 + 6p_3^2 = 1, \tag{3.19}$$

where the constant 3 arises from the fact that the orbit set O_1 connects with O_2 through 3 edges in the full graph and the constant 6 is due to the 6 edges between O_2 and O_3. By applying the Lagrange multiplier method, this optimization problem can be converted to a generalized eigenvalue problem:

$$(A - \sigma B) \cdot \boldsymbol{p} = 0 \quad \text{subject to} \quad p_1^2 + 3p_2^2 + 6p_3^2 = 1, \tag{3.20}$$

where $\boldsymbol{p} = (p_1, p_2, p_3)^T$, $A = \begin{bmatrix} 3a & -3a & 0 \\ -3a & 3a+6b & -6b \\ 0 & -6b & 6b \end{bmatrix}$ and $B = \begin{bmatrix} 1 & 0 & 0 \\ 0 & 3 & 0 \\ 0 & 0 & 6 \end{bmatrix}$.
By solving (3.20), one can write the solution σ and p_1, p_2, p_3 in terms of a and b. Then the values of λ and $\boldsymbol{x}$ will be determined since we have

$$\lambda = \sigma, \tag{3.21}$$

$$\boldsymbol{x} = (p_1, p_2, p_2, p_2, p_3, p_3, p_3, p_3, p_3, p_3). \tag{3.22}$$

Plugging Equations (3.21) and (3.22) back in the gradient system (3.9)-(3.10) and combining with the constraints (3.3), (3.4) and (3.5) will give a system of five equations with five unknown variables a, b, c, μ, τ and two constants P and Q. Note that the value of λ equals the Dirichlet energy by Equation (3.9) and we may have more than one solution of (3.20). If the minimum value of σ is negative, then we will have an energy lower than which of the consensus state, which indicates a probability of the existence of a stable non-consensus state. Thus by detecting the value of $\sigma_{\min}$ we can find a threshold on the opinion variance $\nu^2 := P - Q^2$ for negative energy. To examine the stability of such a new-born state, we linearize the flow around the equilibria and count the number of negative eigenvalues of the resulting linear map. Recall that the critical points of the flow are precisely the constrained extrema of the Dirichlet energy D, i.e. the critical points of $\mathscr{D}$. A standard Lyapunov function argument gives us a new threshold on ν^2 for a stable state.

3.2.3. *Non-consensus States*

In this section, we will focus on non-consensus states of our system. According to what we discussed in section 3.2.1, the system converges to a consensus state for small variance $\nu^2 = P - Q^2$, as one might expect. However, for a larger value of the variance, we have observed convergence to two different stable states, one balanced state and one unbalanced state, as what we will deliberate below.

We start with the balanced state. This is depicted in Figure 3.3, which reflects numeric for $Q = 1$ and $\sqrt{P - Q^2} = 2$. In this state, we have a magnate with strong negative opinion denoted by the vertex v_1 and nine opponents who take positive positions denoted by the other vertices in the graph. The edge between every pair of vertices v_i and v_j represents the degree of friendliness between actor i and actor j, with $\gamma_{ij}(t) > 0$, associated with a solid edge, representing friendliness; and $\gamma_{ij}(t) < 0$, associated with a dashed edge, antagonism. Note that the ten vertices are grouped into three camps: each one is associated with an orbit under an automorphism group $S_2 \times S_3$. More precisely, we have a fixed element v_1, a 3-element orbit $\{v_2, v_3, v_4\}$ and a 6-element orbit $\{v_4, v_5, v_6, v_7, v_8, v_9, v_{10}\}$. Let p_1, p_2 and p_3 represent their positions (or opinions) and a, b and c represent their relationships (a associates with the green dashed edge; b associates with the red

solid edge; and c associates with the black solid edge). Then we have an opinion vector

$$\begin{aligned} \boldsymbol{X} &= \{x_1, x_2, x_3, ..., x_9, x_{10}\} \\ &= \{p_1, p_2, p_2, p_2, p_3, p_3, p_3, p_3, p_3, p_3\}, \end{aligned} \tag{3.23}$$

and a relationship vector

$$\begin{aligned} \boldsymbol{\Gamma} &= \{\gamma_{12}, \gamma_{13}, \gamma_{14}, \gamma_{25}, \gamma_{29}, \gamma_{36}, \gamma_{37}, \gamma_{48}, \gamma_{410}, \gamma_{57}, \gamma_{58}, \gamma_{68}, \gamma_{69}, \gamma_{710}, \gamma_{910}\} \\ &= \{a, a, a, b, b, b, b, b, b, c, c, c, c, c, c\}. \end{aligned} \tag{3.24}$$

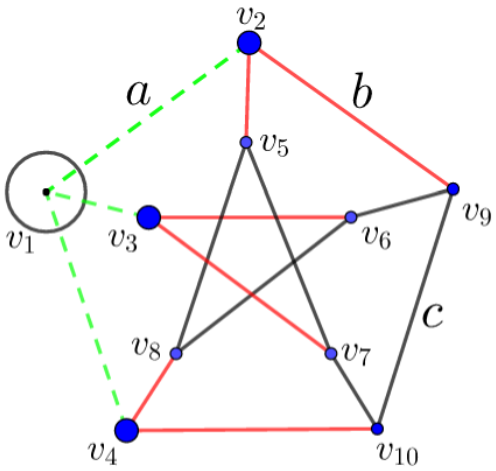

Figure 3.3: A balanced state on the Petersen graph

Now applying our method of reduction, the original optimization problem

$$\underset{\boldsymbol{x},\boldsymbol{\gamma}}{\text{minimize}}\ D(\boldsymbol{x},\boldsymbol{\gamma}) = \sum_{(i,j)\in E} \gamma_{ij}(x_i - x_j)^2,$$

subject to the constraints g_1, g_2 and g_3 (3.3)-(3.5) is equivalent to a generalized eigenvalue problem. (In fact, we used this state as an example to illustrate the reduction method and derived such eigenvalue problem in section 3.2.2. We restate it here simply for completeness.)

$$(A - \sigma B)\cdot \boldsymbol{p} = 0 \quad \text{subject to} \quad p_1^2 + 3p_2^2 + 6p_3^2 = 1, \tag{3.25}$$

where $\boldsymbol{p} = (p_1, p_2, p_3)^T$, $A = \begin{bmatrix} 3a & -3a & 0 \\ -3a & 3a+6b & -6b \\ 0 & -6b & 6b \end{bmatrix}$ and $B = \begin{bmatrix} 1 & 0 & 0 \\ 0 & 3 & 0 \\ 0 & 0 & 6 \end{bmatrix}$.

Clearly, A is symmetric and B is positive definite, so σ's are real. And since B is invertible, solving $\det(B^{-1}A - \sigma I) = 0$ gives us σ, i.e., σ is the regular eigenvalue of $B^{-1}A$ and $\boldsymbol{p}$ is the regular

eigenvector of $B^{-1}A$. Direct computation gives us the eigenvalues as follows:

$$\mathbf{\Lambda} = \begin{bmatrix} \sigma_1 \\ \\ \sigma_2 \\ \\ \sigma_3 \end{bmatrix} = \begin{bmatrix} 0 \\ \\ 2a + \frac{3b}{2} - \frac{\alpha}{2} \\ \\ 2a + \frac{3b}{2} + \frac{\alpha}{2} \end{bmatrix},$$

and the corresponding eigenvectors are

$$\mathbf{v_1} = \begin{bmatrix} 1 \\ \\ 1 \\ \\ 1 \end{bmatrix}, \quad \mathbf{v_2} = \begin{bmatrix} -\frac{1}{2b}(9b - 12a + 3\alpha) \\ \\ -\frac{1}{2b}(4a + b - \alpha) \\ \\ 1 \end{bmatrix}, \quad \mathbf{v_3} = \begin{bmatrix} \frac{1}{2b}(12a - 9b + 3\alpha) \\ \\ -\frac{1}{2b}(4a + b + \alpha) \\ \\ 1 \end{bmatrix},$$

where $\alpha = \sqrt{16a^2 - 16ab + 9b^2}$.

Now, taking the other two constraints g_1 and g_2 into consideration, we obtain the following equation system:

$$\begin{cases} L\vec{x} = \sigma\vec{x} & (3.26) \\ (p_1 - p_2)^2 = \frac{\mu}{15} + \frac{2\tau}{15}a & (3.27) \\ (p_2 - p_3)^2 = \frac{\mu}{15} + \frac{2\tau}{15}b & (3.28) \\ (p_3 - p_3)^2 = 0 = \frac{\mu}{15} + \frac{2\tau}{15}c & (3.29) \\ \frac{1}{15}(3a + 6b + 6c) = Q & (3.30) \\ \frac{1}{15}(3a^2 + 6b^2 + 6c^2) = P. & (3.31) \end{cases}$$

By Equation (3.26), we can write p_1, p_2 and p_3 in terms of a and b. So in fact we have five equations (3.27) – (3.31) and five unknown variables a, b, c, μ and τ. By solving this equation system, we can write a and b in terms of P and Q, and so that σ can be rewritten as a function of P and Q. Notice that the Dirichlet energy is

$$3a(p_1 - p_2)^2 + 6b(p_2 - p_3)^2 = \vec{x}A\vec{x}^T = \vec{x}B(B^{-1}A\vec{x}^T) = \sigma\vec{x}B\vec{x}^T = \sigma.$$

So if negative energy exists, it should be achieved by the smallest non-zero eigenvalue at the value

$$\sigma_{min} = \sigma_2 = 2a + \frac{3b}{2} - \frac{\alpha}{2}.$$

Corresponding to σ_2, we have an associated eigenvector

$$\begin{bmatrix} p_1 \\ p_2 \\ p_3 \end{bmatrix} = \begin{bmatrix} -\frac{1}{2b}(9b - 12a + 3\alpha) \\ -\frac{1}{2b}(4a + b - \alpha) \\ 1 \end{bmatrix}.$$

By plugging in the values of p_1, p_2 and p_3, the above system of equations can be rewritten as follows.

$$\begin{cases} \frac{\mu}{15} + \frac{2\tau}{15}a = \frac{1}{b^2}(8a - 4b - 2\alpha)^2 & (3.32) \\ \frac{\mu}{15} + \frac{2\tau}{15}b = (\frac{1}{2b}(4a + b - \alpha) + 1)^2 & (3.33) \\ \frac{\mu}{15} + \frac{2\tau}{15}c = 0 & (3.34) \\ a + 2b + 2c = 5Q & (3.35) \\ a^2 + 2b^2 + 2c^2 = 5P, & (3.36) \end{cases}$$

where $\alpha = \sqrt{16a^2 - 16ab + 9b^2}$. Solving this equation system gives us the following result of the balanced state.

Theorem 3.4. *The Dirichlet energy turns negative when the variance $\nu^2 = P - Q^2 > 0.25$.*

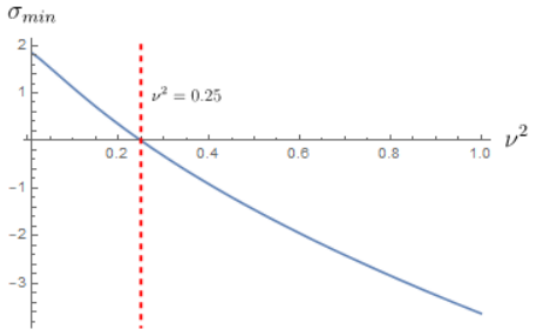

Figure 3.4: Minimum energy for the balanced state

To investigate the stability of such a balanced state, it is natural to check eigenvalues of the Hessian matrix of $\mathscr{D}$ at critical points, since it is known that the gradient flow near critical points is stable if the Hessian is negative definite [55].

Lemma 3.5 (Agbanus-Bronski)**.** *Define a phase space*

$$\Omega = \{(\boldsymbol{x}, \boldsymbol{\gamma}) \in \mathbb{R}^{10} \times \mathbb{R}^{15} : g_1 = Q, g_2 = P, g_3 = 1\}$$

and suppose $\omega_0 \in \Omega$ is a critical point of $\mathscr{D}$ i.e. a local extremum of D subject to the constraints

(3.3)-(3.5). Let $H(\omega_0)$ be the associated Hessian:

$$H(\omega_0) = -\begin{bmatrix} \frac{\partial^2 \mathscr{D}}{\partial x_i \partial x_k} & \frac{\partial^2 \mathscr{D}}{\partial \gamma_{lk} \partial x_i} \\ \frac{\partial^2 \mathscr{D}}{\partial x_k \partial \gamma_{ij}} & \frac{\partial^2 \mathscr{D}}{\partial \gamma_{lk} \partial \gamma_{ij}} \end{bmatrix}\Big|_{\omega_0} \tag{3.37}$$

and $T_{\omega_0}\Omega$ be the tangent space to Ω at ω_0. If $H(\omega_0)|_{T_{\omega_0}\Omega}$ is negative definite, then $\mathscr{D}$ has a strict local minimum at ω_0 and thus the gradient flow is stable near ω_0.

By direct computation, we obtain

$$\begin{cases} \partial^2_{\boldsymbol{x}} \mathscr{D} = 2(L - \lambda I) \\ \partial^2_{\boldsymbol{\gamma}} \mathscr{D} = -\frac{2\tau}{|E|} I_{|E|\times|E|} \\ \frac{\partial^2 \mathscr{D}}{\partial x_k \partial \gamma_{ij}} = 2(x_i - x_j)(\delta_{ik} - \delta_{jk}) \\ \frac{\partial^2 \mathscr{D}}{\partial \gamma_{ij} \partial x_k} = 2(x_i - x_j)(\delta_{ik} - \delta_{jk}). \end{cases} \tag{3.38}$$

Suppose $\boldsymbol{B}$ is a 10×15 matrix with entries $B_{k,ij} = \frac{\partial^2 \mathscr{D}}{\partial \gamma_{ij} \partial x_k}$, then we have

$$\boldsymbol{H} = \begin{bmatrix} -2(L - \lambda I) & -\boldsymbol{B} \\ -\boldsymbol{B}^T & \frac{2\tau}{|E|} I_{|E|\times|E|}, \end{bmatrix}. \tag{3.39}$$

Taking the gradient of the constraints g_1, g_2 and g_3 with respect to time t, we have

$$\begin{cases} \sum \frac{d\gamma_{ij}}{dt} = 0 \\ \sum \gamma_{ij} \frac{d\gamma_{ij}}{dt} = 0 \\ \sum x_i \frac{dx_i}{dt} = 0. \end{cases} \tag{3.40}$$

Define three 25×1 vectors (10 components associate with vertices and 15 associate with edges.):

$$\boldsymbol{v}_1 = \begin{pmatrix} \vec{0} \\ \vec{1} \end{pmatrix}, \quad \boldsymbol{v}_2 = \begin{pmatrix} \vec{0} \\ \Gamma \end{pmatrix}, \quad \boldsymbol{v}_3 = \begin{pmatrix} X \\ \vec{0} \end{pmatrix}, \tag{3.41}$$

where Γ and X are as defined in (3.23) and (3.24). Then from (3.40) we see $\boldsymbol{v}_1, \boldsymbol{v}_2$ and $\boldsymbol{v}_3$ form a orthogonal space of $T_{\omega_0}\Omega$. More explicitly, let $A = (\boldsymbol{v}_1, \boldsymbol{v}_2, \boldsymbol{v}_3)^\perp$, then

$$T_{\omega_0}\Omega = (\text{span}\{\nabla g_1, \nabla g_2, \nabla g_3\})^\perp = (\text{span}\{\boldsymbol{v}_1, \boldsymbol{v}_2, \boldsymbol{v}_3\})^\perp = \text{Nullspace}(A).$$

Clearly, Nullspace(A) is a 22-dimensional vector space. Onto computing $H|_{T_{\omega_0}\Omega}$, it suffices to find a basis for Nullspace(A): $\{\boldsymbol{w}_1, \boldsymbol{w}_2, ..., \boldsymbol{w}_{22}\}$ since

$$(H|_{T_{\omega_0}\Omega})_{ij} = \langle \boldsymbol{w}_i, H\boldsymbol{w}_j \rangle. \tag{3.42}$$

Computing the number of non-negative eigenvalues of $H|_{T_{\omega_0}\Omega}$ numerically leads to the following theorem.

Theorem 3.6. *There exists a constant $c_0 \in (1.01, 1.02)$ such that the balanced state is stable when the variance $\nu^2 = P - Q^2 > c_0$.*

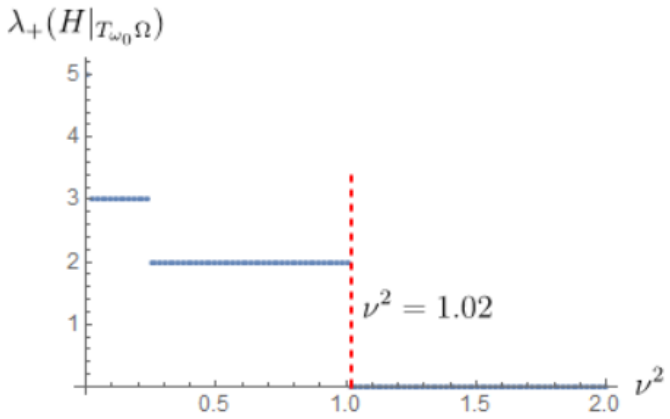

Figure 3.5: Number of non-negative eigenvalues for the balanced state

Following the same methodology, one can also explore the unbalanced state analytically. This state is depicted in Figure 3.6, which reflects numerics for $Q = 1$ and $\sqrt{P - Q^2} = 2$. In this state, ten actors belong to three different factions: one with positive opinions (supporters), one with negative opinions (opponents), and the other sits on the fence (neutrals). The opposition has a leader v_1 with two followers v_2 and v_4. Similarly there is a lead supporter v_3 with two followers v_6 and v_7. The remaining four actors v_5, v_8, v_9 and v_{10} are neutrals. In fact, this unbalanced state is invariant under $D_4 = C_4 \times Z_2$, the symmetry group of the square, as a subgroup of an automorphism group of S_5. The cyclic group C_4 fixes the factions: the leaders of the positive and negative factions are invariant under this group, and the followers and neutral people are permuted by this group. Additionally, there is a Z_2 subgroup corresponding to reflections of the square that switches the positive and negative factions and leaves the neutral faction fixed. More precisely, under a group action of D_4, the ten vertices fall in three different orbits: a 2-element orbit $\{v_1, v_3\}$, a 4-element orbit $\{v_2, v_4, v_6, v_7\}$ and another 4-element orbit $\{v_5, v_8, v_9, v_{10}\}$. Let p_1, p_2 and p_3 represent their positions (or opinions), then clearly $p_3 = 0$ representing the neutral position. Let a, b, c and d represent their relationships (a associates with the green dashed edge; b associates with the red solid edge; c associates with the blue solid edge; and d associates with the black solid edge). Then

we have an opinion vector

$$\begin{aligned} \boldsymbol{X} &= \{x_1, x_2, x_3, ..., x_9, x_{10}\} \\ &= \{-p_1, -p_2, p_1, -p_2, 0, p_2, p_2, 0, 0, 0\}, \end{aligned} \tag{3.43}$$

and a relationship vector

$$\begin{aligned} \boldsymbol{\Gamma} &= \{\gamma_{12}, \gamma_{13}, \gamma_{14}, \gamma_{25}, \gamma_{29}, \gamma_{36}, \gamma_{37}, \gamma_{48}, \gamma_{410}, \gamma_{57}, \gamma_{58}, \gamma_{68}, \gamma_{69}, \gamma_{710}, \gamma_{910}\} \\ &= \{b, a, b, c, c, b, b, c, c, c, d, c, c, c, d\}. \end{aligned} \tag{3.44}$$

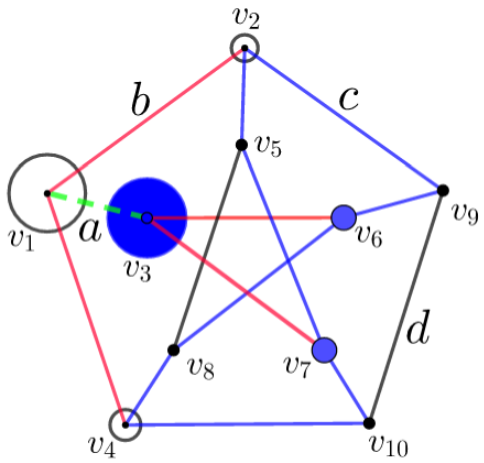

Figure 3.6: An unbalanced state on the Petersen graph

Similarly as above, applying the method of reduction will eventually give us a system of equations:

$$\begin{cases} \frac{\mu}{15} + \frac{2\tau}{15}a = \frac{1}{b^2}(2a + b - 2c - \beta)^2 & (3.45) \\ \frac{\mu}{15} + \frac{2\tau}{15}b = (\frac{1}{2b}(2a + b - 2c - \beta) + 1)^2 & (3.46) \\ \frac{\mu}{15} + \frac{2\tau}{15}c = 1 & (3.47) \\ \frac{\mu}{15} + \frac{2\tau}{15}d = 0 & (3.48) \\ a + 4b + 8c + 2d = 15Q & (3.49) \\ a^2 + 4b^2 + 8c^2 + 2d^2 = 15P, & (3.50) \end{cases}$$

where $\beta = \sqrt{4a^2 + 4ab - 8ac + 9b^2 - 4bc + 4c^2}$.
The corresponding minimum energy can be expressed as

$$\sigma_{min} = \frac{1}{2}(2a + 3b + 2c - \beta). \tag{3.51}$$

Solving the equation system (3.45)-(3.50) numerically gives us the following result of the unbalanced

state.

Theorem 3.7. *The Dirichlet energy turns negative when the variance* $\nu^2 = P - Q^2 > c_1$ *where* $c_1 \in (0.21, 0.22)$.

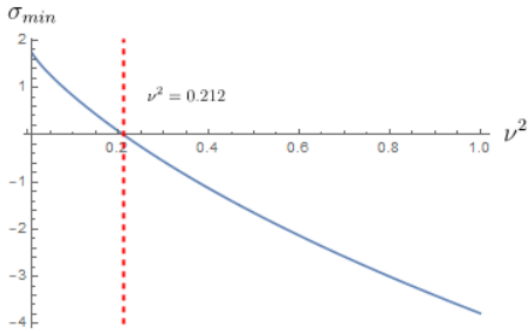

Figure 3.7: Minimum energy for the unbalanced State

The stability of the unbalanced state relies on the eigenvalues of its border Hessian matrix $H(\omega_0)|_{T_{\omega_0}\Omega}$, as what we discussed above for the balanced state. Computing the number of non-negative eigenvalues of $H|_{T_{\omega_0}\Omega}$ numerically leads to our next result.

Theorem 3.8. *All solutions of the unbalanced state corresponding to the negative Dirichlet energy is stable. More precisely, the unbalanced state is stable when the variance* $\nu^2 = P - Q^2 > c_1$ *where* $c_1 \in (0.21, 0.22)$.

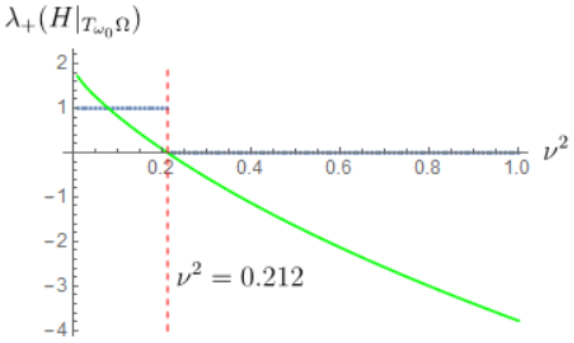

Figure 3.8: Number of non-negative eigenvalues for the unbalanced state

In Figure 3.8, corresponding to different values of ν^2, the blue dots represent the number of non-negative eigenvalues of $H|_{T_{\omega_0}\Omega}$ and the green line the Dirichlet energy. We see that when $\nu^2 \approx 0.212$, the energy turns negative and there are no non-negative eigenvalues, i.e., all eigenvalues of $H|_{T_\omega\Omega}$ are negative, which implies the stability of the unbalanced state.

To study other non-consensus states except for the balanced and the unbalanced state discussed above, we again seek aid from the symmetry of the Petersen graph. In other words, we consider

all the remaining subgroups of the automorphism group of the Peterson graph (except for the one associated with the balanced state and the one with the unbalanced state) given by (∗). States that are invariant under these subgroups provide possible stable steady solution on the Petersen graph that minimizes the Dirichlet energy. Following the same procedure as above, we computed the threshold of negative energy on the variance ν^2 and derived the eigenvalues of the associated boundary Hessian matrix. It turns out all other non-consensus states we found using the graph symmetry are unstable. To avoid redundancy, we omit the analysis process here.

3.2.4. *Summary of Results*

Based on our numerics, only three stable states exist on the Petersen graph that minimizes the Dirichlet energy (3.2) subject to three constraints (3.3)-(3.5) including one consensus state and two non-consensus states: a balanced state and an unbalanced state. Regarding these steady states, two questions were addressed:

1. When does the Dirichlet energy D become negative?
2. When does each state become stable?

We showed that both of the questions depend on the variance of opinions $\nu^2 = P - Q^2$. Recall Q represents the mean of actors' opinions. W.l.o.g., we assume $Q = 1$ in this part for simplification. Then the point of the Dirichlet energy turning negative will be determined by a threshold value of P for each state, and so will the state's stability. More precisely, we have the following results:

1. For the consensus state S_0, the Dirichlet energy $D \equiv 0$ regardless of any value of P, and the state stays stable when $P < p_0 := \frac{31}{30}$.
2. For the balanced state S_1, the Dirichlet energy D becomes negative when $P > p_1 :\approx 1.25$ and the states becomes unstable when $P > p_1' :\approx 2$.
3. For the unbalanced state S_2, the Dirichlet energy D becomes negative and the state becomes unstable simultaneously when $P > p_2 :\approx 1.2$.

States	Threshold of negative energy	Threshold of stable state
Consensus (S_0)	$D \equiv 0$	$P < p_0 = 31/30$
Balanced (S_1)	$P > p_1 \approx 1.25$	$P > p_1' \approx 2$
Unbalanced (S_2)	$P > p_2 \approx 1.2$	$P > p_2 \approx 1.2$

Table 3.1: A comparison among three stable states

In Figure 3.9, we present a comparison among the above three stable states. The stable region is marked blue and the unstable region red. As we can see from the graph, the minimum energy is achieved by a consensus state when the variance ν is small and the minimum energy is zero. We rigorously proved that the consensus state is a global minimizer when $\nu < P_0 - 1$. As the

variance ν increases to $P_2 - 1$, a stable unbalanced state occurs with negative energy and it stays stable regardless of how large the variance grows. Keep increasing ν towards $P_1 - 1$, the energy associated with a balanced state starts being negative and the state comes to be stable as ν exceeds $P_1' - 1$. From then on, two stable states coexist in the system. The balanced state crosses with the unbalanced state when $P = P^* \approx 8.16$. From this point of intersection onward, the whole social network reaches its lowest energy at the balanced state.

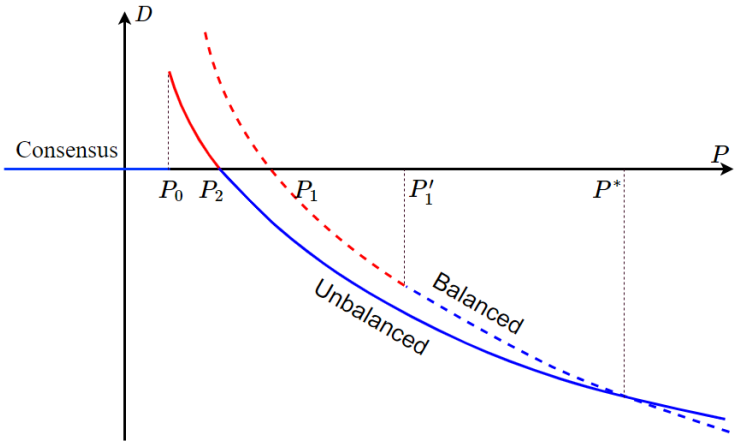

Figure 3.9: A comparison among three stable states

3.3. Social Dynamics on Erdös-Rényi Graph

3.3.1. *Notation and Preliminaries*

The Erdös-Rényi model, one of the most famous and fundamental models generating random graphs, was firstly proposed and studied by two Hungarian mathematicians Paul Erdös and Alfréd Rényi in the 1950s and 1960s. The graph it generates is called the Erdös-Rény graph denoted by $\mathrm{ER}(n, q)$ where n represents the total number of nodes in the graph and $q \in [0, 1]$ represents the probability that any pair of nodes in the graph are connected. The existence of an edge is independent of all other edges. Note that the probability q here does not depend on n, which ensures strongly connected topology especially when n is large.

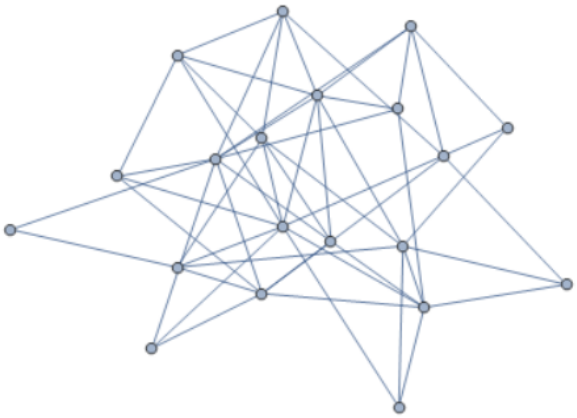

Figure 3.10: An example of the Erdös-Rényi graph

Our goal is to find stable states that minimize the disharmony in a social network with an underlying Erdös-Rényi graph, where the disharmony is measured by a Dirichlet energy (3.2):

$$D(\boldsymbol{x}, \boldsymbol{\gamma}) = \sum_{(i,j)\in E} \gamma_{ij}(x_i - x_j)^2.$$

It is nearly impossible to do such calculation by considering interactions among every pair of vertices, especially when the number of vertices in the graph is large. Moreover, unlike the Petersen graph, the Erdös-Rényi graph lacks a symmetric structure. As a result, directly using the automorphism classes of subgroups to reduce the size of the graph does not apply any further. Instead, a novel method, which we call "nearest-neighbor" mean-field model, is proposed to resolve this problem and will be delved into in the next section.

3.3.2. *Method of Mean Field Analysis*

In general, behaviors of large asymmetric random models are complex and highly nonlinear, which makes it hard to analyze their dynamics in a mathematically elegant way. Mean-field analysis, however, with a concentration on the macroscopic behaviors of the whole system, drastically reduces the dimensionality of the problem and thus the difficulty. It reformulates the dynamics of the system in terms of the "average state" of the system. More precisely, for a given object o, instead of examining the interactions between o and every other individual object, mean-field analysis approximates the interaction on o by considering the averaged effect from all others.

Inspired by the standard mean-field formation, we propose a novel "nearest-neighbor" mean-field model for the Erdös-Rényi graph. The gist is to classify neighbors of a given vertex V_0 in the graph by their distance from it, and approximate the total effect that all other vertices act on V_0 by summing up the averaged effect of each class of V_0's neighbors cross all the classes. In fact,

running the dynamics (3.9)-(3.10):

$$\dot{x}_i = -2 \sum_{j:(i,j)\in E \text{ or } (j,i)\in E} \gamma_{ij}(x_i - x_j) + 2\lambda x_i = -2(L\boldsymbol{x})_i + 2\lambda x_i,$$
$$\dot{\gamma}_{ij} = -(x_i - x_j)^2 + \frac{\mu}{15} + \frac{2\tau}{15}\gamma_{ij},$$

subject to the three constraints (3.3)-(3.5):

$$g_1 := \frac{1}{|E|} \sum_{(i,j)\in E} \gamma_{ij} = Q > 0,$$
$$g_2 := \frac{1}{|E|} \sum_{(i,j)\in E} \gamma_{ij}^2 = P > 0,$$
$$g_3 := \sum_{i=1}^{N} x_i^2 = R > 0,$$

on an Erdös-Rényi graph ER(n, q) for $n = 20$ and $q = 0.3$ with a random initialization gives a steady state as shown below.

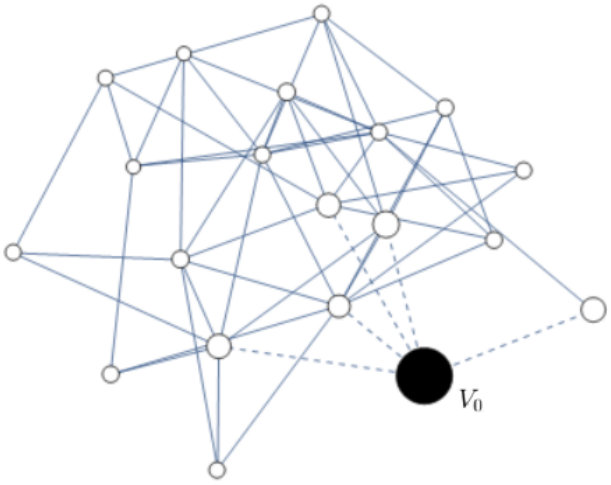

Figure 3.11: A steady state on ER$(20, 0.3)$

From Figure 3.11, it can be seen that there exists a leading vertex V_0 standing at the front line with a strong position on some issue while all its neighbors take weaker positions as they move away from it. Moreover, the vertices with the same distance from V_0 (or in other words, neighbors on the same level) share a common perspective with similar strength. However, as the distance increases, the intensity of attitudes that our actors hold dramatically declines. This striking phenomenon suggests applying a mean-field approach on different levels of neighbors of a given vertex will likely be a valid approximation of the original dynamics. Such approximation will greatly reduce the high dimensionality of our equation system down to just a few dimensions and thus make the problem

much simpler to analyze.

To make a precise "nearest-neighbor" mean-field model formation, we start with an arbitrary vertex in the graph V_0, and regard all its neighbors with distance one as the vertices in the first generation and those with distance two as the second, etc. Also, we regard the origin V_0 itself as its zero generation for convenience. See Figure 3.12 below.

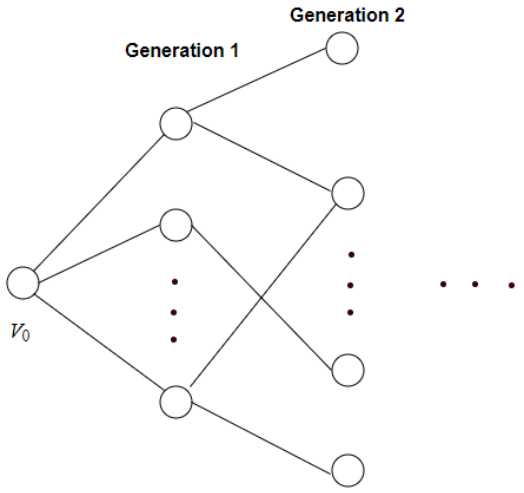

Figure 3.12: Generations of vertices from V_0

Definition 3.9. *Given a vertex V_0 and any $k \in \mathbb{N}$, define v_k as the average number of vertices in the kth generation of V_0 and $e_{k,k+1}$ as the average number of edges between vertices in the kth and $(k+1)$th generations.*

Note that $v_0 = 1$ by Definition 3.9. In fact, for an Erdös-Rényi graph $\mathrm{ER}(n, q)$, a straightforward calculation gives

$$v_k = (n - \sum_{i=0}^{k-1} v_i)(1 - (1-q)^{v_{k-1}}), \tag{3.52}$$

$$e_{k,k+1} = v_k \cdot q \cdot (n - \sum_{i=0}^{k} v_i). \tag{3.53}$$

According to Equation (3.52), we have $v_1 \approx nq$ and $v_2 \approx n - nq$ for large n. So the whole system can be approximated by two generations of a vertex when the system is large enough. We assume actors in the same generation share a common position on some issue, then the resulting reduced model becomes extremely simple since it contains only seven dimensions in total. Let x_i denote the position of the ith generation and γ_{ij} the opinion between actors in the ith and jth generations. Then we have three positions $\{x_0, x_1, x_2\}$ and four opinions $\{\gamma_{01}, \gamma_{11}, \gamma_{12}, \gamma_{22}\}$ (γ_{00} is excluded since we have only one actor in the origin and γ_{02} is also excluded since there exist no

edges between the origin and its second generation).

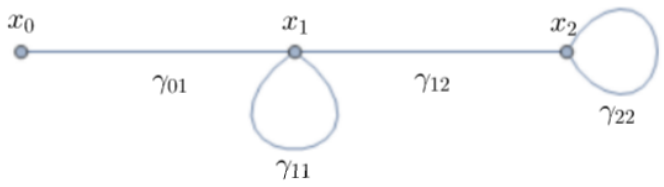

Figure 3.13: An Erdös-Rényi reduced model

Define $\boldsymbol{x} = (x_0, x_1, x_2)$ and $\boldsymbol{\gamma} = (\gamma_{01}, \gamma_{11}, \gamma_{12}, \gamma_{22})$, then for the reduced model, the associated Dirichlet energy is

$$D(\boldsymbol{x}, \boldsymbol{\gamma}) = e_{01}\gamma_{01}(x_0 - x_1)^2 + e_{12}\gamma_{12}(x_1 - x_2)^2, \tag{3.54}$$

and the associated constraints are

$$g_1 := \frac{1}{|E|}(e_{01}\gamma_{01} + e_{11}\gamma_{11} + e_{12}\gamma_{12} + e_{22}\gamma_{22}) = Q > 0, \tag{3.55}$$

$$g_2 := \frac{1}{|E|}(e_{01}\gamma_{01}^2 + e_{11}\gamma_{11}^2 + e_{12}\gamma_{12}^2 + e_{22}\gamma_{22}^2) = P, \tag{3.56}$$

$$g_3 := x_0^2 + v_1 x_1^2 + v_2 x_2^2 = 1, \tag{3.57}$$

where $|E| = e_{01} + e_{11} + e_{12} + e_{22}$. Define $I = \{(0,1), (1,1), (1,2), (2,2)\}$, then the method of Lagrange multipliers gives a constrained free energy

$$\mathscr{D} := D - \mu g_1 - \tau g_2 - \lambda g_3 \tag{3.58}$$

$$= \sum_{(i,j)\in I} \gamma_{ij} e_{ij}(x_i - x_j)^2 - \frac{\mu}{|E|}\sum_{(i,j)\in I} e_{ij}\gamma_{ij} - \frac{\tau}{|E|}\sum_{(i,j)\in I} e_{ij}\gamma_{ij}^2 - \lambda\sum_{i=0}^{2} v_i x_i^2, \tag{3.59}$$

where τ, μ and λ are the three Lagrange multipliers enforcing the constraints (3.55)-(3.57). Based on (3.59), the gradient flows of the positions and opinions are

$$\dot{x}_i = -2\sum_{j:(i,j)\in I \text{ or } (j,i)\in I} e_{ij}\gamma_{ij}(x_i - x_j) + 2\lambda v_i x_i, \tag{3.60}$$

$$\dot{\gamma}_{ij} = -e_{ij}(x_i - x_j)^2 + \frac{\mu}{|E|}e_{ij} + \frac{2\tau}{|E|}e_{ij}\gamma_{ij}, \tag{3.61}$$

with over-dots denoting differentiation with respect to time t. Now taking the derivatives on our

constraints (3.55)-(3.57) gives

$$\sum_{i,j:(i,j)\in I} e_{ij}\dot{\gamma}_{ij} = 0, \tag{3.62}$$

$$\sum_{i,j:(i,j)\in I} e_{ij}\gamma_{ij}\dot{\gamma}_{ij} = 0, \tag{3.63}$$

$$\sum_{i=0}^{2} v_i x_i \dot{x}_i = 0. \tag{3.64}$$

Plugging the gradient flows (3.60) and (3.61) into Equations (3.62)-(3.64) gives

$$\lambda = \frac{\sum_{i=0}^{2} v_i x_i \sum_{j=0}^{2} e_{ij}\gamma_{ij}(x_i - x_j)}{\|\boldsymbol{v}\cdot\boldsymbol{x}\|^2}, \tag{3.65}$$

$$\tau = \frac{|E|}{2(B^2 - AC)}\left(B\sum_{i,j} e_{ij}^2(x_i - x_j)^2 - A\sum_{i,j} e_{ij}^2\gamma_{ij}(x_i - x_j)^2\right), \tag{3.66}$$

$$\mu = \frac{|E|}{(AC - B^2)}\left(C\sum_{i,j} e_{ij}^2(x_i - x_j)^2 - B\sum_{i,j} e_{ij}^2\gamma_{ij}(x_i - x_j)^2\right), \tag{3.67}$$

where $A = \sum e_{ij}^2$, $B = \sum e_{ij}^2\gamma_{ij}$ and $C = \sum e_{ij}^2\gamma_{ij}^2$.

Therefore, our original goal that minimizes the disharmony in a system with a large underlying Erdös-Rényi graph has been successfully boiled down to solving a differential equation system (3.60)-(3.61) with seven variables $(x_0, x_1, x_2, \gamma_{01}, \gamma_{11}, \gamma_{12}, \gamma_{22})$.

3.3.3. *Stable Steady States*

In this section, we will present numerical results on the stable steady solutions of our mean-field reduced model. Starting with an arbitrary initial state $(\boldsymbol{x}(0), \boldsymbol{\gamma}(0))$ that satisfies the constraints (3.55)-(3.57), we run the gradient flow (3.60)-(3.61) using a built-in Mathematica solver "NDSolve". From a considerable amount of numerical experiments, we have observed three stable steady states: a consensus state and two non-consensus states.

1. Consensus State:

In this case, all actors eventually reach an agreement, i.e., $x_1 = x_2 = x_3$. Figure 3.14 shows an example consensus state where all actors hold negative views on some matter to the same extent, denoted by the three hollow nodes with the same size in the bottom graph. Also, the solid edges between nodes represent friendliness whereas the dashed ones represent antagonism. The thickness of an edge represents the strength of the relationship between the two nodes it connects.

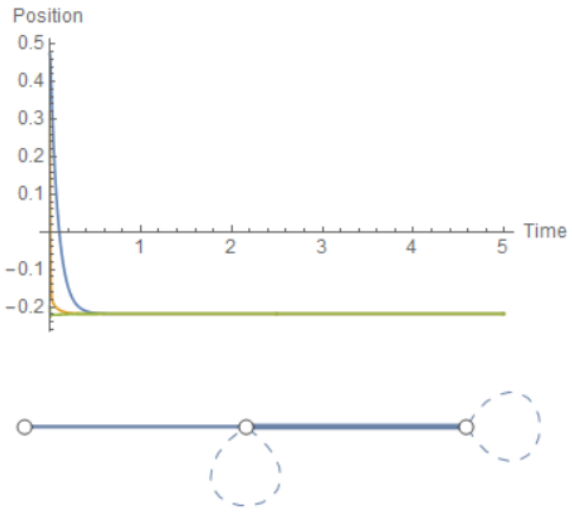

Figure 3.14: A consensus state of the Erdös-Rényi reduced model

2. Type 1 non-consensus state:

In this case, the origin V_0, as an extremist, stands significantly strongly on some matter, which corresponds to the blue curve in the top graph and the big black node in the bottom graph in Figure 3.15. Its two generations take opposite and weaker positions as they move away from V_0. In fact, we have already observed this state for the full model as shown in Figure 3.11.

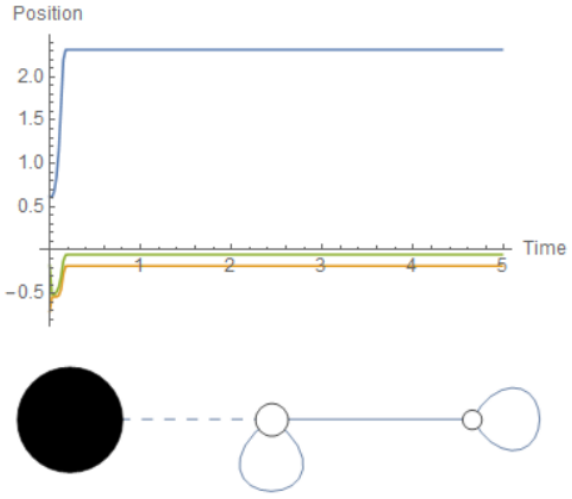

Figure 3.15: Type 1 non-consensus state of the Erdös-Rényi reduced model

3. Type 2 non-consensus state:

Compared with the above non-consensus state, type 2 non-consensus state that we describe here occurs much less often in our numerical experiments. In this state, our origin V_0 has a group of devoted followers constituting its first generation. They stand positively and strongly to a similar

extent on some issue, which are associated with the yellow and blue curves in the top graph and the two black nodes in the bottom graph in Figure 3.16. The actors in the second generation, however, take a weak negative position represented by the green curve and the node with the smallest size.

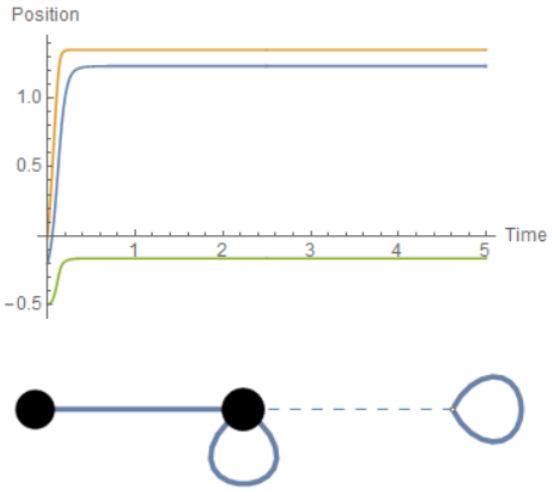

Figure 3.16: Type 2 non-consensus state of the Erdös-Rényi reduced model

For each of the three stable states presented above, the original model has a correspondent state on the full Erdös-Rényi graph with n vertices. To examine whether our mean-field reduced model is a valid approximation of the original full model, we will explore the relation between the variance of opinions $\nu^2 = P - Q^2$ and the probability of the occurrence of each stable state for both our reduced model and the full model.

All simulations are conducted on an Erdös-Rényi graph ER(n, q) with $n = 20$ and $q = 0.5$. We vary the variance of opinions by fixing $Q = 1$ and change the value of P from 1.1 to 5 at a step size of 0.1. For the reduced model, we run 5000 realizations for each value of P on the gradient vector field (3.60)-(3.61) with each realization initializing from a state that satisfies constraints (3.55)-(3.57). And then we compute the ratio of the occurrence of non-consensus states over all stable steady states. For the full model, however, since the system grows dramatically as the number of vertices increases and the simulation then can be intensely time-consuming, we run 100 realizations instead of 5000 on the gradient vector field (3.9)-(3.10) for each value of P. The results are shown in Figure 3.17 and Figure 3.18 as below.

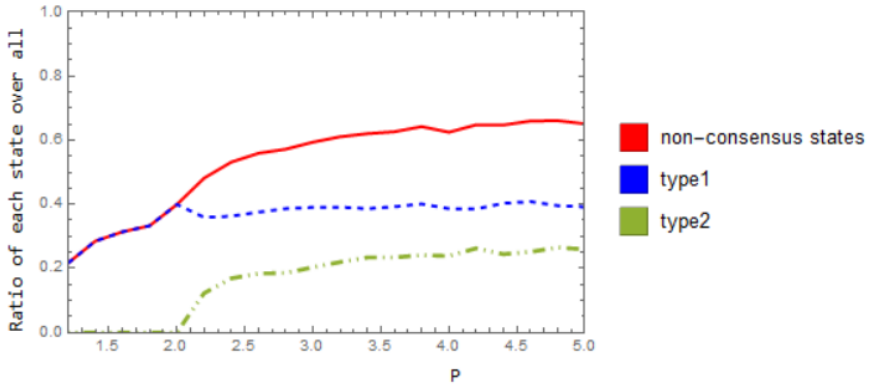

Figure 3.17: Occurrences of non-consensus states for the Erdös-Rényi reduced model

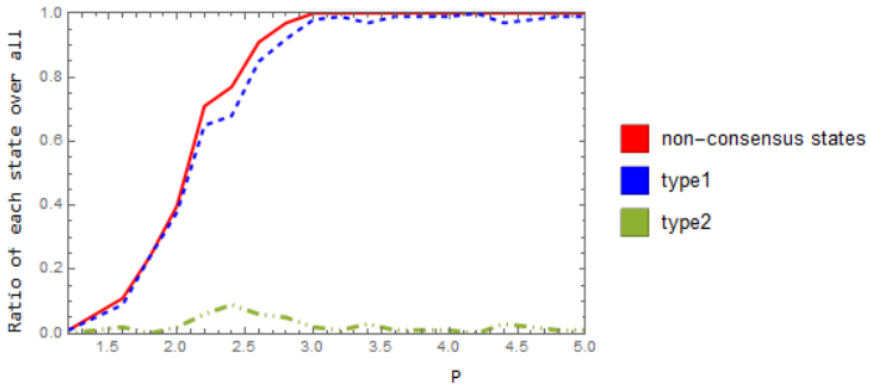

Figure 3.18: Occurrences of non-consensus states for the Erdös-Rényi full model

Several useful observations can be made from the above two figures:

1. As the opinion variance increases, not surprisingly, the frequency that non-consensus states occur rises. In other words, the dynamical system tends to be asynchronous when people's opinions vary much.
2. The type 2 non-consensus states always occur less than the type 1 for both the reduced and the full models. This implies that type 1 non-consensus state yields a more negative Dirichlet energy.
3. For the reduced model, only type 1 non-consensus state exists in a small range of opinion variance; the type 2 non-consensus state arises when the variance is larger than 1 and since then both of these two types of states co-exist. For the full model, however, the type 2 non-consensus state always rarely shows up whatever the value of the opinion variance is.

What we find amazing here is that although we have substantially reduced the large dimensionality of our model to a very small one, the reduced model and the full model share the same set of stable steady states. Meanwhile, it is worth noting that Figure 3.17 and Figure 3.18 display

quantitatively different behaviors on these states. This might be caused by their different initial distributions on the positions. To quantitatively approximate the full model, further adjustments or perhaps a brand new approach is needed, but the analysis process is expected to be much harder than what we proposed in this chapter.

3.4. Conclusion

In this chapter, we propose two approaches to analyze steady states on a simple social network: automorphism reduction method and "nearest-neighbor" mean-field analysis. Both approaches aim to solve the problem of the curse of dimensionality: as the size of the network grows large, the cost of simulation will become absurdly expensive and analytical assessments will be rather difficult. The first approach applies to graphs with a highly symmetric structure such as the Petersen graph and results in a dimension reduction with the aid of the graph automorphism. The second approach applies to large asymmetric systems such as the Erdös-Rényi random networks. It manages to reduce the dimensionality of the whole system to only a few, and the numerical results show that the behaviors on stable steady states of the reduced model and the full model agree qualitatively. However, they do not agree quantitatively: the frequencies of each type of steady state's occurrence do not perfectly match. This is not much out of our expectation due to the different distributions on the initial positions of the full and the reduced models. For a better understanding, further research is required.

So far, whichever underlying graph of our model, we always assumed a simplex relationship embedding, i.e. a single-layer network. However, in reality, reducing a social network to a graph in which actors interact in a pairwise fashion by only a single type of relationship is far from enough to accurately represent a real system. For this reason, researchers started to study social networks with a complex structure in the last twenty years. Such a network has been generally referred to as "multilayer network". We will explore how the multi-layer structure affects the synchronization of the whole dynamical system in the next two chapters.

Chapter 4

Synchronization on Node-aligned Multilayer Networks

4.1. Background

Before the birth of the complex network theory, traditional single-layer network representation was generally used to describe a dynamical system. However, people gradually realized that such representation is an over-simplification of many real-world problems [56]. Multilayer networks, on the other hand, can incorporate multiple channels of connectivity and constitute the natural environment to describe systems interconnected across different types of connections: each channel (relationship, activity, category) is represented by a layer and the same node may have various kinds of interactions (different set of neighbors in each layer) [57]. For instance, in a social network, social interactions rarely occur on a single channel and several relationships may bind individual pairs [56]. Disease transmission, which involves different spreading channels and disease mutations, is another typical example. Wang and five more authors [58] explored the processes of the coevolution and interactions between information and disease transmission by using actual information and a proposed multiplex network spread model. Jiang and Zhou [59] studied the resource control of epidemic spreading through a multilayer network and found that a significantly large amount of the total population may be infected (i.e., an outbreak will occur) if the amount of resource is below a threshold. Not only in biology, researchers have also made progress in the traffic dynamics on multilayer networks. One main intention is to improve the transportation performance by optimizing the topology structures and routing strategies of the network. Recently Wu *et al.* [60] published a survey on the past work of complex traffic dynamic models. One may be able to form a better perspective on the traffic flow on a multilayer network after reading the next chapter. In the current chapter, we will mainly focus on the topology of inter-layer connections and explore how it will affect the synchronization of the whole dynamic.

In the last two decades, a large amount of study has been conducted on dynamical systems with multiple layers of connectivity. However, the inconsistency of the usage of terminology arose a great confusion at the initial stage of research until a general framework for multilayer networks was brought up in Kivela's paper [61] in 2014. In the same year, Boccaletti *et al.* [57] gave a more straightforward definition of a multilayer network in a comprehensive review, which we will use in this chapter. For more details, we refer the interested readers to the books by Newman [62] and Barabási [63].

Definition 4.1. *A **multilayer network** is a pair* $\mathcal{M} = (\mathcal{G}, \mathcal{C})$ *where* $\mathcal{G} = \{G_\alpha : \alpha \in \{0, 1, ..., M-1\}, M \geq 2\}$ *is a family of graphs* $G_\alpha = (V_\alpha, E_\alpha)$ *(called layers of* $\mathcal{M}$*) and* $\mathcal{C} = \{E_{\alpha\beta} \subseteq V_\alpha \times V_\beta : \alpha, \beta \in \{0, 1, ..., M-1\}, \alpha \neq \beta\}$ *is a set of interconnections between nodes of different layers* G_α *and*

*G_β. The set V_α contains all the nodes in the αth layer and E_α contains all the edges. The elements of $\mathcal{C}$ are called **crossed layers**, and the elements of each E_α are called **intra-layer** connections of $\mathcal{M}$ while the elements of each $E_{\alpha\beta}(\alpha \neq \beta)$ are called **inter-layer** connections.*

Definition 4.2. *If a multilayer network satisfies two extra conditions where $V_0 = V_1 = ... = V_{M-1} = V$ and the only possible type of the inter-layer connections are those in which a given node is only connected to its counterpart nodes in **all** the rest of layers, i.e., $E_{\alpha\beta} = \{(x, x) : x \in V\}$ for every $\alpha, \beta \in \{0, 1, ..., M-1\}, \alpha \neq \beta$, then we call it a **multiplex network**. If the second condition is weakened from all the rest of layers to some of them (i.e., not all layers are necessarily to be connected), then we call it a **node-aligned multilayer network**.*

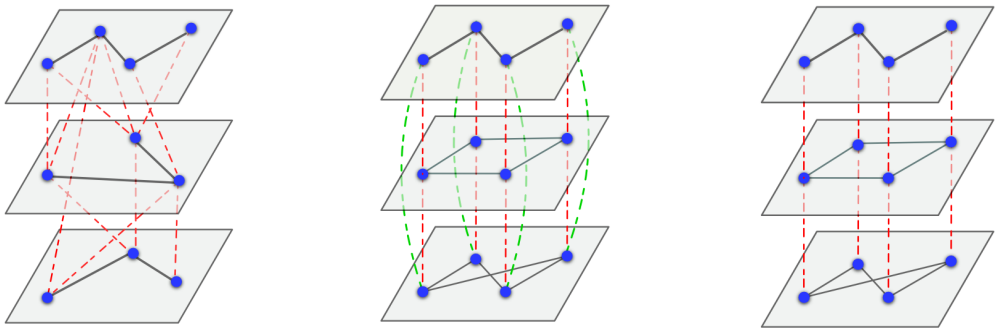

(a) (b) (c)

Figure 4.1: (a) A multilayer network; (b) A multiplex network; (c) A node-aligned multilayer network

Laplacian matrix, as an important tool to understand both the topology of a graph and the dynamics defined on it, is ubiquitously used in the field of geometry and dynamical systems. Similarly, for multilayer graphs, we can define a corresponding supra-Laplacian matrix:

Definition 4.3. *Suppose $\mathcal{G}$ is a multilayer graph with M layers. The supra-Laplacian $\mathcal{L}$ of $\mathcal{G}$ is separated into two contributions:*

$$\mathcal{L} = \mathcal{L}^L + \mathcal{L}^D = \bigoplus_{\alpha=1}^{M} L^{(\alpha)} + \mathcal{L}^D, \tag{4.1}$$

where $\mathcal{L}^L$ is the Laplacian matrix representing the intra-layer topology and $\mathcal{L}^D$ the inter-layer topology. The symbol $\bigoplus$ refers to the direct sum of matrices and $L^{(\alpha)}$ refers to the Laplacian of the graph on the αth layer. In particular, if $\mathcal{G}$ is a node-aligned multilayer network and each layer consists of N nodes, then the supra-Laplacian matrix is

$$\mathcal{L} = \mathcal{L}^L + \mathcal{L}^D = \bigoplus_{\alpha=1}^{M} L^{(\alpha)} + L^D \otimes I_{N\times N}. \tag{4.2}$$

If additionally each layer of $\mathcal{G}$ shares the same structure, i.e., $G_0 = G_1 = ... = G_{M-1}$, then we have $L^{(0)} = L^{(1)} = ... = L^{(M-1)} = L$ which results in

$$\mathcal{L} = \mathcal{L}^L + \mathcal{L}^D = I_{M\times M} \otimes L + L^D \otimes I_{N\times N}, \tag{4.3}$$

where $\otimes$ refers to the Kronecker product of matrices.

To make the definition more clear, we present a geometric interpretation of the supra-Laplacian matrix as in Figure 4.2 for a node-aligned multilayer network with 3 layers and 3 nodes on each layer.

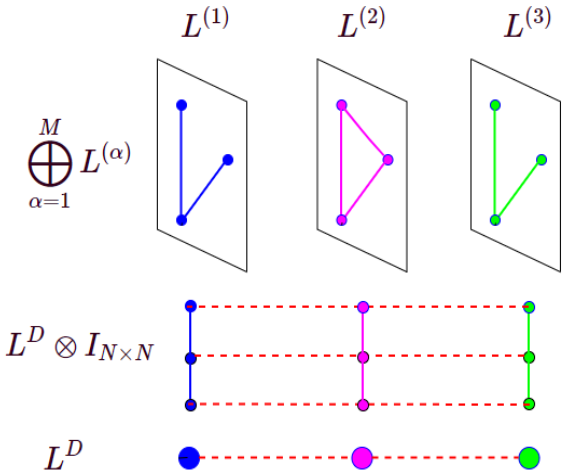

Figure 4.2: An interpretation of the supra-Laplacian matrix when $M = 3$ and $N = 3$.

One can show directly from the definition of supra-Laplacian matrix and the definition of eigenvalues/eigenvectors that the following theorem holds for any node-aligned multilayer networks with the same topology on each layer.

Theorem 4.4. *If $\vec{w}$ is an eigenvector of L with eigenvalue λ and $\vec{v}$ is an eigenvector of L^D with eigenvalue μ, i.e., $L\vec{w} = \lambda\vec{w}$ and $L^D\vec{v} = \mu\vec{v}$, then for the supra-Laplacian matrix $\mathcal{L} = I_{M\times M} \otimes L + L^D \otimes I_{N\times N}$, the eigenvector is*

$$\vec{x} = \begin{bmatrix} v_1\vec{w} \\ v_2\vec{w} \\ \vdots \\ v_M\vec{w} \end{bmatrix}$$

and the corresponding eigenvalue is $\lambda + \mu$, where v_i is the ith component of the vector $\vec{v}$.

Definition 4.5. *Given a matrix M, define $n_+(M)$, $n_-(M)$ and $n_0(M)$ as the number of positive, negative and zero eigenvalues of M respectively. The inertia of a matrix is defined as a tuple (n_+, n_0, n_-).*

The goal of this chapter is to study how the inter-layer connections will enhance or impede the phase-locking of the whole system. Computing the eigenvalues of the supra-Laplacian matrix $\mathcal{L}$ is essential to answer this question. In particular, for a node-aligned multilayer network with the same structure on each layer, according to Theorem 4.4, it boils down to examining the inertia of the matrix L^D. If L^D exists at least one positive eigenvalue, i.e., $n_+(L^D) > 0$, then the phase-locking states will be desynchronized/destabilized. If L^D exists no positive eigenvalues, i.e., $n_+(L^D) = 0$, then the largest eigenvalue of $\mathcal{L}$ is the same as which of $\mathcal{L}^L$, which implies the inter-layer connections do not qualitatively affect the system synchronization/stability.

Throughout the whole chapter, we will consider a node-aligned multilayer network $\mathcal{G}$ with M layers $\{G_0, G_1, ..., G_{M-1}\}$ and each layer consists of N nodes following the same Kuramoto dynamic. More precisely, the phase of the ith oscillator on the αth layer satisfies the equation

$$\frac{d\theta_i^\alpha}{dt} = \omega_i + \sum_{j:j\sim i} \gamma_{ij} \sin(\theta_j^\alpha - \theta_i^\alpha) + \sum_{\beta:(\alpha,\beta)\in E} \tau \sin(\theta_i^\beta - \theta_i^\alpha) \tag{4.4}$$

for $i \in \{1, 2, ..., N\}$ and $\alpha \in \{0, 1, ..., M-1\}$. Here, all the constants: ω_i, the natural frequency of the ith oscillator; γ_{ij}, the intra-layer coupling strength between the ith and jth oscillators; and τ, the inter-layer coupling strength, are all independent of the layers. In other words, the structure of each layer is identical, which will make the eigenvalue analysis procedure mathematically tractable. Furthermore, for the first summation, the subscript $j : j \sim i$ refers to the indices of the oscillators that are on the same layer with the ith oscillator and are connected to it; for the second summation, E in the subscript refers to the set consisting of all the pairs (α, β) if the αth and βth layers are connected. Hence the first summation represents the intra-layer connections while the second the inter-layer connections. We will, w.l.o.g., always assume $\tau = 1$.

Finding the phase-locked solution of Equation (4.4) and exploring the effect of the inter-layer connections on its stability is generally hard. For instance, if the inter-layer connections form a cycle, many stable phase-locked states may exist, but as one adds more edges in the graph, namely adding more pairs in E, the stable states either go away or becomes unstable. Fortunately, for specific inter-layer topologies, one can prove the existence of twisted phase-locked states (will be defined later) and computing the eigenvalues of the Jacobian of Equation (4.4) at such states is feasible. In this chapter we will mainly discuss two inter-layer topologies that allow twisted states:

- A complete graph, i.e., E contains all pairs of layers.
- A cycle-tree graph, i.e. a graph containing only cycles and the cycles are connected in a tree.

For the first scenario, the multilayer network becomes a multiplex network with an additional condition that all layers share the same structure. This is the easiest possible multilayer topology. We will discuss it in the next section. For the second scenario, the layers are only connected in cycles and no cycles share the same edge. To conclude on the inter-layer effect of such a graph, we follow a path from the simplest case, a single cycle, to a graph with multiple cycles connecting with

a single hub that we call a cycle-flower, and finally to a general cycle-tree graph. We will discuss it in the third section. At any above scenario, the Jacobian of Equation (4.4) at the twisted states is a supra-Laplacian matrix with a simple structure:

$$\mathcal{L} = I_{M\times M} \otimes L + L^{\mathrm{D}} \otimes \mathrm{I}_{N\times N}.$$

Finding eigenvalues of L^D, or more specifically, $n_+(L^D)$, then becomes a primary task. For the complete or single cycle inter-layer topology, the eigenvalue computation is straightforward. For the cycle-flower graph, we will conduct perturbation analysis on a rank-one-perturbed matrix to approximate the eigenvalues. For the cycle-tree graph, however, we will instead seek help from algebraic graph theory since the increasing rank of perturbation will make the normal perturbation analysis hard.

4.2. Complete Inter-layer-connected Multilayer Networks

In this section, we consider a multilayer Kuramoto system with complete inter-layer connections, i.e. a multiplex Kuramoto model, the dynamic (4.4) then becomes

$$\frac{d\theta_i^\alpha}{dt} = \omega_i + \sum_{j:j\sim i} \gamma_{ij} \sin(\theta_j^\alpha - \theta_i^\alpha) + \sum_{\beta\neq\alpha} \sin(\theta_i^\beta - \theta_i^\alpha) \tag{4.5}$$

for $i \in \{1, 2, ..., N\}$ and $\alpha \in \{0, 1, ..., M-1\}$. An example of complete inter-layer connections is depicted in Figure 4.3 as below.

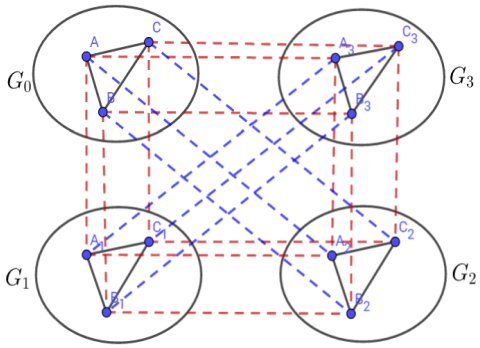

Figure 4.3: An example of a four-layer multiplex network.

Suppose θ_i^0 is a solution on layer zero (i.e., $\alpha = 0$) that satisfies

$$\frac{d\theta_i^0}{dt} = \omega_i + \sum_{j:j\sim i} \gamma_{ij} \sin(\theta_j^0 - \theta_i^0) \tag{4.6}$$

for $i \in \{1, 2, ..., N\}$, then the twisted state defined as

$$\theta_i^\alpha = \theta_i^0 + \frac{2\alpha q\pi}{M}, \ \alpha = 0, 1, ..., M-1 \tag{4.7}$$

is a solution of Equation (4.5) for any winding number $q \in \mathbb{Z}$. The Jacobian at this solution is a supra-Laplacian matrix $\mathcal{L} = I_{M\times M} \otimes L + L^D \otimes I_{N\times N}$, where the entry at the ith row and jth column of L is

$$L_{ij} = \begin{cases} -\sum\limits_{k:k\sim i} \gamma_{ik} \cos(\theta_k^\alpha - \theta_i^\alpha), & i = j \\ \gamma_{ij} \cos(\theta_j^\alpha - \theta_i^\alpha), & i \sim j \end{cases} \tag{4.8}$$

with $i \sim j$ meaning the ith and jth nodes are connected in the graph, and the entry at the $(\alpha+1)$th row and $(\beta+1)$th column of L^D is

$$L^D_{\alpha+1,\beta+1} = \begin{cases} -\sum\limits_{\phi\neq\alpha} \cos(\theta_1^\phi - \theta_1^\alpha), & \alpha = \beta \\ \cos(\theta_1^\beta - \theta_1^\alpha), & \alpha \neq \beta \end{cases} \tag{4.9}$$

$$= \begin{cases} 1, & \alpha = \beta \\ \cos(\frac{2q\pi(\beta-\alpha)}{M}). & \alpha \neq \beta \end{cases} \tag{4.10}$$

Here, from Equation (4.9) to (4.10), we used the fact that $\sum_{i=0}^{M-1} \cos(2q\pi i)/M = 0$.

Theorem 4.6. *The eigenvalues of $\mathcal{L}$ at the twisted states (4.7) are*

$$\begin{aligned} \lambda_{ik} &= \lambda_i, \quad k \in \{1, 2, ..., M-2\} \\ \lambda_{ik} &= \lambda_i + M/2, \quad k = M-1, M, \end{aligned} \tag{4.11}$$

for any $i \in \{1, 2, ..., N\}$ regardless of the value of the winding number q, where λ_i is an eigenvalue of the Laplacian L. Therefore, $\lambda_{\max}(\mathcal{L}) > \lambda_{\max}(L)$, which implies the inter-layer connections always destabilize the twisted states.

The proof of Theorem 4.6 follows directly from the following two lemmas.

Lemma 4.7. *The rank of the Laplacian matrix L^D is two.*

Proof. To prove $\text{rank}(L^D) = 2$, it suffices to make an observation that

$$L^D = v \otimes v + w \otimes w$$

where

$$v = \begin{bmatrix} \sin(\theta_1^0) \\ \sin(\theta_1^1) \\ \vdots \\ \sin(\theta_1^{M-1}) \end{bmatrix} \text{ and } w = \begin{bmatrix} \cos(\theta_1^0) \\ \cos(\theta_1^1) \\ \vdots \\ \cos(\theta_1^{M-1}) \end{bmatrix}.$$

■

Lemma 4.8. *Suppose* $\lambda_1 \leq \lambda_2 \leq ... \leq \lambda_{M-1} \leq \lambda_M$ *are eigenvalues of* L^D*, then* $\lambda_1 = \lambda_2 = ... = \lambda_{M-2} = 0$ *and* $\lambda_{M-1} = \lambda_M = \frac{M}{2}$.

Proof. By Lemma 4.7, we know $M-2$ eigenvalues are zero eigenvalues. To compute the remaining two non-zero eigenvalues, we firstly find the eigenvalues of $v \otimes v$ and $w \otimes w$ separately. W.l.o.g., assume $\theta_1^0 = 0$, then

$$v = \begin{bmatrix} 0 \\ \sin(\frac{2q\pi}{M}) \\ \sin(\frac{4q\pi}{M}) \\ \vdots \\ \sin(\frac{2q(M-1)\pi}{M}) \end{bmatrix} \text{ and } w = \begin{bmatrix} 0 \\ \cos(\frac{2q\pi}{M}) \\ \cos(\frac{4q\pi}{M}) \\ \vdots \\ \cos(\frac{2q(M-1)\pi}{M}) \end{bmatrix}.$$

Since the trace of $v \otimes v$ is

$$\begin{aligned} Tr(v \otimes v) &= \sum_{\alpha=1}^{M-1} (\sin(\frac{2q\alpha\pi}{M})^2) = \sum_{\alpha=1}^{M-1} \frac{1}{2} \left(1 - \cos(\frac{4q\alpha\pi}{M})\right) \\ &= \frac{1}{2}(M-1) - \frac{1}{2} \sum_{\alpha=1}^{M-1} \cos(\frac{4q\alpha\pi}{M}) = \frac{M}{2}, \end{aligned}$$

the unique non-zero eigenvalue of $v \otimes v$ is $\frac{M}{2}$. Similar computation shows that $\frac{M}{2}$ is also the unique non-zero eigenvalue of $w \otimes w$. Also, notice that v is orthogonal to w since $v \cdot w = \sum_{\alpha=0}^{M-1} \sin(\frac{2q\alpha\pi}{M}) \cos(\frac{2q\alpha\pi}{M}) = 0$. It is not hard to show that if $\vec{z}$ is an eigenvector of $w \otimes w$ corresponding to its non-zero eigenvalue, then it is an eigenvector of $v \otimes v$ corresponding to its zero eigenvalue. In fact, note that $w \otimes w = ww^T$ and $v \otimes v = vv^T$. For a vector $\vec{y} = ww^T\vec{x}$ where $\vec{x}$ is any $M \times 1$ non-zero vector, we have

$$ww^T\vec{y} = w(w^Tw)w^T\vec{x} = \sum_{\alpha=1}^{M-1} \left(\sin(\frac{2q\alpha\pi}{M})\right)^2 ww^T\vec{x} = \frac{M}{2}(ww^Tx) = \frac{M}{2}\vec{y},$$

so that $\vec{y}$ is an eigenvector of $w \otimes w$ with an eigenvalue $\lambda = \frac{M}{2}$. Also,

$$vv^T\vec{y} = v(v^Tw)w^T\vec{x} = 0$$

shows that $\vec{y}$ is an eigenvalue of $v \otimes v$ with an eigenvalue $\lambda = 0$. Moreover, since rank$(w \otimes w)$=1, we have $\vec{z} = c\vec{y}$ for some constant c. We proved that for the non-zero eigenvalue $\lambda = \frac{M}{2}$, the corresponding eigenspaces of $w \otimes w$ and $v \otimes v$ are orthogonal. Therefore, $\lambda_{M-1} = \lambda_M = \frac{M}{2}$. ■

4.3. Cycle-tree Inter-layer-connected Multilayer Networks

In section 4.2, we proved that the complete inter-layer connections always destabilize the twisted phase-locked states of the multilayer Kuramoto system. In this section, however, we consider a system where the inter-layer graph contains only cycles and all cycles are connected in a tree. Especially, for the twisted states with the winding number $q = 1$, we conclude that the inter-layer connections destabilize the system only if there exists at least one cycle containing less than four layers.

To validate our conclusion, we will walk the following path, illustrated in Figure 4.4, from the most specific case to the most general one: first, we consider a simple single cycle and compute its eigenvalues directly; then we study a cycle flower and find eigenvalues by perturbation analysis; eventually, we take into the account a cycle tree and compute the corresponding eigenvalues with the help of algebraic graph theory.

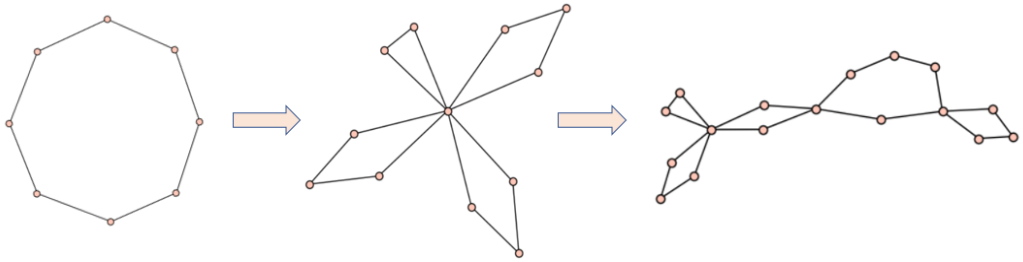

Figure 4.4: Walk-through: a single cycle → a cycle flower → a cycle tree.

Indeed, a single cycle and a cycle flower are special cases of a cycle tree, where the results that hold for a cycle tree apply automatically. The aforementioned workflow alleviated the difficulty of studying the general case directly, and hence leading to a clearer argument.

4.3.1. *A Single Cycle*

When all layers are connected in a cycle, i.e., $E = \{(\alpha, \beta) : \alpha \in \{0, 1, ..., M-1\}, \beta = (\alpha \pm 1) \bmod M\}$, the phase of the ith oscillator on the αth layer satisfies the dynamic

$$\frac{d\theta_i^\alpha}{dt} = \omega_i + \sum_{j:j\sim i} \gamma_{ij} \sin(\theta_j^\alpha - \theta_i^\alpha) + \left(\sin(\theta_i^{\beta_1} - \theta_i^\alpha) + \sin(\theta_i^{\beta_2} - \theta_i^\alpha)\right) \tag{4.12}$$

for $i \in \{1, 2, ..., N\}$ and $\alpha \in \{0, 1, ..., M-1\}$, where $\beta_1 = (\alpha+1) \bmod M$ and $\beta_2 = (\alpha-1) \bmod M$. Similarly as the complete graph case discussed above, one can check that the twisted state

$$\theta_i^\alpha = \theta_i^0 + \frac{2\alpha q\pi}{M}, \ i \in \{1, 2, ..., N\} \text{ and } \alpha = 0, 1, ..., M-1 \tag{4.13}$$

is a solution of Equation (4.12) for any $q \in \mathbb{Z}$, where θ_i^0 corresponding to the phase of the ith oscillator on layer zero satisfies $\dot{\theta_i^0} = \omega_i + \sum \gamma_{ij} \sin(\theta_j^0 - \theta_i^0)$. Then for the supra-Laplacian at this state $\mathcal{L} = I_{M\times M} \otimes L + L^D \otimes I_{N\times N}$, the entry at the $(\alpha+1)$th row and $(\beta+1)$th column of matrix L^D is

$$L^D_{\alpha+1,\beta+1} = \begin{cases} -2\cos(\frac{2q\pi}{M}), & \alpha = \beta \\ \cos(\frac{2q\pi}{M}), & \beta = (\alpha \pm 1) \bmod M \\ 0, & \text{else.} \end{cases} \tag{4.14}$$

Let $a = \cos(\frac{2q\pi}{M})$, then $L^D = -aL^D_M$ where

$$L^D_M := \begin{bmatrix} 2 & -1 & 0 & 0 & \dots & 0 & -1 \\ -1 & 2 & -1 & 0 & \dots & 0 & 0 \\ 0 & -1 & 2 & -1 & \dots & 0 & 0 \\ \vdots & \vdots & \vdots & \vdots & \ddots & \vdots & \vdots \\ -1 & 0 & 0 & 0 & \dots & -1 & 2 \end{bmatrix}$$

is a $M \times M$ toeplitz matrix.

Theorem 4.9. *For the twisted state (4.13) with a winding number $q \in \mathbb{Z}$, we have*
(1) If the multilayer network contains less than $4q$ layers and more than $\lceil \frac{4q}{3} \rceil$ layers, i.e., $\frac{4q}{3} < M < 4q$, then the inter-layer connections destabilize the system.
(2) If the multi-layer network contains at least $4q$ layers, i.e., $M \geq 4q$, then the inter-layer connections do not qualitatively affect the system stability.

Proof. The proof follows directly from the fact that the eigenvalues of the supra-Laplacian $\mathcal{L}$ at the twisted states are

$$\lambda_{ik} = \lambda_i - \cos(q\theta)\,(2 - 2\cos(k\theta)) \tag{4.15}$$

for $i \in \{1, 2, ..., N\}$ and $k \in \{0, 1, ..., \frac{M}{2}\}$, where $\theta = \frac{2\pi}{M}$ and λ_i is an eigenvalue of the Laplacian L. This fact can be derived immediately by combining the following lemma and Theorem 4.4. ■

Lemma 4.10. *The eigenvalues of L^D_M are $\lambda_k = 2 - 2\cos(\frac{2\pi k}{M})$ with eigenvectors*

$$x_n(k) = \sin(\frac{2\pi kn}{M})$$
$$y_n(k) = \cos(\frac{2\pi kn}{M})$$

where $x_n(k)$ or $y_n(k)$ denotes the nth component of the eigenvector associated with the eigenvalue λ_k and $0 \leq k \leq \frac{M}{2}$.

Proof. Suppose λ is an eigenvalue of L_M^D and $\vec{z}$ is an associated eigenvector, then we have

$$\begin{aligned} 2z_1 - z_2 - z_M &= \lambda z_1, \\ -z_1 - z_{M-1} + 2z_M &= \lambda z_M, \\ -z_{k-1} + 2z_k - z_{k+1} &= \lambda z_k,\ 1 \le k \le M-1, \end{aligned}$$

where z_n is the nth component of $\vec{z}$ for $n = 1, 2, ..., M$. As usual for such equations one seek the solution with the form $z_n = A^n$. Plugging this solution into the above equations gives us $A^M = 1$ so that $A_k = e^{\frac{2\pi k i}{M}}$. As a result, the kth eigenvalue and its associated eigenvector are

$$\begin{aligned} \lambda_k &= 2 - 2\cos(\frac{2\pi k}{M}), \\ z_n(k) &= A^{kn} = \cos(\frac{2\pi kn}{M}) + i\sin(\frac{2\pi kn}{M}),\ 1 \le n \le M. \end{aligned}$$

Since L_M^D and λ_k are real, $\vec{z}$ should be real, which implies both the real and imaginary parts of $\vec{z}$ are invariant under L_M^D. Therefore, $x_n(k) = \cos(\frac{2\pi kn}{M})$ and $y_n(k) = \sin(\frac{2\pi kn}{M})$ serve as the nth component of the eigenvectors associated with $\lambda_k = 2 - 2\cos(\frac{2\pi k}{n})$ for $0 \le k \le \frac{M}{2}$. More precisely, when M is odd, we have one eigenvector $\vec{x}(0)$ for $\lambda_0 = 0$ ($\vec{y}(0) = \vec{0}$), and two eigenvectors $\vec{x}(k)$ and $\vec{y}(k)$ for all $0 < k < \frac{M}{2}$; when M is even, we have one eigenvector $\vec{x}(0)$ for $\lambda_0 = 0$ ($\vec{y}(0) = \vec{0}$), two eigenvectors $\vec{x}(k)$ and $\vec{y}(k)$ for all $0 < k < \frac{M}{2}$ and one eigenvector $\vec{x}(\frac{M}{2})$ for $\lambda_{\frac{M}{2}} = 4$ ($\vec{y}(\frac{M}{2}) = \vec{0}$). ■

Example 4.11. In this example, we consider a node-aligned multilayer Kuramoto network with 3 layers connected in a cycle and each layer consists of 20 oscillators, i.e., $M = 3$ and $N = 20$. More precisely, we have

$$\frac{d\theta_i^\alpha}{dt} = \omega_i + \sum_{j:j\sim i} \gamma_{ij}\sin(\theta_j^\alpha - \theta_i^\alpha) + \Big(\sin(\theta_i^{\beta_1} - \theta_i^\alpha) + \sin(\theta_i^{\beta_2} - \theta_i^\alpha)\Big) \tag{4.16}$$

for $i \in \{1, 2, ..., 20\}$ and $\alpha \in \{0, 1, 2\}$, where $\beta_1 = (\alpha + 1) \bmod 3$ and $\beta_2 = (\alpha - 1) \bmod 3$. For convenience, assume $\gamma_{ij} = 1$ for any $i, j \in \{1, 2, ..., 20\}$. The natural frequencies $\omega_1, \omega_2, ..., \omega_{20}$ are chosen to be uniform random variables in the range of $[0, 1.6]$. We first ignore the last term in the right hand-side of the above equation, or in other words, we only consider the intra-layer connections. Then the phase of oscillators on each layer satisfies

$$\frac{d\theta_i}{dt} = \omega_i + \sum_{j:j\sim i} \sin(\theta_j - \theta_i) \tag{4.17}$$

for $i \in \{1, 2, ..., N\}$. Solving this gradient flow numerically gives us a phase-locked solution. The straight lines in Figure 4.5 represent the evolution of the 20 oscillators' phases as time t increases from 0 to 100. It is clear that all oscillators move at a common frequency.

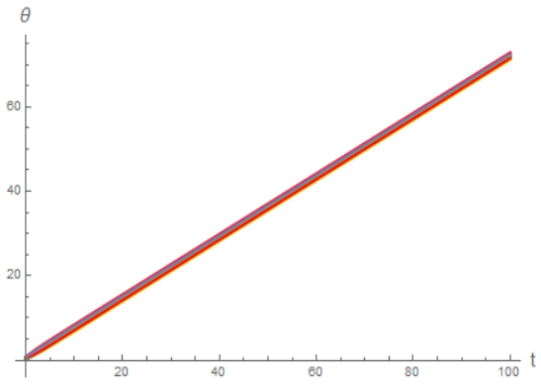

Figure 4.5: Evolution of oscillators' phases on a single layer

Let θ_i for $i \in \{1, 2, ..., 20\}$ denote this phase-locked solution, then $\theta_i^\alpha = \theta_i + 2\alpha\pi/3$ for $i \in \{1, 2, ..., 20\}$ and $\alpha \in \{0, 1, 2\}$ is a solution of Equation (4.16). We then compare the eigenvalues of the intra-layer matrix $\mathcal{L}^L$ associated with θ_i and the eigenvalues of the full matrix $\mathcal{L}$ associated with θ_i^α. The result is shown as below.

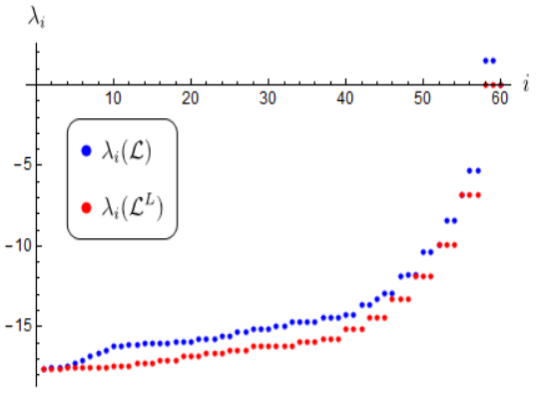

Figure 4.6: A comparison between eigenvalues of $\mathcal{L}$ and $\mathcal{L}^L$

In Figure 4.6, the x-axis represents the indices of eigenvalues and the y-axis represents the eigenvalues themselves. Clearly, $\lambda(\mathcal{L}^L) \leq \lambda(\mathcal{L})$. In fact, all eigenvalues of $\mathcal{L}^L$ are non-positive so without the inter-layer connections we have a stable solution. However, with the inter-layer connections, $\mathcal{L}$ has positive eigenvalues implying the system following Equation (4.16) is not stable anymore. Therefore, this example shows that the inter-layer connections destabilize the system when $M = 3$.

4.3.2. *A Cycle Flower*

In this part, we consider a flower-like graph. Instead of all layers connecting in a single cycle as discussed above, they now form multiple cycles linked with a single hub, which we call a **cycle flower**. More precisely, given M layers $G_0, G_1, ..., G_{n_1-1}, G_{n_1+1}, ..., G_{n_2-1}, ..., G_{n_{l-1}+1}, ..., G_{n_l-1}$,

suppose layers $G_0, G_1, ..., G_{n_1-1}$ are connected in a cycle C_1, $G_0, G_{n_1+1}, ..., G_{n_2-1}$ in a cycle C_2, $\cdots\cdots$, and $G_0, G_{n_{l-1}+1}, ..., G_{n_l-1}$ in a cycle C_l, i.e., $E = E_1 \cup E_2 \cup E_3 \cup E_4$ where

$$
\begin{aligned}
E_1 &= \{(\alpha, \beta) : n_{i-1} + 2 \leq \alpha \leq n_i - 2, \beta = \alpha \pm 1, i = 1, 2, ..., l\}, \\
E_2 &= \{(\alpha, \beta) : \alpha = 0, \beta = n_{i-1} + 1 \text{ or } n_i - 1, i = 1, 2, ..., l\}, \\
E_3 &= \{(\alpha, \beta) : \alpha = n_{i-1} + 1, \beta = 0 \text{ or } \alpha + 1, i = 1, 2, ..., l\}, \\
E_4 &= \{(\alpha, \beta) : \alpha = n_i - 1, \beta = 0 \text{ or } \alpha - 1, i = 1, 2, ..., l\}.
\end{aligned}
$$

Here, the layer G_0 is a hub that connects all the cycles. Clearly, the ith cycle has $n_i - n_{i-1}$ nodes (assume $n_0 = 0$) for $i \in \{1, 2, ..., l\}$, and $M = 1+(n_1-1)+(n_2-n_1-1)+...+(n_l-n_{l-1}-1) = n_l-l+1$. An example with $l = 4$ cycles is shown as below.

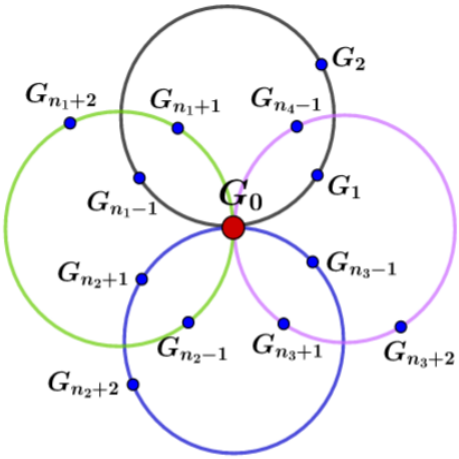

Figure 4.7: Four cycles with a single layer G_0 as a hub.

Same as before, assume θ_i^0 is a solution on layer zero (i.e., $\alpha = 0$) that satisfies $\frac{d\theta_i^0}{dt} = \omega_i + \sum_j \gamma_{ij} \sin(\theta_j^0 - \theta_i^0)$ for $i \in \{1, 2, ..., N\}$, then the twisted state

$$
\theta_i^{\alpha_j} = \theta_i^0 + \frac{2(\alpha_j - n_{j-1})q\pi}{n_j - n_{j-1}}, \quad n_{j-1} \leq \alpha_j \leq n_j - 1, \tag{4.18}
$$

serves as a solution of Equation (4.4) for $i \in \{1, 2, ..., N\}$ and $j \in \{1, 2, ..., l\}$, where q is an arbitrary fixed integer. Let

$$
a_j = \cos(\frac{2q\pi}{n_j - n_{j-1}}), \quad 1 \leq j \leq l, \tag{4.19}
$$

and f^{α_j} be the inter-layer coupling between the α_jth layer and other layers, i.e.,

$$
f^{\alpha_j} = \sum_{(\alpha_j, \beta) \in E} \sin(\theta^\beta - \theta^{\alpha_j}). \tag{4.20}
$$

Then for $\alpha_j \neq 0$ we have

$$\frac{df^{\alpha_j}}{d\theta^\beta} = \begin{cases} a_j, & \beta = \alpha_j \pm 1, n_{j-1} \leq \alpha_j \leq n_j - 1 \\ -2a_j, & \beta = \alpha_j, \end{cases} \tag{4.21}$$

and

$$\frac{df^0}{d\theta^\beta} = \begin{cases} a_j, & \beta = n_j - 1, j = 1, 2, ..., l \\ a_j, & \beta = n_j + 1, j = 0, 1, ..., l - 1 \\ -2 \sum_{k=1}^{l} a_k, & \beta = 0, \end{cases} \tag{4.22}$$

so that our Laplacian matrix L^D can be written as a block diagonal matrix plus a rank-two perturbation:

$$L^D = \begin{pmatrix} -2\sum_{k=1}^{l} a_k & & & & \\ & A_1 & & & \\ & & A_2 & & \\ & & & \ddots & \\ & & & & A_l \end{pmatrix} + \begin{pmatrix} 0 & a_1 & 0 & \cdots & a_l \\ a_1 & & & & \\ 0 & & & & \\ \vdots & & \mathbf{0} & & \\ a_l & & & & \end{pmatrix}$$

$$=: A + P, \tag{4.23}$$

where each diagonal block $A_j =$

$$a_j \begin{bmatrix} -2 & 1 & 0 & \dots & 0 \\ 1 & -2 & 1 & \dots & 0 \\ 0 & 1 & -2 & \dots & 0 \\ \vdots & \vdots & \vdots & \ddots & \vdots \\ 0 & 0 & 0 & \dots & -2 \end{bmatrix}$$

is a $(n_j - n_{j-1} - 1) \times (n_j - n_{j-1} - 1)$ tridiagonal matrix embodying the inter-layer connections within the jth cycle. The $M \times M$ matrix P embodies the inter-layer connections between the hub G_0 and all other layers, of which the entry at the ith row and jth column is

$$P_{ij} = \begin{cases} a_k, & i = 1, j = s_k \text{ or } e_k \\ a_k, & j = 1, i = s_k \text{ or } e_k \\ 0, & \text{else}, \end{cases} \tag{4.24}$$

where $s_k = n_{k-1} - k + 3$ and $e_k = n_k - k + 1$ for $k \in \{1, 2, ..., l\}$.

Example 4.12. In this example, we consider 7 layers of oscillators connected in 2 cycles with a single hub. Each cycle consists of 4 layers. The figure is shown below.

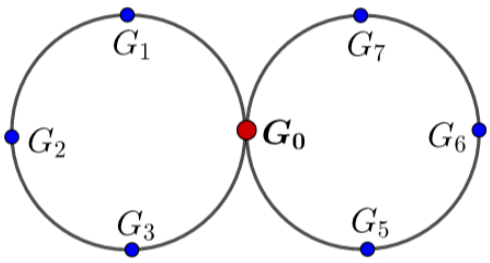

Figure 4.8: Two cycles with a single layer G_0 as a hub.

In this case, $n_0 = 0, n_1 = 4, n_2 = 8$ and $M = 1 + (n_1 - n_0 - 1) + (n_2 - n_1 - 1) = 1 + 3 + 3 = 7$. Let $a_1 = a_2 = \cos(\pi/2)$. The first cycle consists of $n_1 - n_0 = 4$ layers. The inter-layer connections among G_1, G_2 and G_3 are embodied in the matrix $A_1 =$

$$\begin{array}{c} \\ \boldsymbol{G_1} \\ \boldsymbol{G_2} \\ \boldsymbol{G_3} \end{array} \begin{array}{c} \begin{array}{ccc} \boldsymbol{G_1} & \boldsymbol{G_2} & \boldsymbol{G_3} \end{array} \\ \begin{bmatrix} -2a_1 & a_1 & 0 \\ a_1 & -2a_1 & a_1 \\ 0 & a_1 & -2a_1 \end{bmatrix} \end{array}.$$

Similarly, the second cycle consists of $n_2 - n_1 = 4$ layers. The inter-layer connections among G_5, G_6 and G_7 are embodied in the matrix $A_2 =$

$$\begin{array}{c} \\ \boldsymbol{G_5} \\ \boldsymbol{G_6} \\ \boldsymbol{G_7} \end{array} \begin{array}{c} \begin{array}{ccc} \boldsymbol{G_5} & \boldsymbol{G_6} & \boldsymbol{G_7} \end{array} \\ \begin{bmatrix} -2a_2 & a_2 & 0 \\ a_2 & -2a_2 & a_2 \\ 0 & a_2 & -2a_2 \end{bmatrix} \end{array}.$$

Finally, the inter-layer connections between the hub G_0 and all other layers are embodied in the following matrix:

$$\begin{array}{c} \\ \boldsymbol{G_0} \\ \boldsymbol{G_1} \\ \boldsymbol{G_2} \\ \boldsymbol{G_3} \\ \boldsymbol{G_5} \\ \boldsymbol{G_6} \\ \boldsymbol{G_7} \end{array} \begin{array}{c} \begin{array}{ccccccc} \boldsymbol{G_0} & \boldsymbol{G_1} & \boldsymbol{G_2} & \boldsymbol{G_3} & \boldsymbol{G_5} & \boldsymbol{G_6} & \boldsymbol{G_7} \end{array} \\ \begin{bmatrix} -2(a_1+a_2) & a_1 & 0 & a_1 & a_2 & 0 & a_2 \\ a_1 & & & & & & \\ 0 & & & & & & \\ a_1 & & & & & & \\ a_2 & & & & & & \\ 0 & & & & & & \\ a_2 & & & & & & \end{bmatrix} \end{array}.$$

Combining all these matrices gives us the Laplacian matrix $L^D = A + P$, which exhibits the complete inter-layer connections.

One can prove that the number of positive eigenvalues of L^D, $n_+(L^D)$, depends on the number of layers within each individual cycle:

Theorem 4.13. *Define a constant a to be*

$$a := \sum_{j=1}^{l} a_j = \sum_{j=1}^{l} \cos(\frac{2q\pi}{n_j - n_{j-1}}), \tag{4.25}$$

where l is the total number of cycles in a multilayer network with M layers. And define sets S_k as

$$S_k := \{j : n_j - n_{j-1} = k \text{ and } k/4 < (q \bmod k) < 3k/4\}, \tag{4.26}$$

for $3 \leq k \leq M$. Let $m_k = |S_k|$, i.e, m_k represents the number of cycles that contain k layers and satisfies $k/4 < (q \bmod k) < 3k/4$. Then for the Laplacian matrix L^D at the twisted state (4.18), we have

$$n_+(L^D) = \sum_{k=3}^{M} (k-1)m_k. \tag{4.27}$$

Moreover, the following inequality holds:

$$n_+(A) - 1 \leq n_+(L^D) \leq n_+(A), \tag{4.28}$$

or more precisely,

$$n_+(L^D) = n_+(A) \quad \text{if } a > 0, \tag{4.29}$$

$$n_+(L^D) = n_+(A) - 1 \quad \text{if } a < 0. \tag{4.30}$$

Notice that Theorem 4.13 implies $n_+(L^D) = 2m$ where $m = |\{j : n_j - n_{j-1} = 3\}|$ when considering the twisted solution with $q = 1$. The number of positive eigenvalues of L^D only depends on the number of cycles with 3 layers in this scenario. This gives the main result of this part as follows.

Theorem 4.14. *For the twisted state (4.18) with $q = 1$, we have*
(1) If there exists an cycle with less than four layers, i.e., $n_{j_0} - n_{j_0-1} < 4$ for some $j_0 \in \{1, 2, ..., l\}$, then the inter-layer connections desynchronize the system.
(2) If all cycles contain at least four layers, i.e., $n_j - n_{j-1} \geq 4$ for $j = 1, 2, ..., l$, then the inter-layer connections do not qualitatively affect the synchronization of the system.

We leave the proof of Theorem 4.13 for later after verifying several lemmas first as follows.

Lemma 4.15. *Except for one eigenvalue $-2\sum_{k=1}^{l} a_k$, all other eigenvalues of A are of the form*

$$\lambda_j^{k_j} = -a_j \left(2 - 2\cos(\frac{k_j\pi}{n_j - n_{j-1}})\right),$$

where $1 \leq k_j \leq n_j - n_{j-1} - 1$ *and* $1 \leq j \leq l$. *Particularly, for* $q = 1$, *if* $n_j - n_{j-1} \geq 4$ *for all* j, *then* A *is a negative semi-definite matrix.*

Proof. Applying the same argument as in Lemma 4.10, one should be able to prove that for each block matrix A_j, the eigenvalues are $\lambda_j^{k_j} = 2 - 2\cos(\frac{k_j\pi}{n_j - n_{j-1}})$ where $1 \leq k_j \leq n_j - n_{j-1} - 1$, with which the eigenvalues of A can be easily obtained. ■

Lemma 4.16. *The perturbation* P *is a rank-two matrix with two non-zero eigenvalues*

$$\lambda = \pm \left(2 \sum_{j=1}^{l} a_j^2 \right)^{\frac{1}{2}} = \pm \left(2 \sum_{j=1}^{l} \cos^2(\frac{2q\pi}{n_j - n_{j-1}}) \right)^{\frac{1}{2}}.$$

Proof. The matrix P being rank-two is obvious. In fact, P can be written as

$$P = v \otimes w + w \otimes v,$$

where $v = (1, 0, ..., 0)^T$ and $w = (0, a_1, ..., a_1, a_2, ..., a_l)^T$ are two $M \times 1$ vectors. More precisely, the ith components of the vectors v and w are

$$v_i = \begin{cases} 1, & i = 1 \\ 0, & \text{else}, \end{cases} \qquad w_i = \begin{cases} a_i, & i = s_i \text{ or } e_i \\ 0, & \text{else}, \end{cases}$$

where $s_k = n_{k-1} - k + 3$ and $e_k = n_k - k + 1$ for $k \in \{1, 2, ..., l\}$.
Plus, solving the characteristic polynomial function $\det(P - \lambda I) = 0$ directly gives P's eigenvalues. ■

Lemma 4.17. *Define a parameter family of operators* $L_t^D = A + tP$. *If* A *is invertible, then* $\det(L_t^D) = 0$ *as a function of* t *has two roots* $t = \pm 1$.

Proof. Clearly $\det(L_t^D)$ is a quadratic function with one root $t = 1$ since $L_1^D = L^D$ is a Laplacian matrix. So only the second root is to be determined. Note that L_t^D has a non-trivial kernel if there is a non-zero vector x such that $L_t^D x = 0$. Let $D = -A$ and replace P with $v \otimes w + w \otimes v$ in L_t^D where v and w are vectors defined in the proof of Lemma 4.16, then we have

$$-Dx + t(\langle v, x\rangle w + \langle w, x\rangle v) = 0. \tag{4.31}$$

Since A is invertible, so is D. Solving for x gives us

$$x = t(\langle v, x\rangle D^{-1} w + \langle w, x\rangle D^{-1} v). \tag{4.32}$$

Taking the inner product with v and w respectively gives

$$\langle v, x\rangle = t\left(\langle v, x\rangle\langle v, D^{-1}w\rangle + \langle w, x\rangle\langle v, D^{-1}v\rangle\right), \tag{4.33}$$

$$\langle w, x\rangle = t\left(\langle v, x\rangle\langle w, D^{-1}w\rangle + \langle w, x\rangle\langle w, D^{-1}v\rangle\right). \tag{4.34}$$

Let $b_1 = \langle v, x\rangle$ and $b_2 = \langle w, x\rangle$, then the above equations can be written in a matrix form as

$$M_t \begin{bmatrix} b_1 \\ b_2 \end{bmatrix} := \begin{bmatrix} t\langle v, D^{-1}w\rangle - 1 & t\langle v, D^{-1}v\rangle \\ t\langle w, D^{-1}w\rangle & t\langle w, D^{-1}v\rangle - 1 \end{bmatrix} \begin{bmatrix} b_1 \\ b_2 \end{bmatrix} = \begin{bmatrix} 0 \\ 0 \end{bmatrix}. \tag{4.35}$$

It is easy to show $b_1 \cdot b_2 \neq 0$. So M_t has a non-trivial kernel if and only if L_t^D has a non-trivial kernel, which leads to finding roots of $\det(M_t) = 0$. Let

$$\tau_1 = \langle v, D^{-1}w\rangle\langle w, D^{-1}v\rangle - \langle v, D^{-1}v\rangle\langle w, D^{-1}w\rangle, \tag{4.36}$$

$$\tau_2 = \langle v, D^{-1}w\rangle + \langle w, D^{-1}v\rangle. \tag{4.37}$$

Then direct calculation gives

$$\det(M_t) = t^2\tau_1 - t\tau_2 + 1. \tag{4.38}$$

Solving for t gives

$$t_{1,2} = \frac{\tau_2 \pm \sqrt{\tau_2^2 - 4\tau_1}}{2\tau_1}. \tag{4.39}$$

Notice that $\tau_1 < 0$ and $\tau_2 = 0$, so $t_{1,2} = \pm\sqrt{-\tau_1}/\tau_1$. Since we have argued $t = 1$ is a root of $\det(M_t) = 0$, $t = -1$ must be the other root, which completes our proof. ■

Now we are ready to prove Theorem 4.13.

Proof of Theorem 4.13. We first make an important observation. Recall we defined a_j as in Equation (4.19):

$$a_j = \cos(\frac{2q\pi}{n_j - n_{j-1}}) \quad 1 \leq j \leq l,$$

and S_k as in Equation (4.26):

$$S_k = \{j : n_j - n_{j-1} = k \text{ and } k/4 < (q \bmod k) < 3k/4\}.$$

Define $S = \bigcup_{k=3}^{M} S_k$. It is not hard to observe that $a_j < 0$ if $j \in S$. According to Lemma 4.15, the eigenvalue of A is either $-2a = -2\sum_{k=1}^{l} a_k$ or

$$\lambda_j^{k_j} = -a_j\left(2 - 2\cos(\frac{k_j\pi}{n_j - n_{j-1}})\right).$$

Thus, the number of positive eigenvalues of A satisfies

$$n_+(A) = \sum_{k=3}^{M}(k-1)|S_k| = \sum_{k=3}^{M}(k-1)m_k \quad \text{if } a > 0, \tag{4.40}$$

$$n_+(A) = \sum_{k=3}^{M}(k-1)|S_k| + 1 = \sum_{k=3}^{M}(k-1)m_k + 1 \quad \text{if } a < 0. \tag{4.41}$$

Now it suffices to find the relation between $n_+(A)$ and $n_+(L^D)$. Recall the parameter family of operators L_t^D as defined in Lemma 4.17 and the vectors v and w as defined in the proof of Lemma 4.16, we can rewrite L_t^D as

$$L_t^D = L^D + (t-1)P = L^D + (t-1)(v \otimes w + w \otimes v). \tag{4.42}$$

We want to detect whether the eigenvalues of L_t^D cross from the left half-plane to the right half-plane or in the opposite direction near $t = 1$ to track the count of positive eigenvalues. Clearly, $L_0^D = A$ and $L_1^D = L^D$. We know L^D has a zero eigenvalue associated with an all-ones eigenvector $\vec{\mathbf{1}}$. Suppose $\lambda_0 = 0$ and $v_0 = \vec{\mathbf{1}}$, then by perturbation theory,

$$\frac{d\lambda_0}{dt}\Big|_{t=1} = \frac{\langle v_0, (\frac{dL_t^D}{dt}|_{t=1})v_0\rangle}{\|v_0\|^2} = \frac{\langle \vec{\mathbf{1}}, P\vec{\mathbf{1}}\rangle}{\|\vec{\mathbf{1}}\|^2}. \tag{4.43}$$

Direct calculation gives us $\frac{d\lambda_0}{dt}|_{t=1} = \frac{4a}{M}$, so the eigenvalue of L_t^D is

$$\lambda \approx \frac{4(t-1)}{M}\sum_{j=1}^{l}\cos\left(\frac{2q\pi}{n_j - n_{j-1}}\right) \tag{4.44}$$

for t close to 1. The sign of the derivative of λ_0 indicates the direction of the zero eigenvalue movement. According to Lemma 4.17, the equation $\det(L_t^D) = 0$ has no root occurring at $t \in (0, 1)$. Keeping this fact in mind, we discuss three cases separately for the twisted state (4.18) with $q = 1$ as the following. The results naturally extend to any integer winding number q.

Case I: $j \notin \bar{S}$ for all $j \in \{1, 2, ..., l\}$:

This is the case where $n_j - n_{j-1} > 4$ implying $a_j > 0$ for all j. So A is negative definite and $\frac{d\lambda_0}{dt}|_{t=1} > 0$. One can expect that one of the L_t^D's negative eigenvalues moves from the left half-plane to zero as t increases to 1. There is no crossing to the right half-plane since $\det(L_t^D) = 0$ has no root occurring at $t \in (0, 1)$. So we have $n_+(L^D) = n_+(A) = 0$. See the figure below, the black crosses represent eigenvalues of L_t^D for $0 \le t < 1$ and the red one represents the zero eigenvalue of L^D $(t = 1)$.

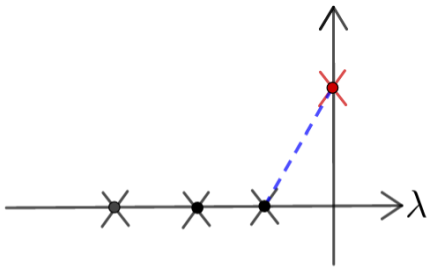

Figure 4.9: Movement of eigenvalues of L_t^D for case I.

Case II: $j \notin S$ for all j and $j \in \partial S$ for some j:

This is the case where $n_j - n_{j-1} \geq 4$ for all j and $n_j - n_{j-1} = 4$ for some j. One can check A is negative semi-definite, $\frac{d\lambda_0}{dt}|_{t=1} \geq 0$ and $\frac{d\lambda_0}{dt}|_{t=0} = 0$. In fact, it is not hard to show that the eigenspace associated with the zero eigenvalue λ_0 satisfies $E_{\lambda_0}(A) \subseteq E_{\lambda^0}(L^D)$ and $\dim(E_{\lambda_0}(A)) = \dim(E_{\lambda_0}(L^D)) - 1$ (See Appendix B for detailed proof). So zero eigenvalues of L_t^D stays zero and one of its negative eigenvalues moves from the left half-plane to zero as t increases to 1. Still, there is no crossing to the right half-plane. So we have $n_+(L^D) = n_+(A) = 0$. See the figure below, same as before, the black crosses represent eigenvalues of L_t^D for $0 \leq t < 1$ and the red ones represent zero eigenvalues of L^D $(t = 1)$.

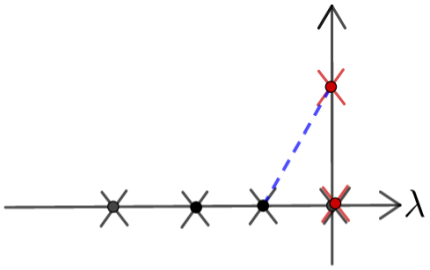

Figure 4.10: Movement of eigenvalues of L_t^D for case II.

Case III: $j \in S$ for some $j \in \{1, 2, ..., l\}$:

This is the case where $n_j - n_{j-1} < 4$ for some j. In this case, A has positive eigenvalues and $\frac{d\lambda_0}{dt}|_{t=1}$ can be either positive or negative. If $\frac{d\lambda_0}{dt}|_{t=1} > 0$, the eigenvalues moves from left to right as t close to 1, corresponding to the left half of Figure 4.11. So we have $n_+(L^D) = n_+(A)$. On the other hand, if $\frac{d\lambda_0}{dt}|_{t=1} < 0$, the eigenvalues moves from right to left as t close to 1, corresponding to the right half of Figure 4.11. So we have $n_+(L^D) = n_+(A) - 1$.

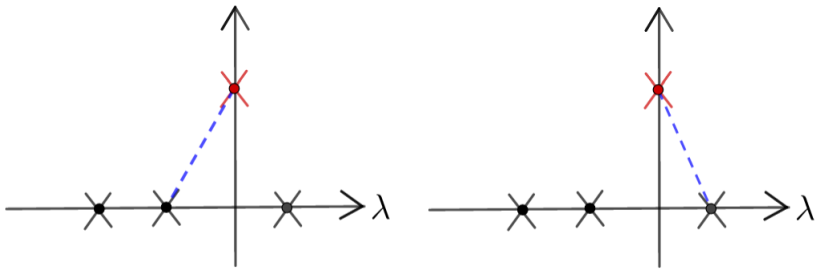

Figure 4.11: Movement of eigenvalues of L_t^D for case III

Combining all these cases, the proof of Theorem 4.13 is finished. ■

Example 4.18 (Case II)**.** In this example, we consider a multilayer Kuramoto network with 13 layers connecting in 3 cycles linked with a single hub. The first cycle consists of 4 layers, the second 5 layers and the third 6 layers, i.e., $n_1 = 4, n_2 = 9, n_3 = 15$. Clearly, this is an example of case II. Direct calculation gives $a := \sum_{j=1}^{3} a_j = \sum \cos(\frac{2\pi}{n_j - n_{j-1}}) \approx 0.8 > 0$ and $m := |\{j : n_j - n_{j-1} = 3\}| = 0$. Based on the proof of Theorem 4.13, we have

$$n^+(L_t^D) = n^+(A) = 0, \quad 0 \le t \le 1, \tag{4.45}$$

$$n^0(L_t^D) = \begin{cases} n^0(A), & 0 \le t < 1 \\ n^0(A) + 1, & t = 1. \end{cases} \tag{4.46}$$

For each fixed time t, L_t^D is a 13×13 matrix with eigenvalues $\lambda_1 \le \lambda_2 \le ... \le \lambda_{13}$. In Figure 4.12, the trend of each eigenvalue λ_i over time t from $t = 0$ to $t = 1$ is drawn by a curve starting from the x-axis. The nine gray curves show that $\lambda_i(L_t^D)$ remains negative over the whole time domain $[0, 1]$ for $i \in \{1, 2, ..., 9\}$. The red curve shows that as t increases from 0 to 1, $\lambda_{10}(L_t^D)$ increases from negative to zero, which increments the kernel dimension of L_t^D by one. The remaining three eigenvalues of L_t^D drawn by the green curves (three curves overlap on the y-axis) remain zero as t increases. All these patterns fit well into Equation (4.45) and (4.46).

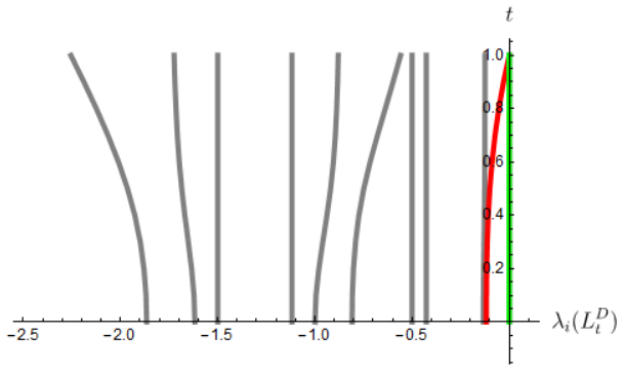

Figure 4.12: Eigenvalues of L_t^D.

According to Theorem 4.14, we know for this case the inter-layer connections do not qualitatively affect the stability of the system. To check this, it suffices to compare the eigenvalues of the intra-layer $\mathcal{L}^L$ and the eigenvalues of the full matrix $\mathcal{L}$. Recall that

$$\mathcal{L} = \mathcal{L}^L + \mathcal{L}^D = I_{M\times M} \otimes L + L^D \otimes I_{N\times N}.$$

The eigenvalues of $\mathcal{L}^L$ are eigenvalues of L each repeating M times, which results in the values shown as red flat bars in Figure 4.13 below. Also, since all eigenvalues of L^D are non-positive, the eigenvalues of $\mathcal{L}$ are expected to be no greater than the eigenvalues of $\mathcal{L}^L$. This explains why the blue curve is always below the red one in Figure 4.13. Finally, since the maximum eigenvalue of L^D is zero, it is expected that $\max(\lambda(\mathcal{L})) = \max(\lambda(\mathcal{L}^L))$. Therefore, the full dynamical system and the same system without inter-layer connections are either both stable or both unstable. The left half of Figure 4.13 represents the eigenvalues of the Supra-Laplacian at a stable solution of Equation (4.18) while the right half at an unstable solution of Equation (4.18).

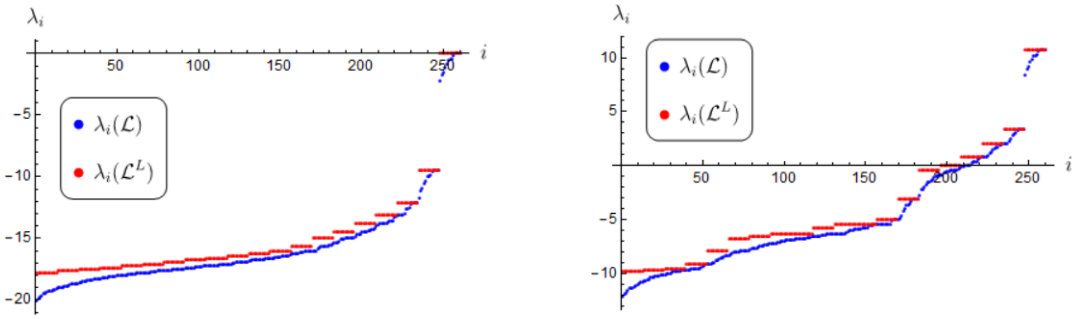

Figure 4.13: A comparison of eigenvalues between $\mathcal{L}$ and $\mathcal{L}^L$

Example 4.19 (Case III)**.** In this example, we consider two multilayer Kuramoto networks corresponding to case III with one satisfying $a < 0$ and one $a > 0$, where the variable a was defined in (4.25).

- A multilayer network with $a < 0$:

Suppose 10 layers are connected in 3 cycles linked with a single hub. The first cycle consists of 3 layers, the second 4 layers, and the third 5 layers, i.e., $n_1 = 3, n_2 = 7, n_3 = 12$. Direct calculation gives $a := \sum_{j=1}^{3} a_j = \sum \cos(\frac{2\pi}{n_j - n_{j-1}}) \approx -0.2 < 0$ and $m := |\{j : n_j - n_{j-1} = 3\}| = 1$. Based on the proof of Theorem 4.13, we have

$$n_+(L_t^D) = \begin{cases} n_+(A) = 3, & 0 \le t < 1 \\ n_+(A) - 1 = 2, & t = 1, \end{cases} \tag{4.47}$$

$$n_0(L_t^D) = \begin{cases} n_0(A), & 0 \le t < 1 \\ n_0(A) + 1, & t = 1. \end{cases} \tag{4.48}$$

In Figure 4.14, the trend of each eigenvalue λ_i over time t from $t = 0$ to $t = 1$ is drawn by a curve

starting from the x-axis. The six gray curves correspond to the trend of eigenvalues $\lambda_i(L_t^D)$ whose signs do not change over the whole time domain $[0, 1]$. The red curve shows that as t increases from 0 to 1, one eigenvalue of L_t^D decreases from positive to zero, which increments the kernel dimension of L_t^D by one. The remaining three eigenvalues of L_t^D drawn by the green curves (three curves overlap on the y-axis) remain zero as t increases. All these patterns fit well into Equation (4.47) and Equation (4.48).

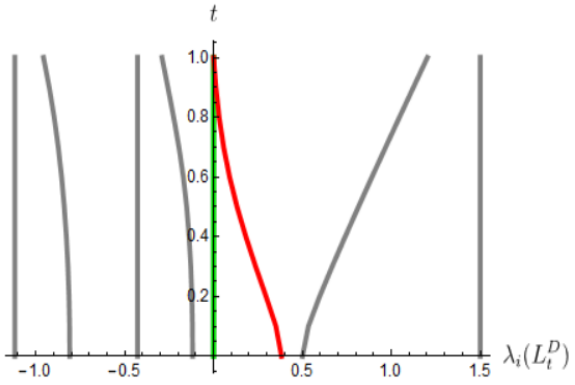

Figure 4.14: Eigenvalues of L_t^D

According to Theorem 4.14, it is expected that the full system will be destabilized by the inter-layer connections since $\max(\lambda(\mathcal{L})) > \max(\lambda(\mathcal{L}^L))$. To check this, we again compare the eigenvalues of $\mathcal{L}$ and $\mathcal{L}^L$ at a solution of Equation (4.4), which gives us Figure 4.15 as below.

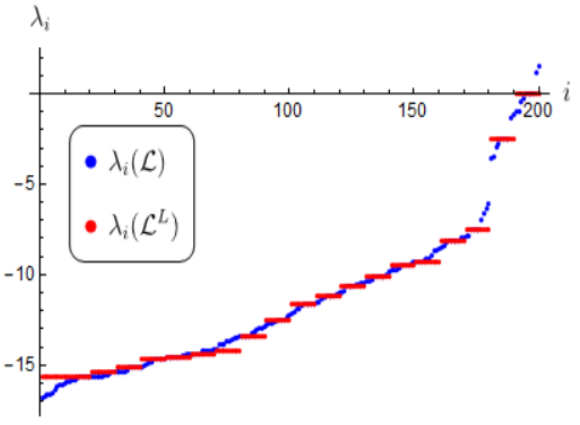

Figure 4.15: A comparison of eigenvalues between $\mathcal{L}$ and $\mathcal{L}^L$

From Figure 4.15 it can be seen that all eigenvalues of $\mathcal{L}^{\mathcal{L}}$ are negative so we have a stable solution without the inter-layer connections. However, after adding the inter-layer connections, $\mathcal{L}$ has positive eigenvalues implying the full system following Equation (4.4) is not stable anymore. So this example shows the fact that the inter-layer connections destabilize the system with the existence of cycles containing less than four layers.

- A multilayer network with $a > 0$:

Suppose 10 layers are connected in 3 cycles linked with a single hub. The first cycle consists of 3 layers, the second 4 layers, and the third 7 layers, i.e., $n_1 = 3, n_2 = 7, n_3 = 14$. Direct calculation gives $a := \sum_{j=1}^{3} a_j = \sum \cos(\frac{2\pi}{n_j - n_{j-1}}) \approx 0.12 > 0$ and $m := |\{j : n_j - n_{j-1} = 3\}| = 1$. Based on Theorem 4.13, we have

$$n_+(L_t^D) = n_+(A) = 2, \quad 0 \le t \le 1, \tag{4.49}$$

$$n_0(L_t^D) = \begin{cases} n_0(A), & 0 \le t < 1 \\ n_0(A) + 1, & t = 1. \end{cases} \tag{4.50}$$

In Figure 4.16, the trend of each eigenvalue λ_i over time t from $t = 0$ to $t = 1$ is drawn by a curve starting from the x-axis, which fits well into Equation (4.49) and Equation (4.50).

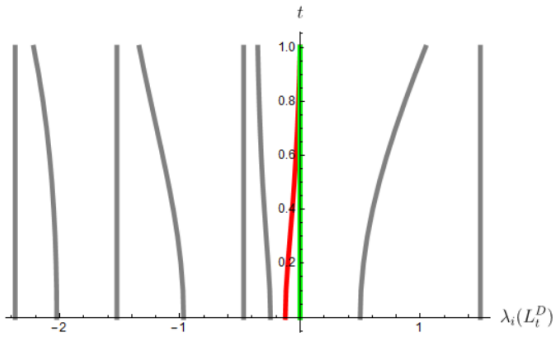

Figure 4.16: Eigenvalues of L_t^D

Similarly as above, comparing the eigenvalues of $\mathcal{L}^L$ and $\mathcal{L}$ shows the fact that the full system can be destabilized by the inter-layer connections. We omit the details here to avoid redundancy.

4.3.3. *A Cycle Tree*

As seen above, for either a single cycle or a graph of multiple cycles with a single hub, the effect of inter-layer connections on the twisted states only depends on the number of layers in each cycle. It is natural to expect the same result for a more general setting where the cycles in a graph are allowed to be connected with different hubs. This leads to the subject of our current subsection: a cycle tree.

Definition 4.20. *If a graph G only contains cycles and these cycles are connected in a tree, i.e., no cycles share edges, then we call it a cycle tree.*

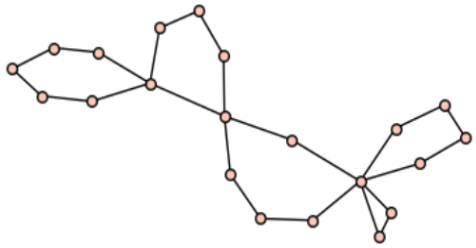

Figure 4.17: A cycle tree

In this case, the method we used for a cycle flower does not apply anymore. This is because the increasing rank of perturbation due to the increasing amount of hubs will make the calculation extremely hard. Instead, we take advantage of Algebraic Graph Theory to do the analysis. In fact, the result for the cycle-flower graph, Theorem 4.14, also holds for the cycle-tree graph. To prove it, fundamental knowledge of graph theory is needed, which can be found in standard lecture notes [64–66]. We review it here for further usage.

Given a connected undirected graph $G = (V, E, O)$, where V is the vertex set, E is the edge set and O is some orientation assigned to the graph. For instance, for the graph below, $V = \{v_1, v_2, v_3, v_4\}$, $E = \{e_1, e_2, e_3, e_4, e_5\}$ and the orientation is given by the edge direction.

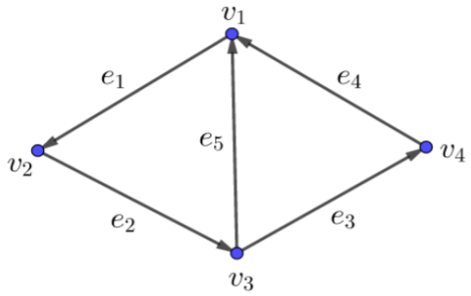

Figure 4.18: A connected undirected graph with some orientation

Definition 4.21 (Incidence vector)**.** *For $G = (V, E, O)$, an incidence vector corresponding to each edge $e \in E$ is defined as a vector I_e with length $|V|$ such that the ith component is*

$$(I_e)_i = \begin{cases} 1 & e \text{ ends at } v_i, \\ -1 & e \text{ starts at } v_i, \\ 0 & \text{else.} \end{cases} \tag{4.51}$$

For instance, for the graph in Figure 4.18, we have

$$\begin{aligned} I_{e_1} &= \{-1, 1, 0, 0\}, \\ I_{e_2} &= \{0, -1, 1, 0\}, \\ I_{e_3} &= \{0, 0, -1, 1\}, \\ I_{e_4} &= \{1, 0, 0, -1\}, \\ I_{e_5} &= \{1, 0, -1, 0\}. \end{aligned}$$

Definition 4.22 (Incidence matrix)**.** *An incidence matrix $B = B(G)$ is a $|V| \times |E|$ matrix with incidence vectors $(I_e)_{e \in E}$ as columns, i.e.,*

$$B_{ij} = \begin{cases} 1 & e_j \text{ ends at } v_i, \\ -1 & e_j \text{ starts at } v_i, \\ 0 & \text{else.} \end{cases} \tag{4.52}$$

For instance, the incidence matrix of the graph in Figure 4.18 is

$$B = \begin{pmatrix} -1 & 0 & 0 & 1 & 1 \\ 1 & -1 & 0 & 0 & 0 \\ 0 & 1 & -1 & 0 & -1 \\ 0 & 0 & 1 & -1 & 0 \end{pmatrix}.$$

Definition 4.23 (Cycle space)**.** *Let $\boldsymbol{F}$ be an arbitrary field. The kernel of the incidence matrix $B(G)$ over $\boldsymbol{F}$ is the cycle space of G denoted by $\mathcal{K}$. In other words,*

$$\mathcal{K} := \{x \in \boldsymbol{F}^E : Bx = 0\}.$$

Definition 4.24 (Fundamental cycles)**.** *Let $T \subset E$ be a spanning tree of G. For each $e \in E \setminus T$, the set $T \cup \{e\}$ contains exactly one cycle C^e. These cycles are the fundamental cycles of G with respect to T.*

Definition 4.25 (Fundamental cycle vectors)**.** *Given a fundamental cycle C^e, the fundamental cycle vector $\vec{v}_{C^e}$ corresponding to C^e is defined as a vector of length $|E|$ such that the ith coordinate is*

$$(\vec{v}_{C^e})_i = \begin{cases} 1 & e_i \in C^e \text{ and } e_i \text{ is clockwise}, \\ -1 & e_i \in C^e \text{ and } e_i \text{ is counterclockwise}, \\ 0 & e_i \notin C^e. \end{cases} \tag{4.53}$$

Let's consider the graph in Figure 4.18 again and pick a random spanning tree $T = \{e_1, e_2, e_3\}$ (the red edges) as shown below.

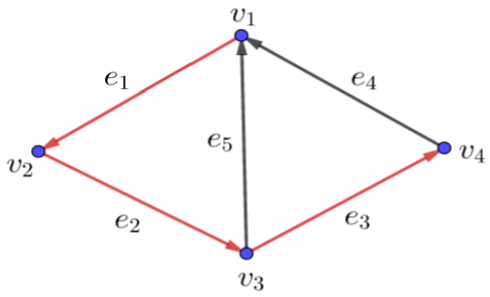

Figure 4.19: A connected undirected graph with a spanning tree

The fundamental cycle vectors with respect to T are

$$\vec{v}_{C^{e_4}} = \begin{pmatrix} -1 \\ -1 \\ -1 \\ -1 \\ 0 \end{pmatrix}, \quad \vec{v}_{C^{e_5}} = \begin{pmatrix} -1 \\ -1 \\ 0 \\ 0 \\ -1 \end{pmatrix}.$$

Remark 4.26. *There are $|E| - |V| + 1$ fundamental cycles for every spanning tree T. The fundamental cycle vectors corresponding to these cycles form a $|E| - |V| + 1$ dimensional vector space, which is independent of the choice of T.*

Lemma 4.27. *Every fundamental cycle vector $\vec{v}_{C^e}$ lies in the cycle space $\mathcal{K}$, i.e., $B\vec{v}_{C^e} = 0$ for any $\vec{v}_{C^e}$, where B is the incidence matrix.*

Theorem 4.28. *Fundamental cycle vectors form a basis of the cycle space $\mathcal{K}$ and* $\dim(\mathcal{K}) = |E| - |V| + 1$. *We call it the cycle basis.*

In a cycle tree, the cycle spaces corresponding to every cycle are orthogonal to each other. This suggests us finding eigenvalues of the whole graph can be reduced to finding eigenvalues of each single cycle. This is essentially why the results for either a single cycle or a cycle flower also hold for a cycle tree.

Theorem 4.29. *Given a cycle tree, there exists a twisted state with the winding number $q = 1$ to the multilayer Kuramoto model, and the corresponding inter-layer Laplacian matrix L^D satisfies $n_+(L^D) = 2m$ where m is the number of cycles containing 3 layers. As a result, we have*
(1) If all cycles contain at least four layers, i.e., $n_j - n_{j-1} \geq 4$ for $j = 1, 2, ..., l$, then the inter-layer connections do not qualitatively affect the stability of the system.
(2) If there exists a cycle with less than four layers, then the inter-layer connections destabilize the system.

Theorem 4.29 can be easily extended to all integer winding numbers as we showed in Theorem

4.13. To prove Theorem 4.29, we need an elegant result from Bronski, Deville, and Ferguson's paper [67] stated as below.

Theorem 4.30 (Bronski, Deville, and Ferguson)**.** *Let $G = (V, E, \Gamma)$ be a connected, weighted graph with weight γ_e on each edge, and let L_G be the Laplacian matrix. Then the number of positive eigenvalues of L_G satisfies*

$$n_+(L_G) = \{e \in E | \gamma_e < 0\} - n_+(Z_G), \tag{4.54}$$

where Z_G is defined as a cycle intersection matrix $Z_G := -Y_G^T D_G^{-1} Y_G$. Here, Y_G is a $|E| \times c$ matrix whose columns are given by y_i, where $\{y_1, ..., y_c\}$ is a basis of the cycle space $\mathcal{K}(G)$, and D_G is a $|E| \times |E|$ matrix whose e'th entry is γ_e.

Lemma 4.31. *Suppose $G = (V, E)$ is composed of l components $G_i = (V_i, E_i)$ for $i \in \{1, ..., l\}$ and these components do not share edges, then the cycle space of G satisfies $\mathcal{K}(G) = \bigoplus_{i=1}^{l} \mathcal{K}(G_i)$.*

Proof. Notice that each component G_i has separate edge set, i.e., $E_i \cap E_j = \emptyset$ for any $i \neq j$. Then by the definition of the cycle space, it can be easily seen that $\mathcal{K}(G_i)$ is a subspace of $\mathcal{K}(G)$ and $\dim(\mathcal{K}(G)) = \sum_{i=1}^{l} \dim(\mathcal{K}(G_i))$. Plus, $\mathcal{K}(G_i) \cap \sum_{j \neq i} \mathcal{K}(G_j) = \{0\}$. Therefore, one can conclude that $\mathcal{K}(G) = \bigoplus_{i=1}^{l} \mathcal{K}(G_i)$. ■

Aside from the main branch of our proof, we would like to mention an interesting observation found along the way. This result is not necessary for the proof of Theorem 4.29, but it provides a nice property of the Laplacian matrix's kernel, which is why we feel it is worth presenting here as Lemma 4.32.

Lemma 4.32. *Given any connected graph G, suppose L_G is the Laplacian matrix and $\tilde{L}_G$ is the principal submatrix of L_G obtained by deleting the first row and column of L_G, then* $\dim(Ker(L_G)) = \dim(Ker(\tilde{L}_G)) + 1$.

Proof. Suppose L_G is an $n \times n$ matrix, we order its eigenvalues in an increasing order: $\lambda_1 \leq \lambda_2 \leq ... \leq \lambda_n$. Then the interlacing theorem gives $\lambda_k(L_G) \leq \lambda_k(\tilde{L}_G) \leq \lambda_{k+1}(L_G)$ for $k \in \{1, ..., n-1\}$. This implies

$$\dim(Ker(\tilde{L}_G)) - 1 \leq \dim(Ker(L_G)) \leq \dim(Ker(\tilde{L}_G)) + 1. \tag{4.55}$$

On the other hand, for any vector $\vec{x} \in Ker(\tilde{L}_G)$, we claim $\vec{y} \in Ker(L_G)$ where $y := \begin{pmatrix} 0 \\ \vec{x} \end{pmatrix}$. In

fact, writing L_G and $\vec{x}$ explicitly gives

$$L_G = \begin{pmatrix} -\sum_{j\neq 1} a_{1j} & a_{12} & \cdots & a_{1n} \\ a_{21} & -\sum_{j\neq 2} a_{2j} & \cdots & a_{2n} \\ \vdots & \vdots & \ddots & \vdots \\ a_{n1} & a_{n2} & \cdots & -\sum_{j\neq n} a_{nj} \end{pmatrix} \text{ and } \vec{x} = \begin{pmatrix} x_2 \\ x_3 \\ \vdots \\ x_n \end{pmatrix},$$

where $a_{ij} = a_{ji}$. Then we have $\sum_{j=2}^{n} a_{ij}(x_j - x_i) - a_{i1}x_i = 0$ for $i = 2, ..., n$ as $\tilde{L}_G\vec{x} = 0$. Summing these $n-1$ equations up gives $\sum_{i=2}^{n}\sum_{j=2}^{n} a_{ij}(x_j - x_i) - \sum_{i=2}^{n} a_{i1}x_i = 0$. The first term is clearly zero by the symmetry, which results in $\sum_{i=2}^{n} a_{1i}x_i = 0$. This implies $L_G\vec{y} = 0$. Furthermore, note that the all-ones vector $\vec{\mathbf{1}}$ lies in $Ker(L_G)$ and it is independent with the vector $\vec{y}$ constructed above, so we have

$$\dim(Ker(L_G)) \geq \dim(Ker(\tilde{L}_G)) + 1. \tag{4.56}$$

Combining the inequalities (4.55) and (4.56) gives

$$\dim(Ker(L_G)) = \dim(Ker(\tilde{L}_G)) + 1, \tag{4.57}$$

which ends the proof. ■

Theorem 4.30, in alliance with the aforementioned lemmas, yields the following proposition.

Proposition 4.33. $n_+(L_G) = \sum_{i=1}^{l} n_+(L_{Gi}) = \sum_{i=1}^{l} n_+(\tilde{L}_{Gi})$.

Proof. Suppose Z_G is the cycle intersection matrix of G defined in Theorem 4.30 and Z_{G_i} is the cycle intersection matrix of G_i. Then by Lemma 4.31, we have

$$\begin{aligned} Z_G &= -Y_G^T D_G^{-1} Y_G \\ &= -\begin{bmatrix} Y_{G_1}^T & & \\ & \ddots & \\ & & Y_{G_l}^T \end{bmatrix} \begin{bmatrix} D_{G_1}^{-1} & & \\ & \ddots & \\ & & D_{G_l}^{-1} \end{bmatrix} \begin{bmatrix} Y_{G_1} & & \\ & \ddots & \\ & & Y_{G_l} \end{bmatrix} \\ &= \begin{bmatrix} Z_{G_1} & & \\ & \ddots & \\ & & Z_{G_l} \end{bmatrix}, \end{aligned}$$

which implies $n_+(Z_G) = \sum_{i=1}^{l} n_+(Z_{G_i})$. Notice that different components of G do not share edges,

i.e., $E_i \cap E_j = \emptyset$ for any $i \neq j$, then Theorem 4.30 gives

$$\begin{aligned} n_+(L_G) &= \{e \in E \mid \gamma_e < 0\} - n_+(Z_G) \\ &= \sum_{i=1}^{l} \{e \in E_i \mid \gamma_e < 0\} - \sum_{i=1}^{l} n_+(Z_{G_i}) = \sum_{i=1}^{l} n_+(L_{G_i}). \end{aligned}$$

Plus, by Lemma 4.32, it is not hard to see that $n_+(L_{G_i}) = n_+(\tilde{L}_{G_i})$. Therefore, we proved $n_+(L_G) = \sum_{i=1}^{l} n_+(L_{Gi}) = \sum_{i=1}^{l} n_+(\tilde{L}_{Gi})$. ■

Proposition 4.33 shows that the number of positive eigenvalues of a cycle-tree graph's Laplacian depends on which of each cycle's Laplacian. This coincides with the result we derived for a cycle flower in section 4.3.2. As a result, Theorem 4.29 holds immediately.

4.4. Conclusion

In this chapter, we discuss a node-aligned multilayer Kuramoto model and show that if the layers are connected into a complete graph or a cycle tree, i.e. a graph containing only no-edge-shared cycles, then a twisted state exists as a phase-locked solution of the Kuramoto model. The Jacobian of the Kuramoto equation at this state is a supra-Laplacian matrix. Our main focus is on the effect of the inter-layer connections on the stability of such a twisted state. For the complete graph, we prove the inter-layer connections always destabilize the system since the value of the eigenvalues of the graph Laplacian is increased due to these connections. For the cycle-tree graph, we prove that whether the inter-layer connections will enhance or impede the phase-locking depends on the number of layers in each cycle. In particular, for the twisted state with a winding number of $q = 1$, the system will only be destabilized if there exists at least one cycle containing less than four layers. Otherwise, the system stability will not be qualitatively affected since the largest eigenvalue remains the same regardless of the inter-layer connections.

We have seen that the inter-layer topology is an important factor in system stability. Another question one may ask is how robust the system stability is towards inter-layer perturbations. Intuitively, the phase locking is enhanced with more inter-layer couplings. However, we will show in the next chapter that, for a duplex Kuramoto model under specific conditions, one of its stable states is always destabilized by an additional weak inter-layer coupling using the standard perturbation theory. This result coincides with the famous Braess's Paradox which we will briefly introduce at the beginning of the next chapter.

Chapter 5

Perturbation Analysis on Duplex Networks

5.1. Background

Back to 1968, a German mathematician Dietrich Braess noticed an interesting phenomenon that an addition of an intuitively helpful road to a network can adversely worsen the traffic and increase the overall journey time, which is totally counter-intuitive [68]. To make it clear, consider a network of two non-interfering routes from s to t. Suppose the traveling time is always one hour on the roads (v, t) and (s, w) regardless of the traffic, i.e., the cost $c(x) = 1$ where x represents the fraction of the traffic on the given route overall routes. Meanwhile, the travelling time on the roads (s, v) and (w, t) is linearly proportional to the traffic, i.e., $c(x) = x$. Therefore, for the initial network shown in Figure 5.1(a), the least total amount of travelling time is $1 + 0.5 = 1.5$ hours since evenly splitting the traffic on (s, v) and (s, w) is the optimal choice. Now, suppose we install a teleportation device allowing drivers to travel instantly from v to w shown as the edge (v, w) in Figure 5.1(b) with $c(x) = 0$. The new route $(s \to v \to w \to t)$ is never worse than the original two routes $(s \to v \to t)$ and $(s \to w \to t)$ and strictly better than the case where some traffic fails to use it. We, therefore, expect all drivers to veer to this new route. And as a result, the total traveling time will be increased to 2 hours due to the full congestion on (s, v) and (w, t). We have made the clogging even worse!

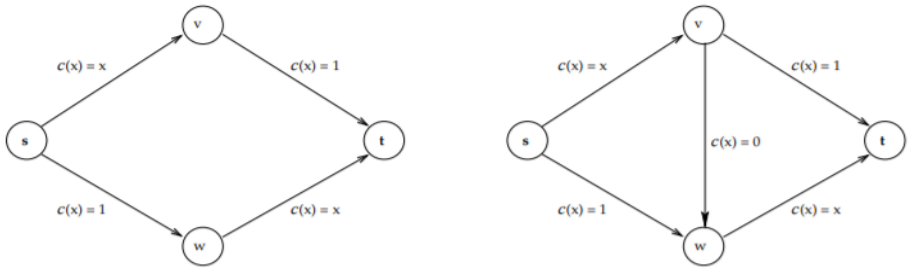

(a) Initial network (b) Augmented network

Figure 5.1: Braess's Paradox [69]

There exists a physical demonstration on Braess's Paradox. As shown in Figure (5.2)(a), we attach one end of a spring to a fixed support and the other end to a taut string S. Another identical spring is attached to the free end of S and carries a heavy weight. In addition, we use two extra strings, one attaches the support and the lower end of S and the other the weight and the upper end of S. Suppose the stretched length of a spring is a linear function of the force applied to it, then this mechanical structure can be viewed as the traffic network depicted in Figure 5.1(b): the two long strings are equivalent to roads (s, w) and (v, t); the taut string is equivalent to (v, w); and finally

the two springs are equivalent to (s, v) and (w, t). Now cutting off the taut string, surprisingly, cause the weight to rise, which corresponds to the better traffic congestion in the network (5.1)(a).

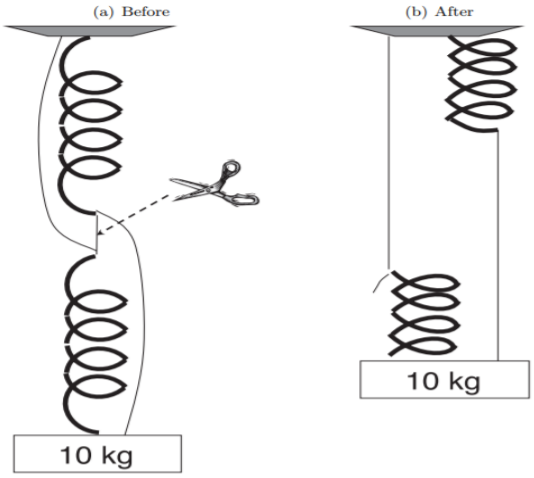

Figure 5.2: A string-springs system: a physical demonstration on Braess's Paradox [69]

In analogy with the Braess's Paradox, a similar phenomenon also occurs in dynamical systems with a population of coupled oscillators. Quite naturally, people expect that connecting a pair of initially uncoupled oscillators would generically favor synchrony. However, Nishikawa and Motter [70] found that a system can be easier to reach synchronization if the average network distance is larger. They presented both numerical results and analytical estimates on the synchronizability of a scale-free network. A few years later, Witthaut and Marc Timme [71, 72] showed that adding specific links could decrease the total grid capacity and thus destroy the locking on the grid, though additional couplings stabilize synchronous states on average. Numerical experiments were performed on both a second-order Kuramoto-like model and a complex network. Very recently, they published a nice review on antagonistic phenomena in network dynamics [73] (we especially refer readers to part one for the phenomena of Braess's paradox). For more related work, we refer readers to the references [74–78].

Although the interest in this field seems to be arising in a recent decade, most of the results are purely numerical. The purpose of this chapter is to provide an analytical treatment of the Braess's paradox in a multilayer Kuramoto model, which is inspired by Coletta and Jacquod's work on linear stability analysis of coupled-oscillator networks [74]. More specifically, we will explore the effect of adding a small coupling between a pair of oscillators on stable synchronous states of a duplex network, i.e. a multiplex network with two layers, using first-order perturbation theory. In particular, when the underlying graph of each layer is a circle, we give a simple elegant result stated in the next section.

5.2. Main Result

Suppose we have a cyclic duplex network, i.e. a two-layer multiplex network with the graph on each layer being a single cycle. Every node in the graph represents a phase oscillator. Suppose each layer contains N oscillators and they satisfy the following Kuramoto dynamic:

$$\frac{d\theta_i^{(1)}}{dt} = \omega + \gamma(\sin(\theta_{i+1}^{(1)} - \theta_i^{(1)}) + \sin(\theta_{i-1}^{(1)} - \theta_i^{(1)})) + \tau_i \sin(\theta_i^{(2)} - \theta_i^{(1)}), \tag{5.1}$$

$$\frac{d\theta_i^{(2)}}{dt} = -\omega + \gamma(\sin(\theta_{i+1}^{(2)} - \theta_i^{(2)}) + \sin(\theta_{i-1}^{(2)} - \theta_i^{(2)})) + \tau_i \sin(\theta_i^{(1)} - \theta_i^{(2)}), \tag{5.2}$$

for $i \in \{1, 2, ..., N\}$ where we assume $\theta_{N+1}^{(\cdot)} = \theta_1^{(\cdot)}$ and $\theta_0^{(\cdot)} = \theta_N^{(\cdot)}$.

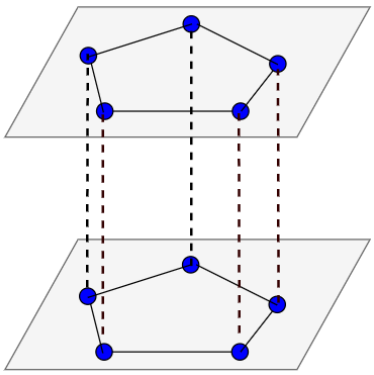

Figure 5.3: A cyclic duplex network

Here, $\theta_i^{(1)}$ refers to the phase of the ith node on the first layer and $\theta_i^{(2)}$ the ith node on the second layer. ω is the natural frequency of each node and γ represents the intra-layer coupling strength. We assume all nodes share the same frequency and the same intra-layer coupling strength. The constant τ_i represents the inter-layer coupling strength between the ith nodes of both layers. Suppose $\tau_1 = \tau_2 = ... = \tau_{N-1} = \tau > 0$, $\tau_N = 0$ and

$$\boldsymbol{\theta} = (\boldsymbol{\theta}^{(1)}, \boldsymbol{\theta}^{(2)}) = (\theta, ..., \theta, -\theta, ..., -\theta) \tag{5.3}$$

is an asymmetric stable consensus state under such dynamic. One can easily check that such stable state exists. The Jacobian matrix of the duplex Kuramoto model (5.1)-(5.2) at this state is negative semi-definite with N eigenvalues $\lambda_1 = 0 > \lambda_2 > ... > \lambda_N$. Since the largest eigenvalue vanishes, the state stability is determined by λ_2. Therefore, we will compute the leading order correction to λ_2 resulting from adding a weak connection between the two layers.

To add a small perturbation on the network, we set τ_N as δ where $0 < \delta \ll 1$, and suppose

$$\tilde{\boldsymbol{\theta}} = (\tilde{\boldsymbol{\theta}}^{(\mathbf{1})}, \tilde{\boldsymbol{\theta}}^{(\mathbf{2})}) = (\tilde{\boldsymbol{\theta}}^{(\mathbf{1})}, -\tilde{\boldsymbol{\theta}}^{(\mathbf{1})}) \tag{5.4}$$

is an asymmetric state for the perturbed dynamic.

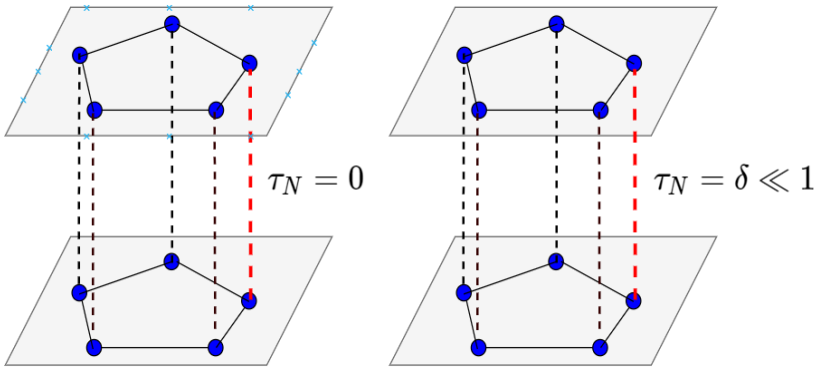

Figure 5.4: An inter-layer perturbation on a duplex network

To determine the stability of this new state, we will apply the method of perturbation analysis to our duplex network later in this section. Before stating our main result, it is necessary to clarify a few notations first.

$$\tilde{\boldsymbol{\theta}} := \boldsymbol{\theta} + \boldsymbol{\delta\theta}, \tag{5.5}$$

$$\theta_{ij}^{(k)} := \boldsymbol{\theta}_i^{(k)} - \boldsymbol{\theta}_j^{(k)},\ k = 1, 2, \tag{5.6}$$

$$\tilde{\theta}_{ij}^{(k)} := \tilde{\boldsymbol{\theta}}_i^{(k)} - \tilde{\boldsymbol{\theta}}_j^{(k)},\ k = 1, 2, \tag{5.7}$$

$$\epsilon_{ij}^{(k)} := \boldsymbol{\delta\theta}_i^{(k)} - \boldsymbol{\delta\theta}_j^{(k)},\ k = 1, 2, \tag{5.8}$$

$$\theta_{ii} := \boldsymbol{\theta}_i^{(1)} - \boldsymbol{\theta}_i^{(2)}, \tag{5.9}$$

$$\tilde{\theta}_{ii} := \tilde{\boldsymbol{\theta}}_i^{(1)} - \tilde{\boldsymbol{\theta}}_i^{(2)}, \tag{5.10}$$

$$\epsilon_{ii} := \boldsymbol{\delta\theta}_i^{(1)} - \boldsymbol{\delta\theta}_i^{(2)}. \tag{5.11}$$

Applying these notations and the asymmetry of our state, we have

$$\begin{cases} \theta_{ij}^{(1)} = \theta_{ij}^{(2)} = 0,\ i \neq j \\ \tilde{\theta}_{ij}^{(1)} = -\tilde{\theta}_{ij}^{(2)},\ i \neq j \\ \theta_{ii} = 2\boldsymbol{\theta}_i^{(1)} = 2\theta, \end{cases} \tag{5.12}$$

$$\begin{cases} \epsilon_{ij}^{(1)} = -\epsilon_{ij}^{(2)},\ i \neq j \\ \epsilon_{ii} = 2\boldsymbol{\delta\theta}_i^{(1)}. \end{cases} \tag{5.13}$$

Now, we are ready to state our main result.

Theorem 5.1. *Suppose* $c_0 = \frac{\tau}{\gamma}\cos(2\theta)$ *where* θ *is defined in (5.3). Define*

$$f_1 = -2(1 + c_0)r_1 + r_1^2 + r_1^N \tag{5.14}$$

$$f_2 = -2(1 + c_0)r_2 + r_2^2 + r_2^N, \tag{5.15}$$

$$g_1 = r_1 + r_1^{N-1} - 2r_1^N \tag{5.16}$$

$$g_2 = r_2 + r_2^{N-1} - 2r_2^N, \tag{5.17}$$

where $r_{1,2} = 1 + c_0 \pm \sqrt{c_0^2 + 2c_0}$, *then the following statements hold:*

(1) For the phase differences defined in (5.8) and (5.11), we have

$$\epsilon_{ij}^{(1)} = \frac{\delta \sin(2\theta)}{\gamma} \frac{1}{f_1 g_2 - f_2 g_1} (f_2(r_1^i - r_1^j) - f_1(r_2^i - r_2^j)) + O(\delta^2), \tag{5.18}$$

$$\epsilon_{ii} = \frac{2\delta \sin(2\theta)}{\gamma} \frac{1}{f_1 g_2 - f_2 g_1} (f_2 r_1^i - f_1 r_2^i) + O(\delta^2). \tag{5.19}$$

(2) After adding the perturbation $\tau_N = \delta$, *the change of the second largest eigenvalue of the Jacobian of our equation system (5.1)-(5.2) is*

$$\Delta\lambda_2 = \sum_{k=1}^{N-1} \frac{2\tau\delta \sin^2(2\theta)}{\gamma} (\boldsymbol{u}_k - \boldsymbol{u}_{N+k})^2 \frac{1}{f_1 g_2 - f_2 g_1} (f_2 r_1^k - f_1 r_2^k) - \delta \cos(2\theta)(\boldsymbol{u}_N - \boldsymbol{u}_{2N})^2 + O(\delta^2), \tag{5.20}$$

where $\boldsymbol{u}$ *is the eigenvector of the original Jacobian without perturbation associated with the second largest eigenvalue. If* $\Delta\lambda_2 > 0$, *then the perturbation destabilizes the dynamic, otherwise it stabilizes the dynamic. In particular, when* $c_0 > 0$ *and* $\sin(2\theta) \neq 0$, *i.e.,* $\theta \in (\ell\pi - \pi/4, \ell\pi) \cup (\ell\pi, \ell\pi + \pi/4)$ *for some* $\ell \in \mathbb{N}$, *we can conclude that, for* N *large, our system is always destabilized by the perturbation since* $\frac{1}{f_1 g_2 - f_2 g_1}(f_2 r_1^k - f_1 r_2^k)$ *is positive for all* $k \in \{1, 2, ..., N-1\}$.

To verify Theorem 5.1, we need to prove the following two lemmas.

Lemma 5.2. *Suppose* A *is a* $n \times n$ *tridiagonal matrix with cornered elements:*

$$A = \begin{bmatrix} c & 1 & 0 & \dots & 0 & 1 \\ 1 & c & 1 & \dots & 0 & 0 \\ & \ddots & \ddots & \ddots & & \\ & & \ddots & \ddots & \ddots & \\ 0 & 0 & \dots & 1 & c & 1 \\ 1 & 0 & 0 & \dots & 1 & d \end{bmatrix}.$$

Then the element at the i*th row and* j*th column of its inverse is*

$$(A^{-1})_{ij} = \begin{cases} P_{ij} & 1 \leq i \leq j \\ Q_{ij} & j < i \leq n, \end{cases} \tag{5.21}$$

where the values of P_{ij} *and* Q_{ij} *are given by*

$$P_{ij} = a_1(j) \cdot r_1^i + a_2(j) \cdot r_2^i, \tag{5.22}$$

$$Q_{ij} = (a_1(j) - z_1(j)) \cdot r_1^i + (a_2(j) - z_2(j)) \cdot r_2^i. \tag{5.23}$$

Here, r_i, z_i *and* a_i *for* $i = 1, 2$ *are defined as*

$$\begin{cases} r_1 = (-c + \sqrt{c^2-4})/2 \\ r_2 = (-c - \sqrt{c^2-4})/2, \end{cases} \tag{5.24}$$

$$\begin{cases} z_1(j) = 1/(r_1^j(r_2 - r_1)) \\ z_2(j) = 1/(r_2^j(r_1 - r_2)), \end{cases} \tag{5.25}$$

and

$$\begin{bmatrix} a_1(j) \\ \\ a_2(j) \end{bmatrix} = \frac{1}{f_1 g_2 - f_2 g_1} \begin{bmatrix} g_2 & -f_2 \\ \\ -g_1 & f_1 \end{bmatrix} \begin{bmatrix} z_1(j) r_1^n + z_2(j) r_2^n \\ \\ z_1(j)(r_1^{n-1} + d r_1^n) + z_2(j)(r_2^{n-1} + d r_2^n) \end{bmatrix}, \tag{5.26}$$

where for $k \in \{1, 2\}$,

$$\begin{cases} f_k = c r_k + r_k^2 + r_k^n \\ g_k = r_k + r_k^{n-1} + d r_k^n. \end{cases} \tag{5.27}$$

Proof. Following the usual argument, we consider the difference equation for $i \in \{2, 3, ..., n-1\}$:

$$r(i-1) + cr(i) + r(i+1) = 0. \tag{5.28}$$

Assume a simple form of $r(i) = r^i$, we then have

$$r^2 + cr + 1 = 0. \tag{5.29}$$

Solving (5.29) for r gives $r_{1,2}$ as shown in (5.24). Define P_{ij} and Q_{ij} as in (5.22) and (5.23):

$$\begin{aligned} P_{ij} &= a_1(j) \cdot r_1^i + a_2(j) \cdot r_2^i, \\ Q_{ij} &= (a_1(j) - z_1(j)) \cdot r_1^i + (a_2(j) - z_2(j)) \cdot r_2^i. \end{aligned}$$

Then it is not hard to see P_{ij} and Q_{ij} are solutions to the equation (5.29) for $i \in \{2, 3, ..., n-1\}$ and $j \in \{1, 2, ..., n\}$, i.e.,

$$P_{i-1,j} + cP_{ij} + P_{i+1,j} = 0, \tag{5.30}$$

$$Q_{i-1,j} + cQ_{ij} + Q_{i+1,j} = 0. \tag{5.31}$$

Suppose

$$(A^{-1})_{ij} = \begin{cases} P_{ij} & 1 \le i \le j \\ Q_{ij} & j < i \le n, \end{cases}$$

as defined in (5.21) and

$$P_{jj} = Q_{jj} \tag{5.32}$$

for $j \in \{1, 2, ..., n\}$. For convenience, we denote $A_{:,j}$ as the jth column of the matrix A. Then

$A \cdot (A^{-1})_{:,j} = I_{:,j}$ for $j \in \{2, 3, ..., n-1\}$ gives equations (5.30), (5.31) and

$$cP_{1j} + P_{2j} + Q_{nj} = 0, \tag{5.33}$$
$$cP_{jj} + P_{j-1,j} + Q_{j+1,j} = 1, \tag{5.34}$$
$$P_{1j} + Q_{n-1,j} + dQ_{n,j} = 0. \tag{5.35}$$

Notice that $cP_{jj} + P_{j-1,j} = -P_{j+1,j}$ by the equation (5.30), so (5.34) can be rewritten as

$$-P_{j+1,j} + Q_{j+1,j} = 1. \tag{5.36}$$

Plugging P_{ij} and Q_{ij} as defined in (5.22) and (5.23) in the equations (5.32) and (5.36) gives us

$$\begin{bmatrix} r_1^j & r_2^j \\ -r_1^{j+1} & -r_2^{j+1} \end{bmatrix} \begin{bmatrix} z_1(j) \\ z_2(j) \end{bmatrix} = \begin{bmatrix} 0 \\ 1 \end{bmatrix}, \tag{5.37}$$

which implies

$$z_1(j) = 1/(r_1^j(r_2 - r_1)),$$
$$z_2(j) = 1/(r_2^j(r_1 - r_2)),$$

as defined in (5.25) for $j \neq 1, n$. On the other hand, plugging P_{ij} and Q_{ij} into equations (5.33) and (5.35) yields

$$f_1 a_1(j) + f_2 a_2(j) = z_1(j) r_1^n + z_2(j) r_2^n, \tag{5.38}$$
$$g_1 a_1(j) + g_2 a_2(j) = z_1(j)(r_1^{n-1} + dr_1^n) + z_2(j)(r_2^{n-1} + dr_2^n), \tag{5.39}$$

where for $k = 1, 2$,

$$f_k = cr_k + r_k^2 + r_k^n, \tag{5.40}$$
$$g_k = r_k + r_k^{n-1} + dr_k^n. \tag{5.41}$$

Solving the equations (5.38) and (5.39) for a_1 and a_2 yields (5.26) for $j \neq 1, n$.
Following the same manner, one can show that $A \cdot (A^{-1})_{:,j} = I_{:,j}$ for $j \in \{1, n\}$ is also guaranteed by the same set of equations (5.32), (5.33), (5.36) and (5.35). This implies our solutions (5.25) and (5.26) also apply for $j = 1$ and $j = n$. The lemma now has been proved. We note that the main idea of this proof comes from Dow's work in 2002 [79]. ■

Lemma 5.3. *Suppose* $c_0 > 0$, $r_{1,2} = 1 + c_0 \pm \sqrt{c_0^2 + 2c_0}$ *and*

$$f_k = -2(1 + c_0)r_k + r_k^2 + r_k^n, \tag{5.42}$$
$$g_k = r_k + r_k^{n-1} - 2r_k^n \tag{5.43}$$

for $k = 1, 2$, then the following inequality

$$\frac{1}{f_1 g_2 - f_2 g_1}(f_2 r_1^i - f_1 r_2^i) > 0 \tag{5.44}$$

is satisfied for any $i \in \{1, 2, ..., n\}$ where $n > 1$ is an arbitrary positive integer.

Proof. To begin with, we make an useful observation that $r_1 \cdot r_2 = 1$. Then fix an arbitrary $i \in \{1, 2, ..., n\}$, we will prove the following inequalities separately:

$$(a) \quad f_2 r_1^i - f_1 r_2^i < 0, \tag{5.45}$$

$$(b) \quad f_1 g_2 - f_2 g_1 < 0. \tag{5.46}$$

Part (a) is much easier to show. Direct calculations give us

$$f_2 r_1^i - f_1 r_2^i = -2(1 + c_0)(r_1^{i-1} - r_1^{1-i}) + (r_1^{i-2} - r_1^{2-i}) - (r_1^{n-i} - r_1^{i-n}), \tag{5.47}$$

which is negative due to the fact that $c_0 > 0$ and $r_1 > 1$.

Part (b) is a bit less trivial to prove. First notice that when $c_0 = 0$, we have $r_1 = r_2 = 1$ and thus $f_1 g_2 - f_2 g_1 = 0$. So it suffices to show the derivative of $f_1 g_2 - f_2 g_1$ with respect to c_0 is negative when $c_0 > 0$. We start with computing the derivatives of f_1, f_2, g_1 and g_2 with respect to c_0 separately. Note that

$$r_1' = \frac{dr_1}{dc_0} = C \cdot r_1, \tag{5.48}$$

$$r_2' = \frac{dr_2}{dc_0} = -C \cdot r_2, \tag{5.49}$$

where $C = 1/\sqrt{c_0^2 + 2c_0}$. Using Equations (5.48) and (5.49) gives

$$f_1' = C \cdot n r_1^n, \tag{5.50}$$

$$f_2' = -C \cdot n r_2^n, \tag{5.51}$$

$$g_1' = C \cdot (r_1 + (n-1) r_1^{n-1} - 2n r_1^n), \tag{5.52}$$

$$g_2' = -C \cdot (r_2 + (n-1) r_2^{n-1} - 2n r_2^n). \tag{5.53}$$

Then $(f_1g_2 - f_2g_1)' =$

$$\begin{aligned}
&f_1'g_2 + f_1g_2' - f_2'g_1 - f_2g_1' \\
&= C \cdot [(4n + 2nc_0 - 2 - 2c_0)(r_1^{n-2} + r_1^{2-n}) - (3n + 4nc_0 + 1)(r_1^{n-1} + r_1^{1-n}) \\
&\quad - (n-1)(r_1^{n-3} - r_1^{3-n}) + 4(1 + c_0)], \\
&\leq C \cdot [(4n + 4nc_0)(r_1^{n-2} + r_1^{2-n}) - (3n + 4nc_0 + 1)(r_1^{n-1} + r_1^{1-n}) \\
&\quad - (n-1)(r_1^{n-3} - r_1^{3-n})], \qquad (5.54)
\end{aligned}$$

where the last inequality is due to $c_0 > 0$ and $r_1^{n-2} + r_1^{2-n} \geq 2$. Now we make another observation on the coefficients of elements inside the parentheses of (5.54):

$$(3n + 4nc_0 + 1) + (n-1) = (4n + 4nc_0). \qquad (5.55)$$

Define $f(x) = x + 1/x$, $c_1 = (3n+4nc_0+1)/(4n+4nc_0), c_2 = (n-1)/(4n+4nc_0)$ and $x_0 = r_1^{n-2} > 1$. Then to show $(f_1g_2 - f_2g_1)' \leq 0$, it is sufficient to prove

$$f(x_0) \leq c_1 f(r_1 x_0) + c_2 f(x_0/r_1). \qquad (5.56)$$

Since the function f is convex and $c_1 + c_2 = 1$, we have

$$c_1 f(r_1 x_0) + c_2 f(x_0/r_1) \geq f(c_1 r_1 x_0 + c_2 x_0/r_1). \qquad (5.57)$$

Note that $c_1 r_1 + c_2/r_1 = c_1 r_1 + c_2 r_2 = \frac{1}{4n+4nc_0}[(1 + c_0)(4n + 4nc_0) + (2n + 4nc_0 + 2)\sqrt{c_0^2 + 2c_0}] \geq 1 + c_0 \geq 1$, and also, $f(x)$ is increasing when $x \geq 1$. This implies $f(c_1 r_1 x_0 + c_2 x_0/r_1) \geq f(x_0)$ which yields the inequality (5.56). Thus part (b) is also proved.

Combining the two inequalities (5.45) and (5.46) gives our result (5.44). ■

Now, it is time to prove our main theorem.

Proof of Theorem 5.1. We will prove part (1) and (2) separately as below.

(1) Plugging $\tilde{\boldsymbol{\theta}}$ into the equations (5.1)-(5.2) and applying the first-order Taylor expansion $\sin(\boldsymbol{\theta} + \boldsymbol{\delta\theta}) \approx \sin(\boldsymbol{\theta}) + \boldsymbol{\delta\theta}\cos(\boldsymbol{\theta})$ yield

$$J \cdot \boldsymbol{\delta\theta} = \delta \sin(\tilde{\theta}_{NN}) \cdot \boldsymbol{v} \qquad (5.58)$$

where J is the Jacobian matrix of (5.1)-(5.2) at $\boldsymbol{\theta}$, $\tilde{\theta}_{NN} = \tilde{\theta}_N^{(2)} - \tilde{\theta}_N^{(1)}$ and $\boldsymbol{v}^T = \left(\boldsymbol{v}^{(1)}, \boldsymbol{v}^{(2)}\right)$ is a $1 \times 2N$ vector. Here $\boldsymbol{v}^{(1)}$ is a $N \times 1$ vector with all zero components except for the last one being 1, and $\boldsymbol{v}^{(2)}$ is a $N \times 1$ vector with all zero components except for the last being -1. The matrix J

is of dimension $2N \times 2N$ and can be written in the form of

$$J = \left[\begin{array}{c|c} A & B \\ \hline B & A \end{array}\right], \tag{5.59}$$

where A is a $N \times N$ tridiagonal Toeplitz matrix and B is a $N \times N$ diagonal matrix with

$$A_{ij} = \begin{cases} \gamma & i \sim j \\ -2\gamma - B_{ii} & i = j, \end{cases} \quad B_{ii} = \begin{cases} \tau\cos(2\theta) & i \neq N \\ 0 & i = N. \end{cases} \tag{5.60}$$

Notice that $\boldsymbol{\delta\theta}^{(1)} = -\boldsymbol{\delta\theta}^{(2)}$, the equation (5.58) gives

$$(A - B)\boldsymbol{\delta\theta}^{(1)} = \delta\sin(\tilde{\theta}_{NN})\boldsymbol{v}^{(1)}, \tag{5.61}$$

which implies $\boldsymbol{\delta\theta}^{(1)} = \delta\sin(\tilde{\theta}_{NN})(A - B)^{-1}\boldsymbol{v}^{(1)}$. Thus

$$\epsilon_{ij}^{(1)} := \delta\theta_i^{(1)} - \delta\theta_j^{(1)} = \delta\sin(\tilde{\theta}_{NN})\left((A - B)_{iN}^{-1} - (A - B)_{jN}^{-1}\right). \tag{5.62}$$

Then to the first order in δ, we will have

$$\epsilon_{ij}^{(1)} \approx \delta\sin(\theta_{NN})\left((A - B)_{iN}^{-1} - (A - B)_{jN}^{-1}\right). \tag{5.63}$$

Here, $(A - B)_{ij}^{-1}$ represents the element at the ith row and jth column of the inverse matrix of $A - B$. Now, let's find the inverse of $A - B$. Define $c_0 = \tau\cos(2\theta)/\gamma$, then

$$A - B = \gamma\begin{bmatrix} -2 - 2c_0 & 1 & 0 & \dots & 0 & 1 \\ 1 & -2 - 2c_0 & 1 & \dots & 0 & 0 \\ & \ddots & \ddots & \ddots & & \\ & & \ddots & \ddots & \ddots & \\ 0 & 0 & \dots & 1 & -2 - 2c_0 & 1 \\ 1 & 0 & 0 & \dots & 1 & -2 \end{bmatrix}. \tag{5.64}$$

Applying Lemma 5.2 by taking $c = -2 - 2c_0$ and $d = -2$ gives

$$(A - B)_{iN}^{-1} = \frac{1}{\gamma(f_1 g_2 - f_2 g_1)}(f_2 r_1^i - f_1 r_2^i), \tag{5.65}$$

where f_1, f_2, g_1, g_2 and $r_{1,2}$ are defined in Theorem (5.1). So (5.63) gives the equation (5.18). The equation (5.19) can be proved following the same argument.

(2) Suppose J is the Jacobian matrix of the original system (5.1)-(5.2) valued at the solution

$\boldsymbol{\theta}$ and $\tilde{J}$ is the Jacobian of the perturbed system (by setting $\tau_N = \delta$) at the solution $\tilde{\boldsymbol{\theta}}$. Then

$$\tilde{J} = J + \Delta J + O(\delta^2), \tag{5.66}$$

where

$$\Delta J = \left[\begin{array}{c|c} -D & D \\ \hline D & -D \end{array}\right] \tag{5.67}$$

composed with a diagonal matrix D with

$$D_{ii} = \begin{cases} -\tau\epsilon_{ii}\sin(2\theta) & i \neq N \\ \delta\cos(2\theta) & i = N. \end{cases} \tag{5.68}$$

Suppose $\boldsymbol{u}$ is the eigenvector of J associated with its second largest eigenvalue and $\Delta\lambda_2$ is the difference between the second largest eigenvalue of J and $\tilde{J}$, then

$$\Delta\lambda_2 \approx \boldsymbol{u}^T \cdot \Delta J \cdot \boldsymbol{u} = \sum_{k=1}^{N-1} \tau\epsilon_{kk}\sin(2\theta)(\boldsymbol{u}_k - \boldsymbol{u}_{N+k})^2 - \delta\cos(2\theta)(\boldsymbol{u}_N - \boldsymbol{u}_{2N})^2. \tag{5.69}$$

Equation (5.69) together with (5.19) that we proved in part (1) gives our result in the second part (5.20). In particular, when $\theta \in (\ell\pi - \pi/4, \ell\pi) \cup (\ell\pi, \ell\pi + \pi/4)$ for some $\ell \in \mathbb{N}$, we have $c_0 > 0$ and $\sin(2\theta) \neq 0$, and thus by Lemma 5.3 we know $\epsilon_{kk}\sin(2\theta) > 0$ for any $k \in \{1, 2, ..., N-1\}$. Also note that any vector $\boldsymbol{v}$ such that $\boldsymbol{v}_k = \boldsymbol{v}_{N+k}$ for $k = 1, 2, ..., N-1$ and $\boldsymbol{v}_N \neq \boldsymbol{v}_{2N}$ is not an eigenvector of J. These imply that, for δ small and N large, we have $\Delta\lambda_2 > 0$. Therefore, our dynamical system will be destabilized by the perturbation. ■

5.3. Conclusion

In this chapter, we focus on a duplex Kuramoto network and study analytically how an additional weak inter-layer connection would affect the system's stability. Originally, the system has an asymmetric stable consensus state $\boldsymbol{\theta} = (\boldsymbol{\theta}^{(1)}, \boldsymbol{\theta}^{(2)}) = (\theta, ..., \theta, -\theta, ..., -\theta)$. After adding a weak coupling between the two layers, we obtain a perturbed system and an associated new asymmetric state $\tilde{\boldsymbol{\theta}}$ is found. The effect of the perturbation on the state stability is measured by the change of the second largest eigenvalue of the Jacobian of the Kuramoto model $\Delta\lambda_2$. We derive an explicit expression of $\Delta\lambda_2$ using the standard perturbation theory. In particular, we prove that, for a large system, when $\theta \in (\ell\pi - \pi/4, \ell\pi) \cup (\ell\pi, \ell\pi + \pi/4)$ for some $\ell \in \mathbb{N}$, our system is always destabilized by the perturbation due to a positive $\Delta\lambda_2$.

APPENDIX A

Proof in Chapter 2

A.1. Proof of Proposition 2.12

Proof. Suppose J is the Jacobian matrix of (2.2) at θ^*, $\lambda_1, \lambda_2, ..., \lambda_N$ are N eigenvalues of J and $v_1, v_2, ..., v_N$ are the corresponding eigenvectors. Since θ^* is a stable fixed point, by definition, $\lambda_N \leq \lambda_{N-1} \leq ... \leq \lambda_2 < \lambda_1 = 0$. And clearly, $v_1 = \hat{\mathbf{1}} = (1, 1, ..., 1)$. Let $V = Ker(J) = \text{span}\{\hat{\mathbf{1}}\}$ and $W = \text{span}\{v_2, v_3, ..., v_N\}$, then $V \oplus W = \mathbb{R}^N$.

Consider any solution of Equation (2.15) that is close to θ^*, i.e., $\theta = \theta^* + \tilde{\theta}$ where $\|\tilde{\theta}\|$ is small. Then we have

$$\dot{\theta}_i = \dot{\tilde{\theta}}_i = \omega_i + \frac{\gamma}{N}\sum_j \sin(\theta_j^* - \theta_i^* + (\tilde{\theta}_j - \tilde{\theta}_i)) + \epsilon f_i(\theta, t) \tag{A.1}$$

$$= \omega_i + \frac{\gamma}{N}(\sum_j \sin(\theta_j^* - \theta_i^*) + \sum_j \cos(\theta_j^* - \theta_i^*)(\tilde{\theta}_j - \tilde{\theta}_i) - \sum_j \sin(\xi_{i,j})\frac{(\tilde{\theta}_j - \tilde{\theta}_i)^2}{2}) \tag{A.2}$$

$$+ \epsilon f_i(\theta, t) \qquad \text{where } \xi_{ij} \text{ is between } (\theta_j^* - \theta_i^*) \text{ and } (\theta_j - \theta_i) \tag{A.3}$$

$$= \frac{\gamma}{N}\sum_j \cos(\theta_j^* - \theta_i^*)(\tilde{\theta}_j - \tilde{\theta}_i) - \frac{\gamma}{N}\sum_j \sin(\xi_{i,j})\frac{(\tilde{\theta}_j - \tilde{\theta}_i)^2}{2} + \epsilon f_i(\theta, t) \tag{A.4}$$

$$= (J\tilde{\theta})_i - \frac{\gamma}{N}\sum_j \sin(\xi_{i,j})\frac{(\tilde{\theta}_j - \tilde{\theta}_i)^2}{2} + \epsilon f_i(\theta, t), \tag{A.5}$$

where $(J\tilde{\theta})_i$ refers to the ith row of the matrix $J\tilde{\theta}$.

By our definition of semi-norm (2.9), $\|\theta\|^2 = \|\theta\|_\Omega^2 = \frac{1}{N}\sum_{1 \leq i \leq j \leq N}(\theta_i - \theta_j)^2 = \frac{1}{N}\theta^T M\theta$, where

$$M = \begin{pmatrix} N-1 & -1 & -1 & ... & -1 \\ -1 & N-1 & -1 & ... & -1 \\ & & ..... & & \\ -1 & -1 & -1 & ... & N-1 \end{pmatrix}.$$

Notice that M has an eigenvalue 0 with multiplicity 1 and an eigenvalue N with multiplicity $N-1$, so M is positive semi-definite. By computing the derivative of this semi-norm for $\tilde{\theta} \in W$, we have

$$
\begin{aligned}
\frac{d}{dt}\|\tilde{\theta}\|^2 &= \frac{1}{N}\frac{d}{dt}\tilde{\theta}^T M\tilde{\theta} = \frac{2}{N}\tilde{\theta}^T M\dot{\tilde{\theta}} \\
&\le \frac{2}{N}\tilde{\theta}^T MJ\tilde{\theta} + \frac{\gamma}{N^2}\sum_{i,j}|\sin(\xi_{i,j})[(\tilde{\theta}_i-\tilde{\theta}_j)^2\sum_k(\tilde{\theta}_i-\tilde{\theta}_k)]| + \frac{2}{N}\epsilon\tilde{\theta}^T Mf \\
&\le \frac{2}{N}\tilde{\theta}^T MJ\tilde{\theta} + \frac{\gamma}{N^2}\sum_{i,j}[(\tilde{\theta}_i-\tilde{\theta}_j)^2\sum_k|\tilde{\theta}_i-\tilde{\theta}_k|] + \frac{2\epsilon}{N}\|\tilde{\theta}^T M\|\cdot\|f\| \\
&\le \lambda_2\frac{2}{N}\tilde{\theta}^T M\tilde{\theta} + \frac{\gamma}{N^2}\sum_{i,j}(\tilde{\theta}_i-\tilde{\theta}_j)^2(\sum_k(\tilde{\theta}_i-\tilde{\theta}_k)^2)^{1/2}N^{1/2} + \frac{2\epsilon}{N}(N\tilde{\theta}^T M\tilde{\theta})^{1/2}\cdot(N^{1/2}C) \\
&\le 2\lambda_2\|\tilde{\theta}\|^2 + \gamma\|\tilde{\theta}\|^3 + 2\epsilon CN^{1/2}\|\tilde{\theta}\|.
\end{aligned}
$$

For $\tilde{\theta}\in V$, $\|\tilde{\theta}\|=0$. In this case, since $M\cdot J$ is negative semi-definite, we still have above inequality. Thus for any small $\tilde{\theta}\in\mathbb{R}^N$, we have

$$
\frac{d}{dt}\|\tilde{\theta}\|^2 \le 2\lambda_2\|\tilde{\theta}\|^2 + \gamma\|\tilde{\theta}\|^3 + 2\epsilon CN^{1/2}\|\tilde{\theta}\|.
$$

To find the basin of attraction, it suffices to find the domain of $\|\tilde{\theta}\|$ such that

$$
2\lambda_2\|\tilde{\theta}\|^2 + \gamma\|\tilde{\theta}\|^3 + 2\epsilon CN^{1/2}\|\tilde{\theta}\| < 0, \tag{A.6}
$$

which will be satisfied if

$$
\begin{cases} 2\epsilon CN^{1/2}\|\tilde{\theta}\| < c_1|\lambda_2|\|\tilde{\theta}\|^2 \\ \gamma\|\tilde{\theta}\|^3 < c_2|\lambda_2|\|\tilde{\theta}\|^2, \end{cases} \tag{A.7}
$$

where $c_1>0, c_2>0$ and $c_1+c_2\le 2$. So we need

$$
\frac{2\epsilon CN^{1/2}}{c_1|\lambda_2|} < \|\tilde{\theta}\| < \frac{c_2|\lambda_2|}{\gamma}. \tag{A.8}
$$

It is clear to see (A.8) makes sense only when $\epsilon < \frac{c_1c_2|\lambda_2|^2}{2CN^{1/2}\gamma}$. Since $c_1c_1 \le (\frac{c_1+c_2}{2})^2 \le 1$, the loosest bound on ϵ is $\frac{|\lambda_2|^2}{2CN^{1/2}\gamma}$, when $c_1=c_2=1$.

Let $r(\epsilon)=2\epsilon CN^{1/2}/|\lambda_2|$ and $R=|\lambda_2|/\gamma$, then by Gronwall's inequality [42], the semi-norm of $\tilde{\theta}$ is exponentially decreasing when $\tilde{\theta}$ is in the annulus of the radii $r(\epsilon)$ and R, and then stays in the ball of radius $r(\epsilon)$ forever. So statements (1) and (2) in Proposition 2.12 have been proved. ■

A.2. Proof of Proposition 2.22

Proof. The goal is to prove Equation (2.36):

$$\lim_{N\to\infty} \mathbb{P}(|g(K,N) - g_\infty(\frac{K}{N})| \leq N^{-\frac{1}{2}+\epsilon}) = 1,$$

in other words, we need

$$\lim_{N\to\infty} \mathbb{P}(g \leq g_\infty + N^{-\frac{1}{2}+\epsilon}) = 1, \tag{A.9}$$

$$\lim_{N\to\infty} \mathbb{P}(g \geq g_\infty - N^{-\frac{1}{2}+\epsilon}) = 1. \tag{A.10}$$

For simplicity, define $a = F^{-1}(1-\frac{\rho}{2})$ so that we have $g_\infty = 2a$ and define $\delta = \frac{1}{2}N^{-\frac{1}{2}+\epsilon}$, then Equations (A.9) and (A.10) can be rewritten as

$$\lim_{N\to\infty} \mathbb{P}(g \leq 2(a+\delta)) = 1, \tag{A.11}$$

$$\lim_{N\to\infty} \mathbb{P}(g \geq 2(a-\delta)) = 1. \tag{A.12}$$

Let's prove Equation (A.11) first. In fact, we will show $\mathbb{P}(g \leq 2a)$ tends to one as $N \to \infty$. Define $X_i =$

$$\begin{cases} 1, & \text{if } \omega_i \in [-a,a] \\ 0, & \text{if } \omega i \notin [-a,a]. \end{cases} \tag{A.13}$$

Then $X_i's$ are i.i.d random variables since $\omega_i's$ are i.i.d random variables. Let $X = X_1+X_2+...+X_N$, then X represents the number of ω_i such that $\omega_i \in [-a,a]$. By strong law of large number theorem, $\frac{X}{N}$ converges to $\mathbb{E}(X_i)$ almost surely, i.e., $\mathbb{P}(\lim_{N\to\infty}\frac{X}{N} = \int_{-a}^{a} f(x)dx) = 1$. Notice that $\int_{-a}^{a} f(x)dx = 1-\rho$, so we have $\mathbb{P}(\lim_{N\to\infty}\frac{X}{N} = 1-\rho) = 1$. Moreover, we know $g(\rho) \leq 2a$ if $X = (1-\rho)N$ by the definition of the function g. Therefore, $\mathbb{P}(g(\rho) \leq 2a) = 1$ as $N \to \infty$. Equation (A.11) has been proved.

The other direction Equation (A.12) is less trivial to prove. Intuitively, we want to show that with high probability no intervals with length $g_\infty - 2\delta$ contain more than $(1-\rho)N$ points. To show this, we need to firstly make two important observations. First, notice that if no intervals of Length L with ω_k at an endpoint contain more than m points then no any other interval does. So we can only focus on N intervals $\{[\omega_i, \omega_i + L] : i = 1, 2, ..., N\}$. Second, the interval centered at zero maximizes the probability that a point lies in the interval, i.e., $I = [-L/2, L/2]$ gives the largest $\mathbb{P}(x \in I)$ among all intervals of length L. The proof follows from the fact that for $\mu = \int_a^{a+L} f(x)dx$, its derivative $\frac{d\mu}{da} = f(a+L) - f(a)$ is zero when $a = -\frac{L}{2}$. As a result, the probability that the interval of length L with ω_k at an endpoint contains more than m points is less than the probability that $[-L/2, L/2]$ contains more than m points. Now, fix $L = 2(a-\delta)$ where δ is defined at the beginning of the proof. Define A_k as the event that interval $[\omega_k, \omega_k + L]$ containing more than

$(1-\rho)N$ points, A as the event that there exists an interval with length L containing more than $(1-\rho)N$ points, and B as the event that $[-L/2, L/2]$ contains more than $(1-\rho)N$ points. Clearly, our goal is to prove

$$\mathbb{P}(A) \to 0 \text{ as } N \to \infty. \tag{A.14}$$

Due to the above two observations and the union bound, we have

$$\mathbb{P}(A) = \mathbb{P}(\cup_{k=1}^{N} A_k) \leq \sum_{k=1}^{N} \mathbb{P}(A_k) \leq N \cdot \mathbb{P}(B). \tag{A.15}$$

Note that

$$\mathbb{P}(B) = N \sum_{M=(1-\rho)N}^{N} \binom{N}{M} p^M (1-p)^{N-M}, \tag{A.16}$$

where $1-\rho = \int_{-a}^{a} f(x)dx$ and $p = \int_{-L/2}^{L/2} f(x)dx = \int_{-a+\delta}^{a-\delta} f(x)dx$. we denote the right-hand side of Equation (A.16) as $R(\rho, p, N)$, then it is sufficient to show

$$R(\rho, p, N) \to 0 \text{ as } N \to \infty. \tag{A.17}$$

Define $\tau_{N,M} := \binom{N}{M} p^M (1-p)^{N-M} = \frac{N!}{M!(N-M)!} p^M (1-p)^{N-M}$. Then

$$\log(\tau_{N,M}) = \log(N!) - \log(M!) - \log(N-M)! + M\log(p) + (N-M)\log(1-p).$$

For large N, using Stirling's approximation: $\log(N!) \approx N\log(N) - N + \frac{1}{2}\log(2\pi N)$, we have

$$\begin{aligned}
\log(\tau_{N,M}) &\approx N\log(N) - N + \frac{1}{2}\log(2\pi N) - M\log(M) + M - \frac{1}{2}\log(2\pi M) \\
&\quad - (N-M)\log(N-M) + (N-M) - \frac{1}{2}\log(2\pi(N-M)) \\
&\quad + M\log(p) - (N-M)\log(1-p) \\
&= N\log(N) - M\log(N) - M\log(\frac{M}{N}) - (N-M)\log(N) \\
&\quad - (N-M)\log(\frac{N-M}{N}) + M\log(p) - (N-M)\log(1-p) \\
&\quad + \frac{1}{2}\log\left(\frac{N}{2\pi M(N-M)}\right) \\
&= N\left(-\frac{M}{N}\log(\frac{M}{N}) - (1-\frac{M}{N})\log(1-\frac{M}{N}) + \frac{M}{N}\log(p) + (1-\frac{M}{N})\log(1-p)\right) \\
&\quad + \frac{1}{2}\log\left(\frac{N}{2\pi M(N-M)}\right)
\end{aligned}$$

By setting $x = \frac{M}{N}$, we have

$$\log(\tau_{N,M}) \approx N\left(-x\log(x) - (1-x)\log(1-x) + x\log(p) + (1-x)\log(1-p)\right) + \frac{1}{2}\log\left(\frac{N}{2\pi x(1-x)}\right) - \log(N).$$

Define

$$\phi(x) := -x\log(x) - (1-x)\log(1-x) + x\log(p) + (1-x)\log(1-p), \tag{A.18}$$

then

$$\phi'(x) = \log(\frac{p}{1-p}) - \log(\frac{x}{1-x}) \text{ and } \phi''(x) = \frac{-1}{x(1-x)} < 0. \tag{A.19}$$

So ϕ reaches the largest when $x = p$. And thus, when N is large, the maximum of $\tau_{N,M}$ occurs when $x = \frac{M}{N} = p$. In the neighborhood of the maximum: $x = p + y$, $\phi(x) \approx \frac{-1}{2p(1-p)}y^2$. So we have

$$\log(\tau_{N,M}) = \frac{1}{2}\log(\frac{1}{2\pi p(1-p)N}) - \frac{N}{2p(1-p)}y^2 + O(y), \tag{A.20}$$

and thus

$$\tau_{N,M} \approx \frac{1}{N}\sqrt{\frac{N}{2\pi p(1-p)}}e^{-\frac{Ny^2}{2p(1-p)}+O(y)}. \tag{A.21}$$

Recall that $1-\rho = \int_{-a}^{a} f(x)dx$ and $p = \int_{-a+\delta}^{a-\delta} f(x)dx$ where $\delta = N^{-\frac{1}{2}+\epsilon}$, then $(1-\rho)-p \sim N^{-\frac{1}{2}+\epsilon}$. So for $M \geq (1-\rho)N$, we have $\frac{M}{N} - p \gtrsim N^{-\frac{1}{2}+\epsilon}$, i.e., $y \gtrsim N^{-\frac{1}{2}+\epsilon}$. On the other hand, $y \leq 1-p < 1$. Thus

$$\tau_{N,M} \lesssim \frac{1}{N}\sqrt{\frac{N}{2\pi p(1-p)}}e^{-\frac{N^{2\epsilon}}{2p(1-p)}+O(1)} \tag{A.22}$$

So we have

$$\begin{aligned} R(\rho,p,N) &\leq N \cdot N \cdot \left(\frac{1}{N}\sqrt{\frac{N}{2\pi p(1-p)}}e^{-\frac{N^{2\epsilon}}{2p(1-p)}+O(1)}\right) \\ &= N\sqrt{\frac{N}{2\pi p(1-p)}}e^{-\frac{N^{2\epsilon}}{2p(1-p)}+O(1)}, \end{aligned}$$

which implies $R(\rho,p,N) \to 0$ as $N \to \infty$ for any positive ϵ. The proof of Equation (A.12) is now complete.

With the two equations (A.11) and (A.12), we proved Proposition (2.22).

■

APPENDIX B

Proof in Chapter 4

Proposition B.1. *Define a parameter family of operators $L_t^D = A + tP$ where A and P are defined as in (4.23) and $t \in [0,1]$. If A is negative semi-definite, then as t increases from 0 to 1, the following statements hold:*
(1) zero eigenvalues of L_t^D remain stationary;
(2) negative eigenvalues of L_t^D are in motion below zero and exactly one of them hits zero at $t = 1$.

Proof. Recall $L_0^D = A =$

$$\begin{pmatrix} -2\sum_{k=1}^{l} a_k & & & & \\ & A_1 & & & \\ & & A_2 & & \\ & & & & \\ & & & & A_l \end{pmatrix} \tag{B.1}$$

where each diagonal block $A_j = -a_j\tilde{A}$ with $a_j = \cos(\frac{2q\pi}{n_j - n_{j-1}})$ and $\tilde{A}$ being

$$\begin{bmatrix} 2 & -1 & 0 & \dots & 0 \\ -1 & 2 & -1 & \dots & 0 \\ 0 & -1 & 2 & \dots & 0 \\ \vdots & \vdots & \vdots & \ddots & \vdots \\ 0 & 0 & 0 & \dots & 2 \end{bmatrix},$$

a $(n_j - n_{j-1} - 1) \times (n_j - n_{j-1} - 1)$ tridiagonal matrix. By Lemma 4.10, we know $\tilde{A}$ is positive semi-definite. So $a_j \geq 0$ for $j \in \{1, 2, ..., l\}$ given A is negative semi-definite. Without loss of generality, assume $l = 2$, A_1 is a $n \times n$ matrix and A_2 is a $m \times m$ matrix. Also, assume $a_1 > 0$ and $a_2 = 0$. Then the eigenspace of A associated with its zero eigenvalue λ^0 is

$$E_{\lambda^0}(A) = Span\{e_j : \ n + 2 \leq j \leq 1 + n + m\}, \tag{B.2}$$

where $e_j = (0, \dots, 0, 1, 0, \dots, 0)$ is the standard basis of $\mathbb{R}^{1+n+m}$, with all components equal to 0, except the jth, which is 1. Notice that for each $e_j \in E_{\lambda^0}(A)$, $Pe_j = 0$ since the last m columns of P are all zero vectors due to $a_2 = 0$. So we have $L_t^D e_j = 0$ for any t. Therefore,

$$E_{\lambda^0}(A) \subseteq E_{\lambda^0}(L_t^D), \tag{B.3}$$

we proved statement (1). To prove statement (2), notice that the $(1 + n) \times (1 + n)$ principal

submatrix of A is invertible. Denote the corresponding principal matrix of L_t^D as LS, i.e., $LS =$

$$\begin{bmatrix} -2a_1 & ta_1 & 0 & \dots & ta_1 \\ ta_1 & -2a_1 & a_1 & \dots & 0 \\ 0 & a_1 & -2a_1 & \dots & 0 \\ \vdots & \vdots & \vdots & \ddots & \vdots \\ ta_1 & 0 & 0 & \dots & -2a_1 \end{bmatrix}.$$

Then according to Lemma 4.17, $\det(LS) = 0$ if and only if $t = \pm 1$ so LS is invertible for $0 \leq t < 1$, and thus $L_t^D \vec{x} \neq 0$ for any $\vec{x} \notin E_{\lambda^0}(A)$. Therefore,

$$E_{\lambda^0}(A) = E_{\lambda^0}(L_t^D),\ 0 \leq t < 1. \tag{B.4}$$

As $t = 1$, $LS =$

$$a_1 \begin{bmatrix} -2 & 1 & 0 & \dots & 1 \\ 1 & -2 & 1 & \dots & 0 \\ 0 & 1 & -2 & \dots & 0 \\ \vdots & \vdots & \vdots & \ddots & \vdots \\ 1 & 0 & 0 & \dots & -2 \end{bmatrix}.$$

By Lemma 4.10, there exists only one eigenvector of LS associated with its zero eigenvalue, which is an all ones vector. Therefore,

$$dim(E_{\lambda^0}(L_1^D)) = dim(E_{\lambda^0}(A)) + 1, \tag{B.5}$$

so we proved statement (2). ■

References

[1] S. H. Strogatz, D. M. Abrams, A. McRobie, B. Eckhardt, and E. Ott, "Crowd synchrony on the millennium bridge," *Nature*, vol. 438, pp. 43–44, Nov. 2005.

[2] H. M. Oliveira and L. V. Melo, "Huygens synchronization of two clocks," *Scientific Reports*, vol. 5, jul 2015.

[3] C. M. Gray, "Synchronous oscillations in neuronal systems: mechanisms and functions," *Journal of Computational Neuroscience*, vol. 1, no. (1-2), pp. 11–38, 1994.

[4] V. Torre, "A theory of synchronization of heart pace-maker cells," *Journal of Theoretical Biology*, vol. 61, no. 1, pp. 55–71, 1976.

[5] M. R. Arkady Pikovsky and J. Kurths, *Synchronization: a universal concept in nonlinear sciences*, vol. 12. New York: Cambridge University Press, 2003.

[6] H. Yoon, S. H. Choi, S. K. Kim, H. B. Kwon, S. M. Oh, J.-W. Choi, Y. J. Lee, D.-U. Jeong, and K. S. Park, "Human heart rhythms synchronize while co-sleeping," *Frontiers in Physiology*, vol. 10, Mar. 2019.

[7] A. Palmieri, J. R. Kleinbub, V. Calvo, E. Benelli, I. Messina, M. Sambin, and A. Voci, "Attachment-security prime effect on skin-conductance synchronization in psychotherapists: An empirical study.," *Journal of Counseling Psychology*, vol. 65, pp. 490–499, July 2018.

[8] S. H. Strogatz, *SYNC : How Order Emerges from Chaos in the Universe, Nature, and Daily Life*. New York: Theia, 2003.

[9] A. T. Winfree, "Biological rhythms and the behavior of populations of coupled oscillators," *Journal of Theoretical Biology*, vol. 16, pp. 15–42, July 1967.

[10] S. H. Strogatz, "From Kuramoto to Crawford: exploring the onset of synchronization in populations of coupled oscillators," *Physica D: Nonlinear Phenomena*, vol. 143, pp. 1–20, sep 2000.

[11] J. A. Acebrón, L. L. Bonilla, C. J. P. Vicente, F. Ritort, and R. Spigler, "The Kuramoto model: A simple paradigm for synchronization phenomena," *Reviews of Modern Physics*, vol. 77, pp. 137–185, apr 2005.

[12] Y. Kuramoto, *Chemical Oscillations, Waves, and Turbulence*. Springer Berlin Heidelberg, 1984.

[13] Y. Kuramoto, "Collective synchronization of pulse-coupled oscillators and excitable units," *Physica D: Nonlinear Phenomena*, vol. 50, no. 1, pp. 15–30, 1991.

[14] S. H. Strogatz and R. E. Mirollo, "Stability of incoherence in a population of coupled oscillators," *Journal of Statistical Physics*, vol. 63, pp. 613–635, May 1991.

[15] S. H. Strogatz, R. E. Mirollo, and P. C. Matthews, "Coupled nonlinear oscillators below the synchronization threshold: Relaxation by generalized landau damping," *Physical Review Letters*, vol. 68, pp. 2730–2733, May 1992.

[16] F. D. Smet and D. Aeyels, "Partial entrainment in the finite Kuramoto- Sakaguchi model," *Physica D: Nonlinear Phenomena*, vol. 234, pp. 81–89, oct 2007.

[17] B. Fernandez, D. Gérard-Varet, and G. Giacomin, "Landau damping in the kuramoto model," *Annales Henri Poincaré*, vol. 17, pp. 1793–1823, Dec. 2015.

[18] H. Dietert, "Stability and bifurcation for the kuramoto model," *Journal de Mathématiques Pures et Appliquées*, vol. 105, pp. 451–489, Apr. 2016.

[19] H. Chiba, G. S. Medvedev, and M. S. Mizuhara, "Bifurcations in the kuramoto model on graphs," *Chaos: An Interdisciplinary Journal of Nonlinear Science*, vol. 28, p. 073109, July 2018.

[20] D. Aeyels and J. A. Rogge, "Existence of partial entrainment and stability of phase locking behavior of coupled oscillators," *Progress of Theoretical Physics*, vol. 112, pp. 921–942, dec 2004.

[21] F. Dörfler and F. Bullo, "On the critical coupling for Kuramoto oscillators," *SIAM Journal on Applied Dynamical Systems*, vol. 10, pp. 1070–1099, jan 2011.

[22] S. Boccaletti, J. Kurths, G. Osipov, D. Valladares, and C. Zhou, "The synchronization of chaotic systems," *Physics Reports*, vol. 366, pp. 1–101, Aug. 2002.

[23] E. Mosekilde, Y. Maistrenko, and D. Postnov, *Chaotic Synchronization.* WORLD SCIENTIFIC, Mar. 2002.

[24] J. Fell and N. Axmacher, "The role of phase synchronization in memory processes," *Nature Reviews Neuroscience*, vol. 12, pp. 105–118, Jan. 2011.

[25] M. G. Rosenblum, A. S. Pikovsky, and J. Kurths, "From phase to lag synchronization in coupled chaotic oscillators," *Physical Review Letters*, vol. 78, pp. 4193–4196, June 1997.

[26] N. F. Rulkov, M. M. Sushchik, L. S. Tsimring, and H. D. I. Abarbanel, "Generalized synchronization of chaos in directionally coupled chaotic systems," *Physical Review E*, vol. 51, pp. 980–994, Feb. 1995.

[27] H. D. I. Abarbanel, N. F. Rulkov, and M. M. Sushchik, "Generalized synchronization of chaos: The auxiliary system approach," *Physical Review E*, vol. 53, pp. 4528–4535, May 1996.

[28] W. He and J. Cao, "Generalized synchronization of chaotic systems: An auxiliary system approach via matrix measure," *Chaos: An Interdisciplinary Journal of Nonlinear Science*, vol. 19, p. 013118, Mar. 2009.

[29] J. C. Bronski, L. DeVille, and M. J. Park, "Fully synchronous solutions and the synchronization phase transition for the finite-N Kuramoto model," *Chaos: An Interdisciplinary Journal of Nonlinear Science*, vol. 22, no. 3, p. 033133, 2012.

[30] E. Canale and P. Monzo, "Almost global synchronization of symmetric Kuramoto coupled oscillators," in *Systems Structure and Control*, InTech, aug 2008.

[31] N. Chopra and M. W. Spong, "On exponential synchronization of Kuramoto oscillators," *IEEE Transactions on Automatic Control*, vol. 54, pp. 353–357, feb 2009.

[32] G. Ermentrout, "Synchronization in a pool of mutually coupled oscillators with random frequencies," *Journal of Mathematical Biology*, vol. 22, jun 1985.

[33] S.-Y. Ha, T. Ha, and J.-H. Kim, "On the complete synchronization of the Kuramoto phase model," *Physica D: Nonlinear Phenomena*, vol. 239, pp. 1692–1700, sep 2010.

[34] M. Verwoerd and O. Mason, "Global phase-locking in finite populations of phase-coupled oscillators," *SIAM Journal on Applied Dynamical Systems*, vol. 7, pp. 134–160, jan 2008.

[35] M. Verwoerd and O. Mason, "On computing the critical coupling coefficient for the Kuramoto model on a complete bipartite graph," *SIAM Journal on Applied Dynamical Systems*, vol. 8, pp. 417–453, jan 2009.

[36] Y. Kuramoto and D. Battogtokh, "Coexistence of coherence and incoherence in nonlocally coupled phase oscillators," *Nonlin.Phenom. Complex Syst.*, vol. 5, no. 4, pp. 380–385, 2002.

[37] B. Nicolaenko, B. Scheurer, and R. Temam, "Some global dynamical properties of the kuramoto-sivashinsky equations: Nonlinear stability and attractors," *Physica D: Nonlinear Phenomena*, vol. 16, no. 2, pp. 155 – 183, 1985.

[38] P. Collet, J.-P. Eckmann, H. Epstein, and J. Stubbe, "A global attracting set for the kuramoto-sivashinsky equation," *Communications in mathematical physics*, vol. 152, pp. 203–214, 1993.

[39] J. C. Bronski and T. N. Gambill, "Uncertainty estimates and l2 bounds for the kuramoto–sivashinsky equation," *Nonlinearity*, vol. 19, no. 9, p. 2023, 2006.

[40] R. W. Wittenberg, "Optimal parameter-dependent bounds for kuramoto-sivashinsky-type equations," *Discrete & Continuous Dynamical Systems-A*, vol. 34, no. 12, pp. 5325–5357, 2014.

[41] M. Goldman, M. Josien, and F. Otto, "New bounds for the inhomogenous burgers and the kuramoto-sivashinsky equations," *Communications in Partial Differential Equations*, vol. 40, no. 12, pp. 2237–2265, 2015.

[42] H. K. Khalil, *Nonlinear Systems*. Upper Saddle River, New Jersey 07458: Prentice Hall, 3 ed., 2002.

[43] R. Johnson, "Cantor spectrum for the quasi-periodic schrödinger equation," *Journal of Differential Equations*, vol. 91, pp. 88–110, May 1991.

[44] G. Medvedev and Y. Yoo, "Multimodal oscillations in systems with strong contraction," *Physica D: Nonlinear Phenomena*, vol. 228, pp. 87–106, apr 2007.

[45] S. Wasserman and K. Faus, *Social Network Analysis: Methods and Applications*. New York: Cambridge University Press, 1994.

[46] S. E. Parsegov, A. V. Proskurnikov, R. Tempo, and N. E. Friedkin, "Novel multidimensional models of opinion dynamics in social networks," *IEEE Transactions on Automatic Control*, vol. 62, pp. 2270–2285, may 2017.

[47] A. Das, S. Gollapudi, and K. Munagala, "Modeling opinion dynamics in social networks," in *Proceedings of the 7th ACM international conference on Web search and data mining - WSDM 14*, ACM Press, 2014.

[48] W. Quattrociocchi, G. Caldarelli, and A. Scala, "Opinion dynamics on interacting networks: media competition and social influence," *Scientific Reports*, vol. 4, may 2014.

[49] P. Jia, A. MirTabatabaei, N. E. Friedkin, and F. Bullo, "Opinion dynamics and the evolution of social power in influence networks," *SIAM Review*, vol. 57, pp. 367–397, jan 2015.

[50] A. V. Proskurnikov, A. S. Matveev, and M. Cao, "Opinion dynamics in social networks with hostile camps: Consensus vs. polarization," *IEEE Transactions on Automatic Control*, vol. 61, pp. 1524–1536, jun 2016.

[51] Y. Dong, Z. Ding, L. Martínez, and F. Herrera, "Managing consensus based on leadership in opinion dynamics," *Information Sciences*, vol. 397-398, pp. 187–205, aug 2017.

[52] J. Ghaderi and R. Srikant, "Opinion dynamics in social networks with stubborn agents: Equilibrium and convergence rate," *Automatica*, vol. 50, pp. 3209–3215, dec 2014.

[53] X. Song, W. Shi, Y. Ma, and C. Yang, "Impact of informal networks on opinion dynamics in hierarchically formal organization," *Physica A: Statistical Mechanics and its Applications*, vol. 436, pp. 916–924, oct 2015.

[54] F. Heider, "Attitudes and cognitive organization," *The Journal of Psychology*, vol. 21, pp. 107–112, Jan. 1946.

[55] I. Agbanusi and J. C. Bronski, "Emergence of balance from a model of social dynamics," *SIAM Journal on Applied Mathematics*, vol. 78, pp. 193–225, Jan. 2018.

[56] L. da Fontoura Costa, O. N. Oliveira, G. Travieso, F. A. Rodrigues, P. R. V. Boas, L. Antiqueira, M. P. Viana, and L. E. C. Rocha, "Analyzing and modeling real-world phenomena with complex networks: a survey of applications," *Advances in Physics*, vol. 60, pp. 329–412, June 2011.

[57] S. Boccaletti, G. Bianconi, R. Criado, C. del Genio, J. Gómez-Gardeñes, M. Romance, I. Sendiña-Nadal, Z. Wang, and M. Zanin, "The structure and dynamics of multilayer networks," *Physics Reports*, vol. 544, pp. 1–122, Nov. 2014.

[58] W. Wang, Q.-H. Liu, S.-M. Cai, M. Tang, L. A. Braunstein, and H. E. Stanley, "Suppressing disease spreading by using information diffusion on multiplex networks," *Scientific Reports*, vol. 6, July 2016.

[59] J. Jiang and T. Zhou, "Resource control of epidemic spreading through a multilayer network," *Scientific Reports*, vol. 8, Jan. 2018.

[60] J. Wu, C. Pu, L. Li, and G. Cao, "Traffic dynamics on multilayer networks," *Digital Communications and Networks*, Nov. 2018.

[61] M. Kivela, A. Arenas, M. Barthelemy, J. P. Gleeson, Y. Moreno, and M. A. Porter, "Multilayer networks," *Journal of Complex Networks*, vol. 2, pp. 203–271, July 2014.

[62] M. E. J. Newman, *Networks: an introduction*. Oxford; New York: Oxford University Press, 2010.

[63] A.-L. Barabsi and M. Psfai, *Network science*. Cambridge: Cambridge University Press, 2016.

[64] D. Thesis and A. M. Schwahn, "Minimum Fundamental Cut Basis Problem," no. August, 2005.

[65] B. Skerritt, "Graph Theory Graph theory," *Medium - University of Liverpool*, p. 274, 2018.

[66] M. Loebl, "Lecture 1," *History of Modern Psychology*, no. March, pp. 1–10, 2019.

[67] J. C. Bronski, L. DeVille, and T. Ferguson, "Graph homology and stability of coupled oscillator networks," *SIAM Journal on Applied Mathematics*, vol. 76, pp. 1126–1151, Jan. 2016.

[68] D. Braess, "Über ein paradoxon aus der verkehrsplanung," *Unternehmensforschung Operations Research - Recherche Opérationnelle*, vol. 12, pp. 258–268, Dec. 1968.

[69] T. Roughgarden, *Twenty Lectures on Algorithmic Game Theory*. Cambridge University Press, 2016.

[70] T. Nishikawa, A. E. Motter, Y.-C. Lai, and F. C. Hoppensteadt, "Heterogeneity in oscillator networks: Are smaller worlds easier to synchronize?," *Physical Review Letters*, vol. 91, July 2003.

[71] D. Witthaut and M. Timme, "Braesss paradox in oscillator networks, desynchronization and power outage," *New Journal of Physics*, vol. 14, p. 083036, Aug. 2012.

[72] M. Rohden, A. Sorge, M. Timme, and D. Witthaut, "Self-organized synchronization in decentralized power grids," *Physical Review Letters*, vol. 109, Aug. 2012.

[73] A. E. Motter and M. Timme, "Antagonistic phenomena in network dynamics," *Annual Review of Condensed Matter Physics*, vol. 9, pp. 463–484, Mar. 2018.

[74] T. Coletta and P. Jacquod, "Linear stability and the braess paradox in coupled-oscillator networks and electric power grids," *Physical Review E*, vol. 93, Mar. 2016.

[75] L. xin Yang, J. Jiang, X. jun Liu, and Y. hua Chen, "Adjusting synchronizability of coupled oscillatory power networks via feedback control schemes," *Chaos: An Interdisciplinary Journal of Nonlinear Science*, vol. 29, p. 073112, July 2019.

[76] M. Fazlyab, F. Dörfler, and V. M. Preciado, "Optimal network design for synchronization of coupled oscillators," *Automatica*, vol. 84, pp. 181–189, Oct. 2017.

[77] E. B. T. Tchuisseu, D. Gomila, P. Colet, D. Witthaut, M. Timme, and B. Schäfer, "Curing braess' paradox by secondary control in power grids," *New Journal of Physics*, vol. 20, p. 083005, Aug. 2018.

[78] W. Lin, H. Fan, Y. Wang, H. Ying, and X. Wang, "Controlling synchronous patterns in complex networks," *Physical Review E*, vol. 93, Apr. 2016.

[79] M. Dow, "Explicit inverses of toeplitz and associated matrices," *ANZIAM Journal*, vol. 44, p. 185, Jan. 2008.